PALEOENVIRONMENT OF MARMARA SEA: PALYNOLOGY OF UPPER PLEISTOCENE - HOLOCENE SEDIMENTS IN LONG PISTON CORES

KATHRYN ROBERTS

Paleoenvironment of Marmara Sea: Palynology of Upper Pleistocene – Holocene Sediments in Long Piston Cores

by

© Kathryn Roberts

A Thesis submitted to the

School of Graduate Studies

in partial fulfillment of the requirements for the degree of

Master of Science

Department of Earth Sciences

Memorial University of Newfoundland

September - 2012

St. John's Newfoundland

ABSTRACT

The Marmara Sea along with the straits of Dardanelles and Bosphorus is the marine gateway that connects the Mediterranean and Black seas. Fossil palynomorphs are used to reconstruct the paleoclimate and paleoceanography of the Marmara Sea recorded in piston core MAR02-89P, from a water depth of 257 m on the upper slope basinward of the southeastern Marmara shelf. This is the first core from the region with a high resolution sedimentary record from approximately 30,000 cal. yr BP to early Holocene with the exception of a hiatus from ~14,850 – 12,700 cal. yr BP. The long section of upper Pleistocene glacial and early postglacial sediments in Core MAR02-89P enables a more detailed interpretation of the palynomorphs within the eastern Marmara Sea region than has previously been possible. Geochemical data indicate increased total organic carbon (TOC), and development of more anoxic sedimentary conditions starting around 18,000 cal. yr BP, with a gradual increase in marine production at 12,700 cal. yr BP. The ratio of total sulphur to TOC displays five peaks from ~28,500 – 10,000 cal. yr BP, which correspond to spikes in *Pediastrum* algae and may indicate Black Sea flood events. Pollen records indicate four assemblage zones (5 – 2) within core MAR02-89P. Pleniglacial to late glacial zone 5 represents mixed oro-Mediterranean forest and steppe grassland, indicating some areas with >600 mm rainfall/yr and warm enough to support a *Castanea* (sweet chestnut) refugium. Zone 4 in the cold Heinrich HS1 and warmer Bølling-Allerød equivalent intervals has increased presence of steppe grassland with *Ephedra*. Zone 3 in the Younger Dryas interval consists of predominantly steppe-forest

with sparse oro-Mediterranean forest, suggesting ~300 – 600 mm of annual rainfall. Pre-boreal to early Holocene Zone 2 records mesic euxinian forest with less steppe vegetation, because there is a reduction in pollen characterizing grassland areas and indicating <600 mm per year of rainfall, and an increase in pollen of euxinic forests plants requiring >600 mm of rainfall year-round. Dinoflagellate cyst records show two assemblage zones, with a low salinity *Spiniferites cruciformis-Pyxidinopsis psilata* assemblage being replaced with a more diverse *Operculodinium centrocarpum-Spiniferites* assemblage by 12,700 cal. yr BP. Three subzones in Dinocyst Assemblage Zone 2 (D2) may indicate changes in sea surface salinity (SSS) and temperature (SST). The marker species in the Dinocyst Assemblage subzone D2c indicate ~10 psu and cool water for the pleniglacial. Late glacial subzone D2b has assemblages indicating increased salinity (~13 – 17 psu) while late glacial subzone D2a assemblages suggest warmer SST during the Heinrich HS1 and the start of the Bølling-Allerød equivalent intervals. Dinocyst Assemblage Zone 1 (D1) consists of two subzones: dinocysts in pre-boreal subzone D1b indicate SSS of ~13 – 20 psu and cool to temperate surface water in contrast to subzone D1a Holocene assemblages indicating temperate to sub-tropical SST. From ~30,000 – 14,850 cal. yr BP, the Marmara Sea received water from the Black Sea during flood events. There is no record in core MAR02-89P for the interval of 14,850 – 12,700 cal. yr BP, by the end of this hiatus, sapropel development had begun, and Mediterranean dinocysts indicate Mediterranean water from the Aegean Sea was contributing to the Marmara Sea together with Black Sea water during and after the Younger Dryas event.

ACKNOWLEDGEMENTS

I would like to express my heartfelt thanks and gratitude to my thesis supervisors, Dr. Petra Mudie, Dr. Richard Hiscott, and Dr. Ali Aksu, for providing me with this research project and allowing me to become part of the Eastern Mediterranean research group. A special thanks, to Dr. Petra Mudie for her continual support, guidance, and patience throughout this process. She was there for me unfailingly, and without her, this thesis would never have been possible. I greatly appreciate the encouragement, constructive criticism, editing, and financial support required to complete this project.

I would also like to thank Helen Gillespie (Research Laboratory Coordinator CREAIT Network) and Allison Pye (Stable Isotope Laboratory Coordinator) for all of their help with processing samples and sampling techniques. I greatly appreciate Dr. Lee Bradley for answering countless questions about software and encouragement to complete my palynology analysis. Separate thanks to Dr. Elliott Burden for convincing me that Geology was a good idea, encouraging me to switch from Biology and Dr. James Macquaker for helping me to become more confident in my work.

Thank you to my parents for supporting me through my "course" as they like to call it, putting up with me when I got frustrated, and babysitting Layla. To my best friends Anna Linegar and Michael W. Hamilton, thank you for all of the intense games of dominoes, phone calls, workouts, and emotional support, all while working on your own Masters theses. Thank you to all of my friends for your love and support.

Table of Contents

List of Tables

Chapter 2

List of Figures

Chapter 1

Chapter 2

Chapter 3

List of Plates and Appendices

Introduction

The goal of this thesis is to better understand the climate, vegetation, and oceanography of the Marmara Sea over the past 30,000 years by analyzing the palynology of core MAR02-89P from the Marmara Sea. This study will provide insight and crucial data to understand the controversial history of the Black Sea and Mediterranean Sea reconnection and compare MAR02-89P data with other published data in the Marmara Sea region.

Background Information

The time and rate of development in a marine connection between the Black Sea and the Mediterranean Sea during the Holocene and Late Pleistocene is highly debated (Mudie et al., 2001; Aksu et al., 2002a; Ryan et al., 2003; Hiscott et al., 2007a; Vidal et al., 2010). The Marmara Sea and the Straits of Dardanelles and Bosphorus is the marine gateway that connects these two large bodies of water (Figure 1.1); it is believed that detailed study of the fossils within the sedimentary record of this gateway will clarify controversy concerning the timing of these marine connections following the last deglaciation (Aksu et al., 2002a). Studying the micropaleontology and, particularly, the palynology of acid-resistant organic-walled microfossils in the Marmara Sea sediments may be the most influential tool in settling this debate (Mudie et al., 2001, 2002a,b; Aksu et al., 2002a).

This Masters Project involves analyzing palynomorphs (e.g. pollen, spores, dinoflagellate cysts) and other non-pollen palynomorphs to reconstruct the paleoclimate and paleoceanography of the Marmara Sea over the past 30,000 years. Foraminifera, diatoms, and ostracods are all useful microfossils, but not the most appropriate paleontological tools for study of the low salinity Marmara Sea where diversity of calcareous and siliceous microfossils is low and foraminiferal shells are thin-walled and subject to calcite dissolution (Alavi, 1988). Under these conditions, palynology is more effective because a diversity of organic-walled palynomorphs preserve better in low salinity, high nutrient water, and because pollen and terrestrial spores, including fungal spores, are unique microfossils for correlating marine records with paleoenvironmental events on land (Mudie et al., 2002b).

There have been several Late Pleistocene – Holocene palynological studies made previously from cores taken in the Marmara Sea (Mudie et al., 2001; 2002a,b; 2004; 2007; Caner and Algan, 2002; Londeix et al., 2009), but few of these have long sections of sediment for the Pleistocene interval. The piston core MAR02-89P, from a water depth of 257 m on the upper slope of the southeastern Marmara Sea about 30 km south of the Bosphorus Strait, is the first core that has an almost complete well-dated sedimentary record from about 23,000 conventional radiocarbon years ago (uncalibrated and designated throughout the thesis by units "yr BP") to early Holocene time for the northern Marmara gateway. This 800 cm-long piston core has been dated by multiple radiocarbon ages and provides a key reference section that can be correlated to other radiocarbon-

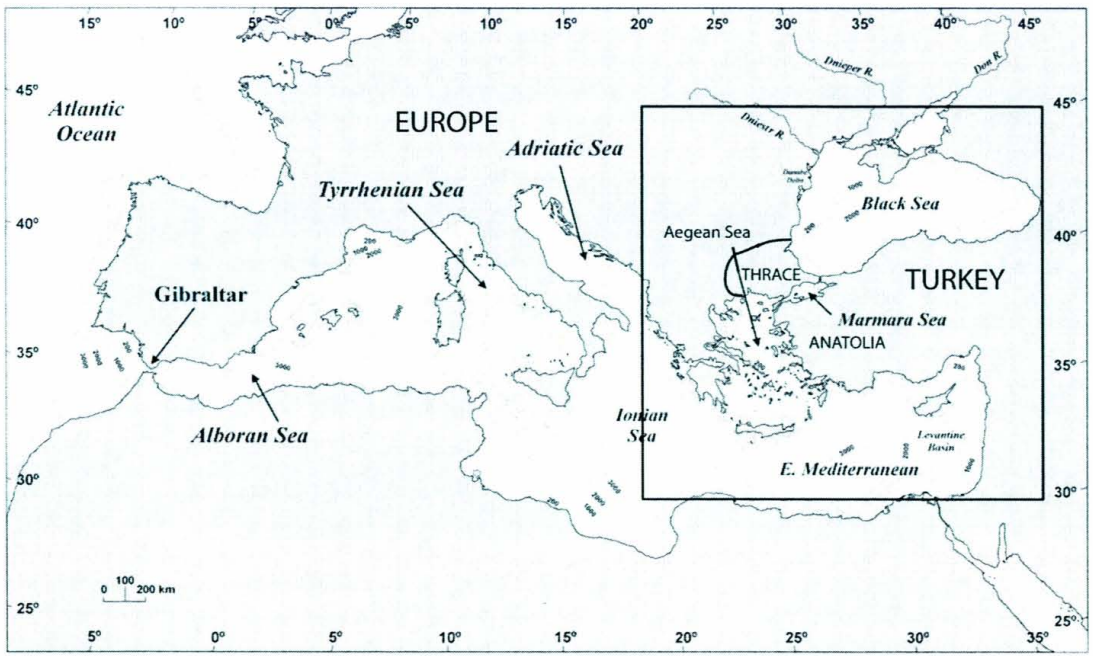

Figure 1.1: Map of the Mediterranean region showing the Marmara Sea study area within the large box. Bathymetry is in meters (from Mudie et al., 2004).

dated cores within the study area. The pre-Holocene pollen records from core MAR02-89P provide a background for comparison with the vegetation before agricultural development in the Marmara Sea region that is thought to be between 10,000 to 6,000 cal. yr BP (e.g. Turney and Brown, 2007; Algan et al., 2009; Özdoğan, 2011). The palynological data from this core may provide indications of human presence such as pollen markers of agriculture and horticulture, fungal spores as indicators of soil erosion and animal husbandry, and charcoal particles as an index of forest fires and crop/grassland burning. Geochemical data (A. Aksu, unpublished) will be analyzed to supplement the palynological proxy-data, to determine the main sources of carbon (terrestrial versus marine) and compare to previous investigations of other Marmara Sea cores (e.g. Abrajano et al., 2002; Vidal et al., 2010). Dinoflagellate cyst (dinocyst) data mark surface water conditions relatively close to the Bosphorus overflow into the Marmara Sea and can be compared to the western basin dinocyst data of Londeix et al. (2009) and with Kaminski et al. (2002) bottom-water data from benthic foraminifera.

1.1.1 Geographical Location

The study area is a small semi-enclosed sea (~11,500 km^2), located along the border between southern Europe and Asia (Figure 1.1). The Marmara Sea is a marine intracontinental basin and today acts as a transitional zone, connecting the Black Sea (via the Bosphorus Strait) to the Aegean Sea (via the Dardanelles Strait). The Pontic

Mountains are adjacent to the Marmara Sea to the south, with the Thracian Plain to the north. The modern climate and vegetation are outlined in section 1.3.1 on pollen sources.

1.1.2 Geology

The Marmara Sea is a transtensional basin that straddles the Eurasian Plate and the Aegean-Anatolian Microplate, forming a negative flower structure (Aksu et al., 2000). This region is prone to faulting and earthquakes due to the westward movement of the Aegean-Anatolian Microplate along the dextral Northern Anatolian Transform Fault that is driven by the collision of the Arabian Microplate with the Eurasian Plate. This seismic activity can have a huge effect on bathymetry (uplift and/or subsidence) within the basin and may displace slope sediments, interrupting sedimentation.

The geology of the Marmara region (Zattin et al., 2010) is composed of small continental fragments: the Sakarya Zone (south), the Istanbul Zone (northeast), and the Strandja-Rhodopian terrane that crops out along the margin of the Thrace Basin. The Sakarya Zone is composed of a deformed and metamorphosed Triassic subduction-accretion complex overlain by Jurassic continental to shallow marine deposits, followed by Cretaceous carbonates, and andesites. The Istanbul Zone is composed of a crystalline Precambrian basement overlain by a continuous transgressive sedimentary succession (Ordovician – Carboniferous), which was deformed during the Paleozoic and is unconformably overlain by a Mesozoic succession with Cretaceous andesites and small

acidic intrusions. The crystalline Strandja-Rhodopian terrane composes the basement of the Thrace Basin, which is filled with shallowing-upward, clastic-dominant successions of early – middle Eocene to Oligocene age. Shales and sandy shales with some coal bearing siliciclastics and carbonates overlie these rocks, and fluvial deposition characterizes the sedimentation from Miocene – Pliocene until the Late Pleistocene.

The MAR02-89P core is located at a water depth of 257 m in the southeastern part of the Marmara Sea, on an elongate ridge at the seaward edge of a perched upper-slope basin and northeast of the mouth of the Kocasu River which is the main supplier of clastic terrigenous sediments (614,000 tons/yr of suspended solids) to the southern Marmara Sea shelf (Ergin et al., 1997; Çağatay et al., 2000). Today, the Kocasu River contributes about 48% of suspended riverine sediment and approximately 80% of total riverine freshwater discharge that flows directly to the Marmara Sea, excluding the input from the Black Sea. Silty mud is the prominent Holocene sediment type within the Marmara Sea and sand and gravel usually make up less than 10% of the total sediment dry weight (Ergin and Bodur, 1999).

1.1.3 Oceanography

The oceanography of the study region has varied throughout the Quaternary Period (Aksu et al., 2002b). Glaciations during the Pleistocene locked large amounts of fresh water into ice sheets at high latitudes and contributed to an ~-125 m fall in global sea

level, causing the Marmara Sea and Black Sea to be landlocked because of the shallower depths of the Dardanelles (~-70 meters below present sea level) and the Bosphorus (~-40 meters below present sea level) straits (Figure 1.2). By the Holocene, the Marmara Sea climate changed from colder to warmer and more humid, and runoff from large rivers that were draining Eastern Europe (Danube, Dnieper, Dniester, Bug, and Don) raised the level of the Black Sea (Aksu et al., 2002b). During the deglaciations, huge amounts of glacial meltwater periodically flooded the Black Sea (Chepalyga, 2007). By ~10,000 – 10,500 yr BP (~11,060 – 11,700 cal. yr BP), the excess Black Sea water spilled into both the Marmara Sea, and then the Aegean Sea. The Marmara Sea was reconnected to the Aegean Sea earlier (~12,000 yr BP; ~ 13,400 cal. yr BP) when the sea level rose above ~-85 to 70 meters below present sea level in the Dardanelles Strait (Çağatay et al., 2000; Aksu et al., 2002a; Eriş et al., 2011). By ~8,500 yr BP (~9,100 cal. yr BP), continued rise of global sea level reconnected the Black Sea to the Mediterranean Sea via the inflow of Aegean Sea water through the Bosphorus Strait (Hiscott et al., 2007b).

The Dardanelles and the Bosphorus straits are relatively shallow and narrow (Figures 1.2 and 1.3) and prevent the exchange of deep water between the Aegean and Black seas, resulting in the development of a steady two-layer flow system within the Marmara Sea (Beşiktepe et al., 1994). The two-layer water circulation system consists of a low salinity upper layer and a high salinity lower layer that are present throughout the

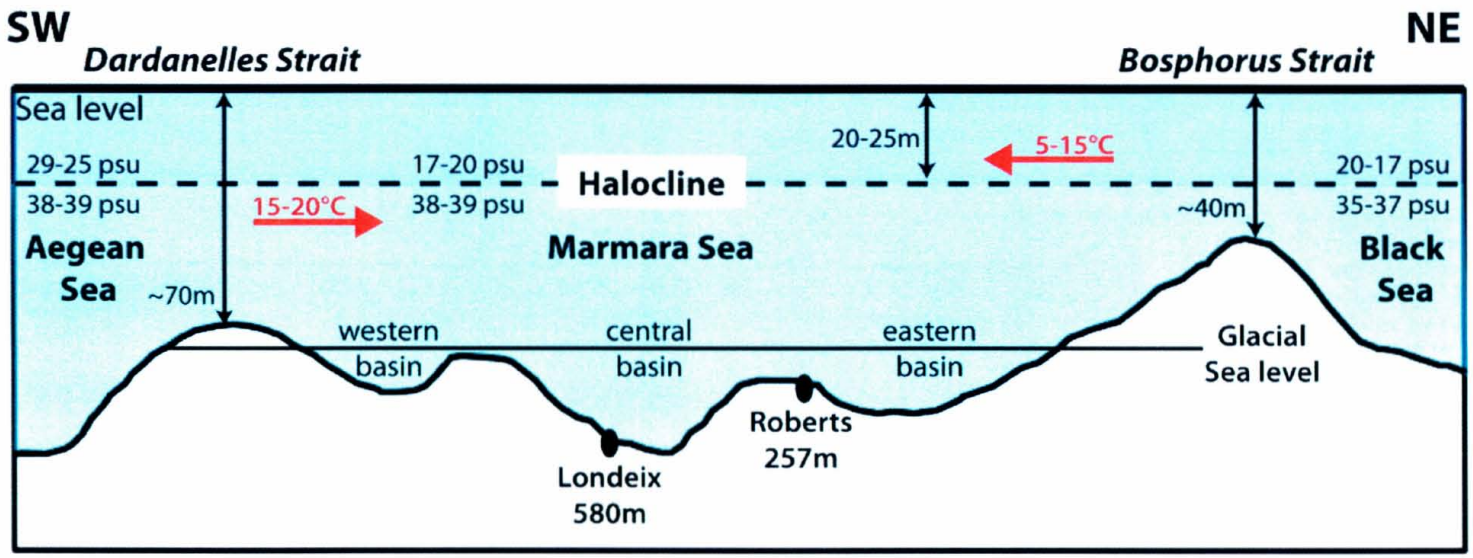

Figure 1.2: Cartoon of present day water circulation, salinity, and temperature within the Marmara Sea showing locations and depth (m) of Roberts and Londeix cores, vertical scale is not quantitative because the three deep basins reach >1000 m depth. Figure modified from Londeix et al. (2009) and Beşiktepe et al. (1994).

entire Marmara Sea (Figure 1.2). Salinity is defined as a Practical Salinity Scale measuring the conductivity ratio of a sea water sample to a standard KCl (potassium chloride) solution; this is a dimensionless quantity with "units" commonly expressed as psu. Cooler (5 – 15°C), low salinity water (17 – 20 psu) from the Black Sea forms a 20 to 25 m-thick westward flowing surface layer that moves into the Marmara Sea with velocities of 10 – 30 cm/s (Beşiktepe et al., 1994). The lower layer is formed of warmer (15 – 20°C), hypersaline marine water, initially 38 – 39 psu, becoming more dilute towards the Bosphorus Strait where it is 35 – 37 psu. The bottom water of Mediterranean origin flows from the Aegean Sea through the Dardanelles Strait, entering the western basin in winter, then gradually occupying the entire Marmara Sea. On entering the Marmara Sea, the Mediterranean water plunges beneath the cooler low salinity surface water layer at velocities of 5 – 25 cm/s, then travels further northeast through the Bosphorus Strait into the Black Sea.

At present, this strong salinity and temperature stratification creates a permanent halocline and sustains an overall estuarine circulation within the Marmara Sea. As a result, the vertical circulation throughout the basin is inefficient, as oxygen is not effectively transported into the deeper portions of the water column (Kaminski et al., 2002; Londeix et al., 2009). The depletion of oxygen in the lower layers of the basin creates suboxic to dysoxic conditions with a limited number of organisms that can survive in this restricted environment. The low oxygenation and restricted bioactivity aid in the preservation of organic matter and periodically promote sapropel deposition; i.e.,

sediments with >2% total organic carbon (Aksu et al., 2002a; Abrajano et al., 2002).

The low salinity surface Black Sea water moves through the Bosphorus Strait and into the Marmara Sea in a southwesterly direction as a narrow current (Figure 1.3). The current crosses the northeastern basin generating weak anticyclonic eddies, then turns west along the southern shelf and finally northwest across the central basin. The current then turns southwest towards the Dardanelles Strait forming another large meander loop with a weak anticyclonic gyre in the central basin.

The circulation of the deep bottom layer presently depends on the influx of water from the Aegean Sea through the Dardanelles Strait (Beşiktepe et al., 1994). As this water enters the Marmara Sea, it forms turbulent plumes below the halocline (20 – 25 m) that sink into the western basin and slowly move eastward, eventually entering the Black Sea via the Bosphorus Strait. The sinking and spreading of the turbulent plumes are seasonal, and during the winter, the plumes sink to the bottom of the deep western basin to depths of 100 to >500 m (Beşiktepe et al., 1994). The movement of water from the western to eastern basin is restricted by deep sills, and can remain stagnant for weeks at certain times of the year. The autumn season in the eastern basin is characterized by high temperature and salinity anomalies just below the halocline.

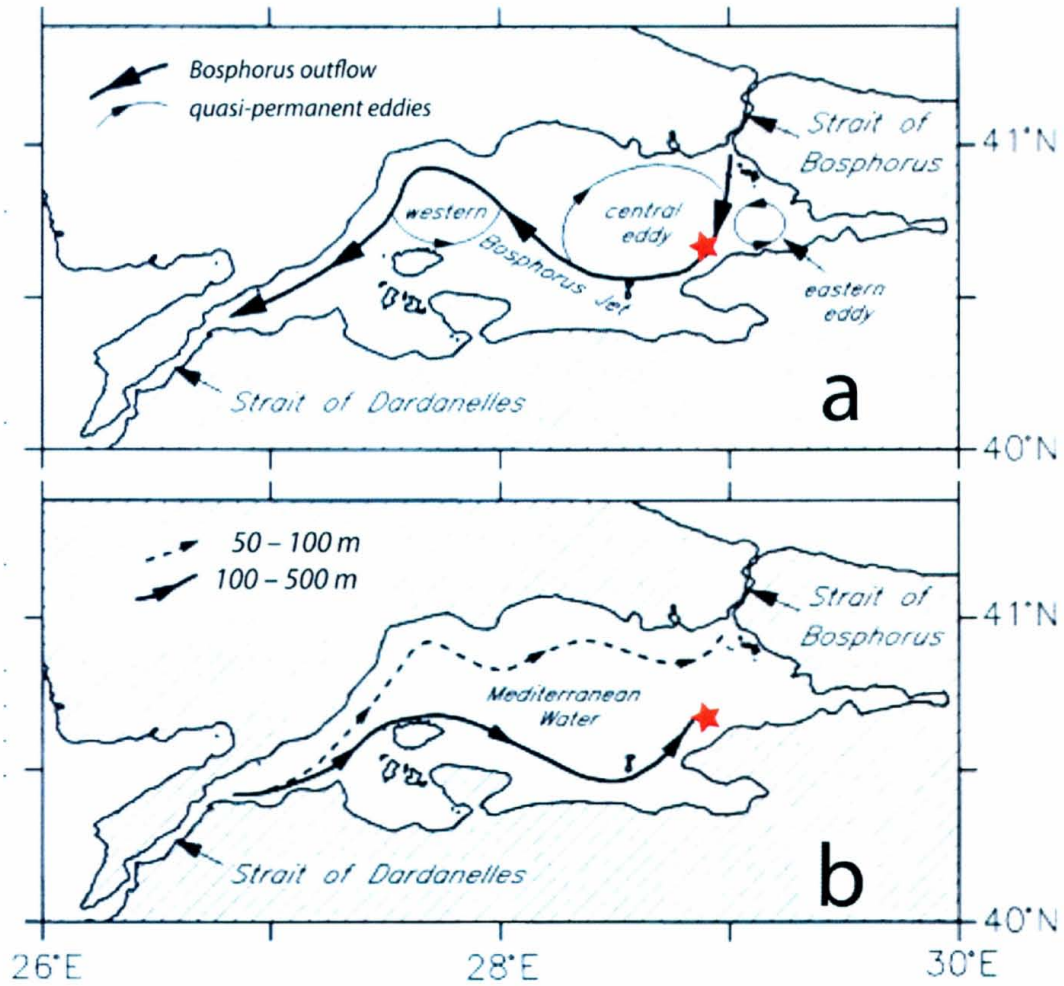

Figure 1.3: Surface (a) and deep (b) water circulation in the Marmara Sea with red star indicating approximate location of core MAR02-89P, modified from Aksu et al. (2002a), based on Beşiktepe et al. (1994).

1.2 Catastrophic vs. Gradual Flooding and Water Level Fluctuations

A widely publicized view of the last marine reconnection between the Mediterranean, Marmara, and Black seas is that reconnection occurred in one large catastrophic very rapid (<100 years duration) flooding event. Ryan et al. (1997) and Ryan and Pitman (1999) proposed this hypothesis and linked it to the biblical "Noah's flood", initially reporting that it took place at approximately 7,150 yr BP (~7,610 cal. yr BP).

There are problems with the above hypothesis and other research groups are working with various forms of paleontology, seismic imaging, and other geological and geochemical techniques in further investigating this "Noah's Flood Hypothesis" (Hiscott et al., 2007a; 2007b; Vidal et al., 2010). If the flood were a catastrophic event, then there would have been a unidirectional flow of marine surface waters into an isolated Black Sea lake through the Bosphorus Strait, rapidly filling it with water, drowning the exposed lake shelves and transporting Mediterranean marine organisms into the Black Sea (Mudie et al., 2001;Kaminski et al., 2002). This increased inflow of Mediterranean water would certainly have destroyed any density stratification of the Marmara Sea, resulting in a well-oxygenated water column (Kaminski et al., 2002). However, in the Marmara Sea, palynological and micropaleontological data from short cores indicate a persistent low salinity surface layer and dysoxic conditions below a stable halocline throughout the early – mid Holocene, which can be explained by sustained outflow of low salinity Black Sea water and gradual inflow of Mediterranean water to the Black Sea (Mudie et al., 2001,

2002; Kaminski et al., 2002; Marret et al., 2009). Other authors (Sperling et al., 2003; Çağatay et al., 2000; Vidal et al., 2010) dispute this scenario because they have collected geochemical data suggesting increasing salinity in the Marmara Sea and thus no or a weak connection with the Black Sea in the early Holocene.

It is presumed that during glacial intervals when global sea level fell, the Black Sea became an isolated lake disconnected from the Marmara and Aegean Seas. There are several published hypotheses regarding the water level fluctuations resulting in the connection between the Aegean, Marmara and Black seas (Figure 1.4; Aksu et al., 1999b; Vidal et al., 2010; Eriş et al., 2011; McHugh et al., 2008). The ages presented in this section are those given by the authors of the models presented in this chapter, but the ages used for this study of core MAR02-89P are from Fletcher and Sánchez- Goñi (2008).

Aksu et al. (1999b) analyzed seismic profiles, geochemistry ($\delta^{18}O$) and mollusk data to reconstruct four phases demonstrating significant stages in the reconnection of the Marmara Sea gateway. 1. At 18,000 yr BP (~23,000 cal. yr BP), all three basins were disconnected during a global ocean low-stand, with the potential of Marmara Sea spillover into the Aegean Sea. 2. From 11,000 yr BP (~13,500 cal. yr BP), glacial melt water began to flow into the Black Sea, and Aegean Sea water breached the Dardanelles Strait, flowing into the Marmara Sea. 3. At 9,500 yr BP (~10,700 cal. yr BP), fresh to brackish Black Sea water flowed into the Marmara Sea on top of marine Mediterranean Sea water, but the marine inflow could not penetrate the Black Sea; this resulted in initial stratification and development of the sapropels S1 in the Aegean Sea and M1 in the

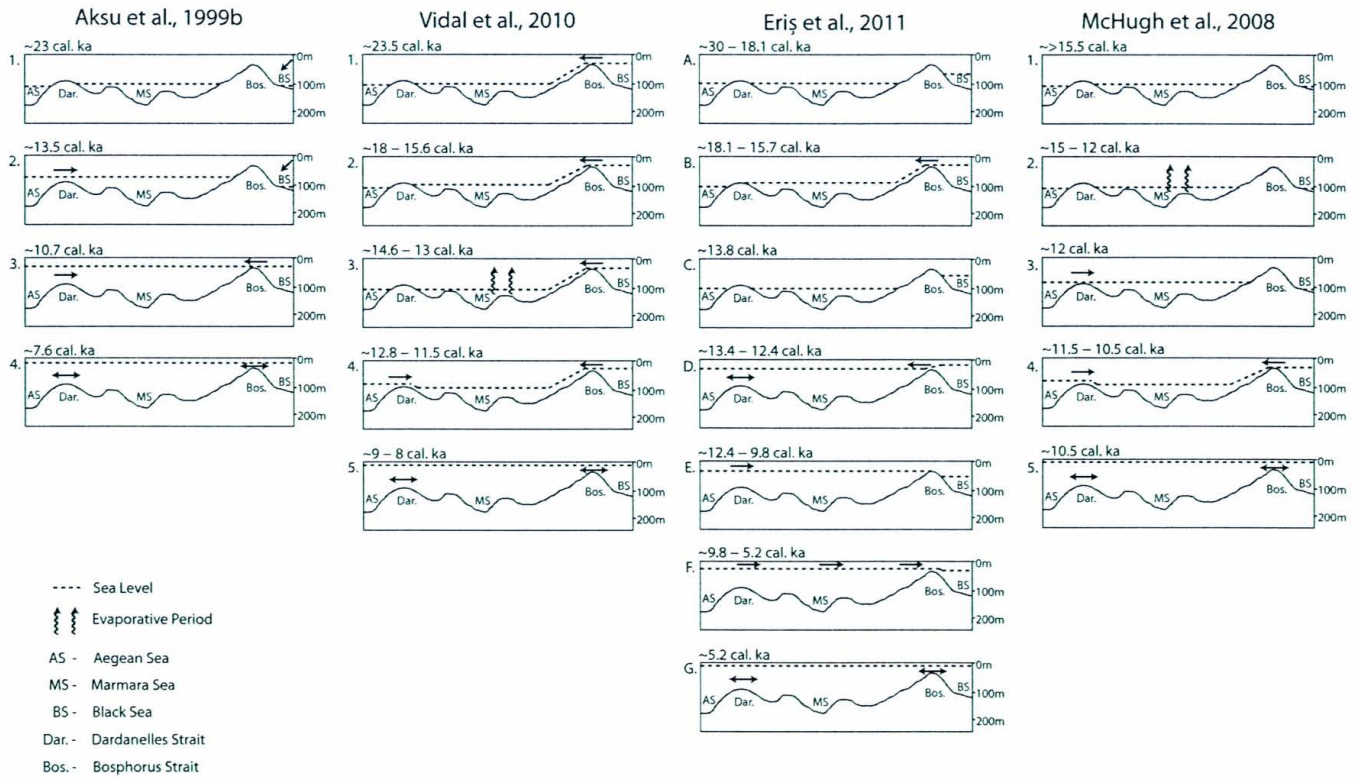

Figure 1.4: Summary diagram of published water level fluctuations in the Marmara Sea region described in this thesis, with arrows indicating water flow direction. Calibrated ages are only approximate because of differences in reservoir correction curves used by the different authors.

Marmara Sea. 4. At 7,150 yr BP (~7,610 cal. yr BP), marine Mediterranean Sea water fully penetrated across the Bosphorus Strait resulting in continuous two-way flow; the deposition of sapropel S1 was nearly complete and sapropel development began in the Black Sea.

Using oxygen ($\delta^{18}O$) and strontium ($\delta^{87}Sr$) isotopes and ostracod data from long cores in the NW Black Sea and the western Marmara Basin, Vidal et al. (2010) described five phases for their reconnection model (Figure 1.4), including the last glacial maximum, the time of Heinrich stadial interval HS1, Bølling-Allerød, Younger Dryas and sapropel deposition. Coinciding with the last glacial maximum (1. ~23,500 cal. yr BP) and Heinrich stadial HS1 interval (2. 18,000 – 15,600 cal. yr BP) their model indicates inflow of melt water that had accumulated in the Black Sea into the Marmara Sea. During the Bølling-Allerød phase (3. ~14,600 – 13,000 cal. yr BP), climate in western Europe is known to have warmed, possibly leading to increased evaporation and salinity in the Marmara Sea and at ~14,700 cal. yr BP both Aegean and Black sea waters penetrated into the Marmara basin. The Younger Dryas phase (4. 12,800 – 11,500 cal. yr BP) is poorly represented in the Vidal et al. (2010) core MD01-2430 from the Marmara Sea, but Londeix et al., (2009) determined outflow from the Black Sea at this time. Vidal et al. (2010) reported an apparent disconnect of the basins along the Marmara Sea gateway from 11,500 – 9,000 cal. yr BP, followed by the reentry of both Mediterranean and Black sea waters into the Marmara Sea. Vidal et al. (2010) found that during the initiation of sapropel development in the interval of weak or no connection, organic matter was

predominatly of terrigenous origin. During the remainder of the M1 sapropel phase (5. between 9,000 – 8,000 cal. yr BP) the basins reconnected, estuarine flow was established and organic matter was primarily of marine origin.

Eriş et al. (2011) analyzed seismic profiles and the sedimentology, including benthic foraminifera, in seven short cores and one long core of Holocene sediment from ~80 – 65 meters below sea level in the eastern Marmara Sea, to determine a seven phase (a – g) model of reconnection (Figure 1.4). During the Late Pleistocene phase A (25,000 – 15,000 yr BP, ~30,000 – 18,100 cal. yr BP), they concluded that the three basins were not connected and fluvial erosion may have lowered the Dardanelles Strait to -85 m, below its present depth. In phase B (15,000 – 13,500 yr BP, ~18,100 – 15,700 cal. yr BP), glacial melt water raised the level of the Black Sea allowing it to export water into the Marmara Sea. In phase C (12,000 ka BP, ~13,800 cal. ka BP), the Black Sea level fell due to evaporative draw-down (during the warm Bølling-Allerød event), and the Marmara Sea level rose significantly, but did not breach the Dardanelles Strait. During phase D (11,500 – 10,500 yr BP, ~13,400 – 12,400 cal. yr BP), global sea-level rose flooding the Marmara Sea with Mediterranean water, and during the Younger Dryas, the Black Sea overflowed into the Marmara Sea, filling it and eventually flowing into the Aegean Sea. Eriş et al. (2011) consider that sea-level rise in the Marmara Sea was interrupted by still stands most likely due to high volumes of Black Sea outflow blocking Aegean Sea inflow over a shallow sill. The end of the Younger Dryas was followed by the onset of sapropel deposition. During phase E, (10,500 – 8,800 yr BP, ~12,400 – 9,800 cal. yr BP), rising

global sea-level fully breached the Dardanelles Strait, and during the mid – late Holocene phase F (8,800 – 4,500 yr BP, ~9,800 – 5,200 cal. yr BP), Marmara Sea water flooded into the Black Sea. The final Phase G from late Holocene to Present (4,500 – 0 yr BP, ~5,200 – 0 cal. yr BP) was when Black Sea water flowed unimpeded into the Marmara Sea, generating the modern two-way flow, more than 4,000 years later than the time of Black Sea outflow established in the other models described above.

McHugh et al. (2008) analyzed cores from the eastern Marmara Sea using lithology, benthic and planktonic foraminifera, mollusk assemblages, diatoms, physical properties (density, magnetic susceptibility and X-ray fluorometry), geochemistry (Br, $CaCO_3$) and oxygen isotopes. McHugh et al. (2008) describe five phases that comprise the reconnection of the Black Sea to the Mediterranean Sea (Figure 1.4). 1. The Marmara lacustrine phase (>15,500 – 12,000 cal. yr BP) occurred after deglaciation of the Eurasian continental ice sheet and was determined to be a cold and dry interval by McHugh et al. (2008). 2. During the Bølling-Allerød conditions warmed, resulting in a drawdown of both the Marmara and Black seas. 3. The marine incursion phase (12,000 cal. yr BP) resulted in the introduction of marine organic matter, decrease in grain size and abundance of calcium carbonate. 4. During the Younger Dryas phase (11,500 – 10,500 yr BP), the Marmara Sea continued to receive marine water inflow along with fresh water outflow from the Black Sea and saw a still stand of sea-level. 5. Periodic mixing of Black Sea and Marmara Sea shelf waters and development of strong stratification accompanied the establishment of two-way flow and increased influx of nutrients from Black Sea water

inflow.

The long core MAR02-89P is located in deeper water of the eastern Marmara Sea than the Eriş et al. (2010) cores. Therefore, this new core potentially might provide a more detailed record of late glacial and early Holocene floodwater events in the southeastern Marmara Sea than could be obtained from the series of short cores in shallower water studied by McHugh et al. (2008) and Eriş et al. (2010).

1.3 Palynomorphs: Fossil Pollen, Dinoflagellate Cysts, and Fungal Remains

Palynomorphs are microfossils produced by organisms that form a cell, tissue, or organ with an organic wall of complex carbohydrates and sterols that are highly resistant to organic decay or inorganic degradation (de Leeuw et al., 2006). They are derived from four of the five biological kingdoms: Protista, Planta, Fungi, and Animalia (Traverse, 1988). The study of palynomorphs preserved in the rock and sedimentary record has practical applications to the Earth and environmental sciences, resources, development and monitoring. Palynomorphs are excellent subjects to study due to their small size and great abundance per gram of sediment, their highly varied morphology and their ability to remain preserved in the geological record wherever sedimentation is rapid and bottom water is not highly oxidizing (Jansonius and McGregor, 1996; Mudie et al., 2001). Palynomorphs include microspores and organic remains that originate both on land and in fresh and salt water environments.

The abundance and resistance of organic-walled palynomorphs to dissolution is an essential feature of palynology. Due to their abundance, palynologists can employ statistics and population studies from detailed counts of pollen grains or dinoflagellate cysts (dinocysts) within a given sample (Traverse, 1988; de Vernal and Marret, 2007). The durability of the palynomorphs, most commonly composed of sporopollenin (pollen), dinosporin (dinoflagellate cysts) or chitin (microforaminiferal linings), allows good preservation in non-oxidizing environments after deposition.

1.3.1 Pollen and Spores in the Marmara Sea Region

The Marmara Sea is surrounded by the western Pontic Mountains and coastal plains in the south and the Thrace Region to the north, which today support a wide variety of vegetation that are the sources of pollen and terrestrial spores in the marine sediments (Mudie et al., 2002a; Caner and Algan, 2002). This vegetation diversity is related to the geomorphology, climate, and recent climate and anthropogenic changes during the late Quaternary in Turkey. Mountain ranges extend along the north coast of Anatolia, while plains and plateaus are found in the central and east Anatolia, creating a transitional region between temperate, humid, tropical and arid climates (Mudie et al., 2002b, their Figure 2; Cordova et al., 2009). The modern climate of the Marmara region is reported to have an average annual precipitation of 686.2 mm and average temperature of 13.7°C (Ünal et al., 2003). Ünal et al. (2003) determined the minimum and maximum average

temperature for the region to be 3.8°C and 25.7°C, respectively. The forests of Northern Anatolia are restricted to specific elevations on the mountain chains, with high altitudes representing Euro-Siberian forest elements, and lower elevations supporting euxinic mesic forest elements in the southeastern section of Marmara Sea. Mediterranean scrub occupies the lower altitudes in the southwestern region. The northern region of the Marmara is characterized by broad-leaved deciduous forests.

Forest is comprised mainly of summer green *Quercus* (broadleaf, deciduous oaks), *Alnus* (alder), *Acer* (maple), *Corylus* (hazel), *Ulmus* (elm), *Fraxinus* (ash), and *Tilia* (linden). The southern Marmara region consists of both broad-leaved and summer-dry forest, mostly represented by *Quercus* (oak), *Olea* (olive), and *Pinus* (pine) along the coastal foothills. Mesic euxinic forest in the Pontic Mountains is dominated by warm temperate deciduous forest trees, including *Juglans* (walnut), *Carpinus* (hornbeam), and *Pterocarya* (wingnut) in addition to the northern temperate elements (Mudie et al., 2002b). By comparing fossil pollen to modern analogues, a paleoclimate can be inferred based on the modern climate requirements of the species present e.g. deciduous *Quercus* indicates warm-dry summers and mild-wet winters, and requires year-round moisture of more than 600 mm and winter temperature about -5°C (Mudie et al., 2002b; 2007). Certain other forest pollen types are also good indicators of glacial/interglacial periods. Species that require relative warm temperature and high moisture are associated with interglacial periods e.g. deciduous *Quercus* (summer green oak), *Fagus* (beech), *Abies* (fir), while scrub and herb species that are resistant to dry, cold climates are linked to

glacial periods and saline soils e.g. *Artemisia* (sage brush) and Chenopodiaceae (saltbush) (Caner and Algan, 2002).

Spores of ferns and mosses are also useful vegetation indicators. *Asplenium* fern occurs in a wide variety of habitats which can be exposed or partially shaded and could indicate conditions of semi-deciduous woodland, wet evergreen forest, and sub-montane rain forest (Lashin, 2012). *Equisetum* horsetails (Sphenopsid) prefer wet sandy soils and are poisonous to animals when eaten in large amounts so they are associated with over-grazing in addition to land clearance. Most polypodiaceae ferns thrive in wet, temperate zones, but some can also survive in summer dry Mediterranean regions. The presence of a perine on polypod spores also indicates better preservation (Mudie et al., 2002b). *Dryopteris*-type forest ferns require more moisture compared to *Polypodium*, agreeing with pollen data that show the early Holocene experience high rainfall (~>600 mm/year; Mudie et al., 2002b). *Pteridium* (bracken fern) can survive in a wide range of soils and often indicates cleared forest (fires) or grazed land (Mcglone et al., 2005). Mosses generally indicate wet conditions, while lycopods (club mosses) represent open and dry conditions that can be hot or cold (Leroy et al., 2010). The liverwort *Anthoceros* can indicate open, wet soils and perennially humid conditions, such as along river banks (Leroy et al., 2010).

1.3.2 Dinoflagellate Cysts in the Marmara Sea Region

Dinoflagellate cysts (dinocysts) are another category of palynomorphs that provide invaluable information about paleoceanography, biostratigraphy, and paleoecology, including presence of brackish and fresh water environments. Dinocysts are the resting spores of phytoplankton that live in the top ~5 – 20 m of water, with some species capable of living at greater depths down to the top of the pycnocline. Species of these phytoplankton have different surface water condition requirements and their cysts can be used to infer past surface water conditions (Mudie et al., 2002a; Marret and Zonneveld, 2003; Sluijs et al., 2005). Dinocysts are found to be abundant and well preserved within the organic-rich Late Pleistocene and Holocene sediments of the Marmara Sea (Mudie et al., 2004). The morphology of some dinocysts, such as *Spiniferites cruciformis* and *Lingulodinium machaerophorum* varies in response to changes in salinity, stratification, and/or stress in the physical environment and may account for the wide range of cyst morphologies that are found within the study area (Mudie et al., 2001, 2004; Marret et al., 2004). In particular, *S. cruciformis* possesses five described morphological forms with a cruciform body and varying processes lengths, and it is a reliable indicator of brackish water to estuarine environments of low salinity in the Marmara and Black Seas (Mudie et al., 2001); spine length of *L. machaerophorum* is related to temperature and salinity at 30 m water depth (Mertens et al., 2009) and to surface water salinity (Mertens et al., 2012).

Previous studies show that the eastern Mediterranean Sea and Aegean Sea regions have a low diversity of dinocyst species (9 – 12), a mixed assemblage of Aegean Sea and

Black Sea species occurs in Marmara Sea, and some species are restricted to either the Aegean or the Black Seas (Mudie et al., 2004). Two geographic groups have been determined. 1. The Aegean group is represented by mainly autotrophic gonyaulacoid taxa and one protoperidinioid that characterize the high salinity Aegean/Mediterranean waters and 2. the Marmara/Black Sea group consists of diverse heterotrophic protoperidinioids and three gonyaulacoids that characterize the low salinity environment. The organic-rich Holocene Marmara Sea and Black Sea sediments provide uniformly good preservation of the thin-walled protoperidinioid species (Mudie et al., 2004). It is to be expected; however, that preservation of the protoperidinioids could be reduced during glacial intervals of shallower water, more oxidizing bottom water and lower organic production (Hopkins and McCarthy, 2002; Zonneveld et al., 2008). When the amount of dinocysts lost by oxidation can be evaluated, then the concentration and influxes of dinocysts can be used as an index of primary productivity.

1.3.3 Algae and Other Non-Pollen Palynomorphs in the Marmara Sea Region

Aquatic algae here mainly refer to colonial forms of green algae such as *Pediastrum* and *Botryococcus* and desmid hemicells that are most abundant in freshwater but also live in brackish water (Mudie et al., 2011). Fossil algae are helpful palynological indicators, e.g. *Botryococcus* (colonial algae) that may be preserved in lake and estuarine marine sediments as organic rich layers, and can exist in a wide spectrum of temperatures

(tropical to sub-polar regions; Cohen, 2003), as well as a range of salinities from <1 – 22 psu in the Marmara Corridor (Mudie et al., 2011). *Pediastrum* is another colonial algae, which generally indicates nutrient-rich, and relatively freshwater conditions and may indicate wetter climatic conditions or higher river discharge (Cohen, 2003; Londeix et al., 2009; Mudie et al., 2010). Within the study area, it is believed that spikes in *Pediastrum* may be an indicator of increased runoff water to the Black Sea (Mudie et al., 2002a). Desmids are a group of green algae generally found in freshwater, but *Cosmarium* is also occasionally present in the modern Black Sea (Mudie et al., 2011); *Staurastrum* is frequently found as a fossil remain in lake sediments due to polyphenolic compounds in the cell wall that protect against bacterial degradation (Bellinger and Sigee, 2010). *Cymatiosphaera* is common in modern sediments of the low salinity Black Sea although Londeix et al. (2009) considers that it is an indicator of marine water and may mark the reconnection of the Aegean Sea in the study area.

Fungal remains are most widespread in terrestrial realms, and some taxa are clear indicators of soil erosion (e.g. *Glomus* sp.; Jansonius and McGregor, 1996), while other air-borne fungal spores are indicators of animal husbandry and/or crop production (Mudie et al., 2011). Many fungal spores are derived from soils in watersheds and fringing marshlands, and are good tracers of soil erosion because there are no aquatic or marine fungi that produce fossilizable fungal palynomorphs (Mudie et al., 2002). Mudie et al. (2004) show that fungal spores are more abundant during intervals of higher river runoff in the early Holocene and that there is an order of magnitude difference of fungal spore

concentration from the Black Sea to the Marmara Sea, with fungal remains mostly absent from the core sites sampled within the Aegean Sea (Mudie et al., 2002).

Animal remains (various zooplankton and zoobenthos) are additional non-pollen palynomorphs, such as copepod and flatworm eggs and forminiferal linings found within the study area (Mudie et al., 2011). For the most part, flatworms (Rhabdocoels) are freshwater organisms and the palynomorphs are represented by egg capsules. Copepods are present in freshwater but are most common in marine environments. Foraminiferal linings may be indicators of a sustained marine connection with the Mediterranean Sea, and based on presence and/or absence within the region, it is known that no planktonic foraminifera and few benthic foraminifera can live in the low surface salinity (<22 psu) and anoxic conditions presently found below 200 – 400 m water depth in the Black Sea (Mudie et al., 2011).

The Black Sea receives ~350 km^3 per year of drainage water from surrounding rivers, and with it comes transported palynomorphs that can be transferred to the Marmara Sea through water circulation (Aksu et al., 2002a). The present-day Marmara Sea has significantly less direct river drainage (~6 km^3 per year), than the Black Sea that also contributes terrestrial palynomorphs to the landlocked Marmara Sea (Aksu et al., 2002a). Previous studies that compared late Holocene cores from the Marmara Sea and a lake on the south shore of the Marmara Sea (Lake Manyas) show that there is very close agreement between the pollen assemblages in the fresh water and marine environment of the small, almost land-locked Marmara Sea (Cordova et al., 2009).

1.4 Human Impact

Noah's flood was said to last for 40 days and 40 nights, and may have wiped out all Neolithic communities farming on the shelves of the Black Sea (Ryan and Pitman, 1999; Turney and Brown, 2007). Some scientists think that the Black Sea was a freshwater lake allowing Neolithic populations to develop agriculture in the region until ~9,400 – 7,500 yr BP (~10,200 – 7,950 cal. yr BP) when the Bosphorus sill was breached by marine water from the Mediterranean Sea (Turney and Brown, 2007). The suggested demise of these farming communities because of the rapid sea level rise may have resulted in a cultural change among the populations and a hypothetical mass migration into Europe.

Pollen records can provide excellent insight into the activity of humans, and deep water Marmara and Black Sea pollen records show no sign of large-scale deforestation or sustained agriculture before ~4,000 yr BP (~3,990 cal. yr BP; Mudie et al., 2002b; 2004). This is also evident from other cores within the Black and Marmara Seas as well as deltas of southwestern Ukraine that only show the presence of cereals, walnuts, and olives being cultivated after 3,000 – 4,000 yr BP (Mudie et al., 2007). However, there are scattered large early Neolithic settlements recorded for the eastern Marmara Sea shores, and more work is required in the southeastern region (Caner and Algan, 2002; Algan et al., 2009; Özdoğan, 2011), especially the shelf area closer to the coastline than the deep basins. Previously described hypotheses by Turney and Brown (2007) are based on

circumstantial evidence and limited archeological data, with little to no marine archeological evidence partly because of the difficulty of underwater archeological excavations at modern water depths of >30 – 100 m and possibly because of absence of arable soils (Mudie et al., 2002b; 2007). It is unlikely that the technology of irrigation agriculture would have been used by these Neolithic people and would have been difficult to manage due to high salt content within the clay soils and the dry climate that is required for lake drawdown in the catastrophic reconnection hypothesis (Mudie et al., 2004).

The presence/absence, and abundance of particular palynomorphs will provide indicators to the vegetation history and potentially improve current knowledge of the appearance and habits of Neolithic communities through the palynological record that is truncated in most regional lakes.

1.5 Research Questions

The most important aspects of this thesis are to produce the following new insights to the Late Pleistocene history of the Marmara Sea Gateway:

1. Pollen-spore diagrams will show changes in vegetation and climate over the past 30,000 cal. yr BP at site MAR02-89P, and may contain records of human occupation in the Marmara region as indicated by agricultural, and cleared-land weed pollen records.

2. The pollen study will provide insight to how the forest flora of the Late Pleistocene and early Holocene evolved in the southeastern Marmara Sea region during part of the late Pleniglacial (30,000 – 21,000 cal. yr BP) and the last glacial maximum (21,000 – 18,000 cal. yr BP). The presence/absence, abundance and influxes of particular palynomorphs in the marine sediments will provide indicators of tree migrations and potentially improve current knowledge of the palynological record that is truncated in most regional lakes.
3. Study of MAR02-89P core will allow comparison of pollen deposition during the Late Pleistocene when glaciation restricted fresh water inflow and allowed deposition of predominately local palynomorphs versus the glacial meltwater phase from ~16,000 – 12,000 yr BP (~18,700 – 13,400 cal. yr BP) when flooding from Black Sea rivers was intense.
4. The presence of a long section of Late Pleistocene glacial and early postglacial sediments within Core MAR02-89P will provide a more refined interpretation of the pre-Holocene palynomorphs within the eastern Marmara Sea region than has previously been possible, and will allow for comparison with time-equivalent palynostratigraphies previously reported for the western Marmara Sea by Caner and Algan (2002) and Mudie et al. (2002; 2007) for pollen, by Londeix et al., (2009) and by Mudie et al. (2004) for dinoflagellate cysts, and by Vidal et al., (2010) and Menot and Bard (2010), using geochemical proxies for the abundance of dinoflagellates.

5. A dinoflagellate cyst diagram for MAR02-89P will show how the oceanography (surface water salinity and primary production) changed over this time, as the sea level changed and as the northern glaciers melted and flooded the Black Sea.
6. A conceptual model/cartoon of how water levels changed in the Marmara Sea for the past 30,000 to ~8,000 cal. yr BP, using the results from the new core MAR02-89P supplemented by published Marmara Sea core data to show reconnection of the Mediterranean and Black Seas.

Materials & Methods

2.1 Field Survey Methods

2.1.1 Seismic Profiling

The MAR02-89P and MAR02-88P core sites were selected and occupied in 2002 based on seismic profiles that were taken on a research cruise of the R/V *Koca Piri Reis* of the Institute of Marine Sciences and Technology, Dokuz Eylül University in 1995 (Figure 2.1). During the 1995 cruise, approximately 2,500 km of seismic reflection profiles were collected using a 40-cubic-inch (655 cm^3) sleeve-gun source and two separate streamers: a 6 m-long, 21-element Nova Scotia Research Foundation Corporation streamer, and a 9 m-long, 50-element Benthos streamer. The incoming data was printed using two EPC 3200S recorders. The depth resolution of the seismic profiles is ~4 m.

2.2.2 Core Analysis

In 2002, piston cores were collected from the R/V *Koca Piri Reis* of the Institute of Marine Sciences and Technology, Dokuz Eylül University. The equipment consisted of a Benthos piston corer, with or without a trigger-weight gravity corer. Two long piston cores, MAR02-89P and MAR02-88P (Table 2.1), were taken from the upper slope of the

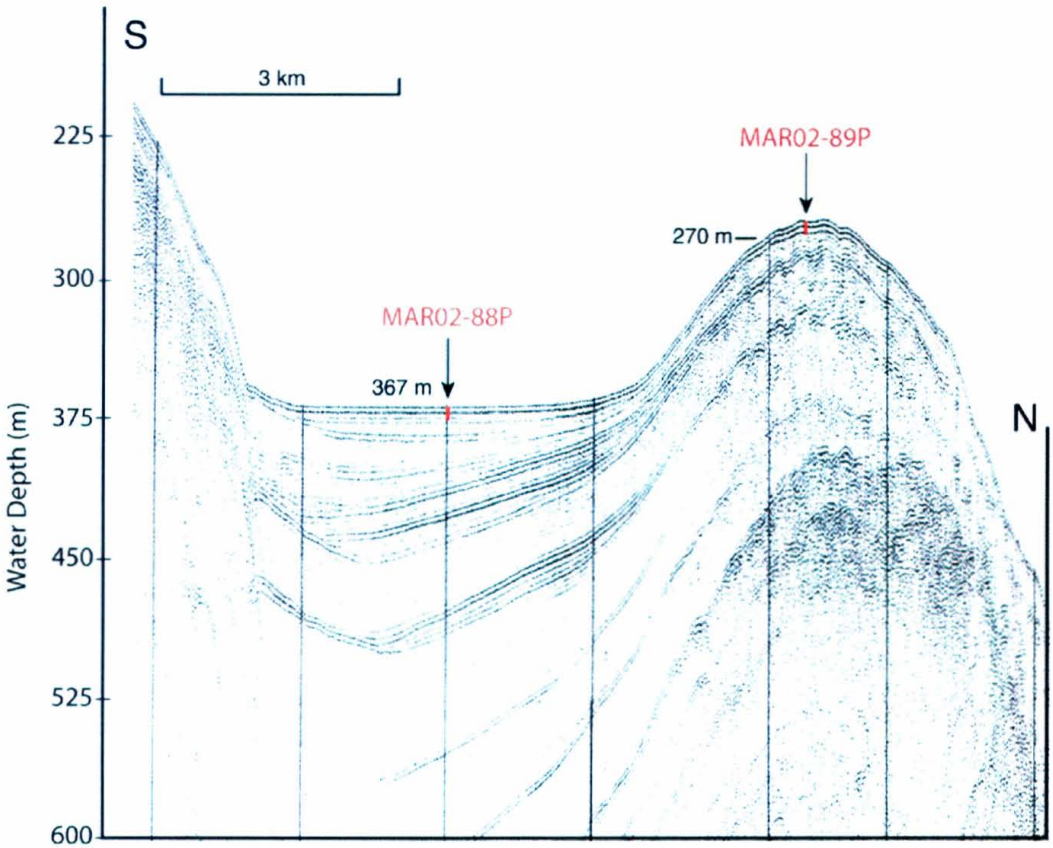

Figure 2.1: Seismic reflection profile containing MAR02-88P and MAR02-89P cores south of the Bosphorus Strait in the eastern Marmara Sea, obtained using a 40-cubic-inch sleeve-gun source, showing a perched basin.

southeastern Marmara Sea. The trigger weight corer was not available for use in this area because of an earlier accident and core MAR02-89P did not recover much of the soft uppermost Holocene sediment.

Table 2.1. Core length, latitude, longitude, and water depth of MAR02-89P and other cores discussed in this study and used for cross-correlation and shown in Figure 3.2.

Core #	Length (cm)	Latitude	Longitude	Water Depth (m)
MAR97-11P	235	40°39.20'N	28°22.67'E	111
MAR98-12P	215	40°50.54'N	27°47.68'E	549
MAR02-88P	682	40°37.99'N	28°50.85'E	367
MAR02-89P	813	40°40.30'N	28°51.39'E	257
MD01-2430	750	40°47.81'N	27°43.51'E	580
DM13	300	~40°45.00'N	~27°48.00'E	710
KL97	540	~40°50.00'N	~28°46.00'E	1,094
MAR94-05P	1008	40°52.26'N	28°06.31'E	850
MD04-2750	1300	40°56.70'N	28°56.15'E	68

The piston cores were kept in a refrigerator and shipped upright to Memorial University of Newfoundland (MUN), where they were split and stored in a refrigerator at 4°C. In 2010, the split cores were run through a GeoTek Multisensor Track (MST) to determine magnetic susceptibility (MS), density, and P-wave velocity, and they were photographed. Sampling for core MAR02-89P geochemistry and palynology began at 800 cm; at a later date (2011) a sample from 810 cm was analyzed for total carbon (TOC), $\delta^{13}C$, total sulphur (TS), and $\delta^{34}S$ and has been included with the geochemistry data presented in this thesis.

2.2 Laboratory Analytical Procedures

2.2.1 Core Analysis and Age Model

Core MAR02-89P was split and described by Dr. Richard Hiscott in July of 2003 and was visually evaluated for colour (Geological Society of America Rock Color Chart), texture, and sedimentary structures. Eight shell samples were extracted from the core at various depths and were sent to either Université Laval or University of Toronto, Canada for radiocarbon dating. The chronology of core MAR02-89P was determined from the eight known core ages together with a known age of ~21,780 cal. yr BP for the Santorini Y2 ash layer (Aksu et al., 2008), and an extrapolated date of ~12,535 cal. yr BP from core MAR98-12P for the base of the Marmara Sea M1 sapropel layer (Aksu et al., 2002a). The calibrated ages for these samples were obtained using internet-based software

OxCal09 with a marine reservoir value of zero years for all samples. The sedimentation rates (cm/ka) were determined using all of the known calibrated ages and the assumption of constant sedimentation rates between the dated levels.

A zero reservoir age was used because appropriate reservoir ages for the MAR02-89P site in 257 m of water are not known, although they are likely greater than 400 – 500 years. The modern shallow-water reservoir age of ~415 years (Siani et al., 2000) is likely too low a value for the deeper waters of the Holocene Marmara Sea because reservoir ages tend to increase with water depth in modern seas and oceans (Stuiver and Braziunas, 1993). Before its reconnection to the world ocean at ~12,000 uncalibrated radiocarbon years, the Marmara Sea was an isolated lake for which the Pleistocene reservoir value(s) are presently unknown. It is for this reason that authors like Londeix et al. (2009) and Eriş et al. (2007) have not made reservoir corrections to their uncalibrated radiocarbon dates in the Marmara Sea. Because a zero value for the reservoir age is used in this thesis (by setting ΔR to -405 years in the Oxcal calibration set-up), the reader should be aware that the true ages of events described in this thesis on the basis of radiocarbon dating might be ~500 years less for Holocene times and a yet unconstrained number of years less for late Pleistocene times.

2.2.2 Age-Depth Conversion

The multiproxy data collected in core MAR02-89P were transformed from the depth domain to age domain (calibrated calendar years BP) using two programs: Ager

and Timer. These programs are part of an Arand software package developed by CLIMAP at Brown University, United States of America (http://www.ncdc.noaa.gov/paleo/softlib/arand/arand.html). The Ager program determines sedimentation rates for each of the dated intervals and uses linear interpolation to assign an age to each measurement point of the time series. The Timer program generates a time series using the output of the Ager program to create equal time increments defined by the user (200 years for this study).

2.3 Sample Preparation

2.3.1 Elemental and Isotopic Measurements

The MAR02-89P core was sampled at 10 cm intervals and samples of approximately 20 cm^3 of sediment were collected for geochemical work (Appendix I). Each 20 cm^3 sample was analyzed by Dr. Ali Aksu, for total organic carbon (TOC), total sulphur (TS), sulphur ($\delta^{34}S$) isotopic composition and the stable carbon ($\delta^{13}C$) and isotopic composition of bulk organic matter. All but the $\delta^{34}S$ data are used in this thesis to support or augment arguments for environmental changes through the Late Pleistocene and early Holocene. The sulphur isotopic data are plotted but not discussed because the dynamics of isotopic fractionation in lakes and during early diagenesis are complex (Jørgensen and Kasten, 2006; Thode, 1991) and beyond the scope of this thesis.

2.3.2 Isotope Ratio Mass Spectrometry - IRMS

Isotope ratio mass spectrometry is used to measure the relative abundance of stable isotopes in a given sample. In this study, the ratios of $^{13}C/^{12}C$ and $^{34}S/^{32}S$ were measured on a Finnigan MAT 252 isotope ratio mass spectrometry system at Memorial University of Newfoundland.

Samples were dried in a fume hood at room temperature for a few days. Dried samples were homogenized with a mortar and pestle, and then 5 g of sample was weighed into a plastic tube and 5 ml of water was added and then treated with acid (20 ml of 30% HCl) to remove carbonates. The acidified samples remained overnight in the fumehood, then they were centrifuged, washed with distilled water until neutral, and dried overnight at ~40°C. The samples were again homogenized and about 15 mg was weighed and sealed along with ~0.2 mg of vanadium pentoxide in 4x6 mm tin sample capsules for isotope ratio mass spectrometry analysis (Abrajano et al., 2002; Hiscott at al., 2007b).

2.3.3 Elemental and Bulk Isotopic Analyses

The Memorial University of Newfoundland system combines an isotope ratio mass spectrometer (Finnigan MAT 252) with a Carlo Erba CNS elemental analyzer (NA 1500) using an automated on-line dry combustion method to measure the total organic carbon

(TOC), total sulphur (TS), $\delta^{13}C$ and $\delta^{34}S$ (Abrajano et al., 2002; and Hiscott at al., 2007b).

Total sulfur and total organic carbon in the samples were converted to SO_2, CO_2, H_2O and other oxidized gases in the oxidation chamber and then passed through a reduction reagent, a $Mg(ClO_4)_2$ water trap and a 1.2 m Poropak QS 50/80 chromatographic column at 70°C for final isolation. TS and TOC quantification from measurement of generated SO_2 and CO_2 was accomplished using an external standard (sulphanilamide, $C_6H_8N_2O_2S$) and a thermal conductivity detector (TCD). The TS and TOC concentrations in the samples were back-calculated as a percentage of dry-weight sediment. From the thermal conductivity detector, the SO_2 and CO_2 were carried by He to a ConFloII interface, allowing a portion of the He and combustion gases to enter directly into the ion source of the IRMS for sulfur and carbon isotopic measurement. All isotopic analyses are reported in standard δ notation referenced to the standards Vienna-Canyon Diablo Troilite (V-CDT) and Pee Dee Belemnite (PDB) for sulfur and carbon, respectively.

2.3.4 TOC and $\delta^{13}C$ Analysis

Total organic carbon is the total amount of carbon derived from dissolved and particulate organic sources, but does not include the carbon incorporated into the shells of foraminifera, mollusks and other calcareous organisms. In the study area, TOC can be

used to identify sapropels (defined as a discrete bed >1 cm thick, with greater than 2.0% TOC by weight) and sapropelic mud layers (characterized by 0.5 – 2.0% TOC by weight; Kidd et al., 1978; Faure, 1986; Aksu et al., 2002b). Carbon isotopes (light ^{12}C and heavy ^{13}C) are fractionated by natural processes, such as photosynthesis and isotope exchange reactions among carbon compounds. For photosynthesis, phytoplankton selectively use the lighter isotope ^{12}C in preference to the heavier isotope, and more negative (lighter) $\delta^{13}C$ values are an index of high primary (plant) production. The standard notation is:

$$\delta^{13}C = \frac{(^{13}C/^{12}C_{sample} - ^{13}C/^{12}C_{PDB})}{^{13}C/^{12}C_{PDB}} \times 1000$$

Most land plants that use only atmospheric carbon and no marine carbon have highly depleted $\delta^{13}C$ values of ~-24‰ to -30‰. Marine carbonates are generally enriched in ^{13}C, while organic matter in marine plants and in plant-eating animals is enriched in ^{12}C (Faure, 1986). Heavier (less negative) $\delta^{13}C$ values are more typical of marine environments where the food chains are more complex than in fresh water. Marine mollusk shells have $\delta^{13}C$ values around zero.

2.3.5 TS Analysis

Sulphur is present in the lithosphere, biosphere, hydrosphere, and atmosphere and occurs as sulphate in the oceans and lakes. The isotopes of sulphur are fractionated during the reduction of sulphate to sulphide by anaerobic bacteria, which produces H_2S

and reacts with iron in the sediments to form metastable monosulphide minerals and eventually pyrite (Faure, 1986). Percentage (by weight) of total sulphur in a sediment sample can be used as a proxy for pyrite in marine sediments and sulphate reduction (Faure, 1986). Changes in sulphur isotopes are determined relative to the iron meterorite standard Vienna-Canyon Diablo Troilite (V-CDT) as follows:

$$\delta^{34}S = \frac{(^{34}S/^{32}S_{sample} - {}^{34}S/^{32}S_{V\text{-}CDT}) \times 1000}{{}^{34}S/^{32}S_{V\text{-}CDT}}$$

The sulphate in present-day Mediterranean water is enriched in $\delta^{34}S$, with a value of about +20‰ (Aksu et al., 1999a), in contrast to values of about +5‰ for well-mixed Canadian fresh water lakes (Eimers et al., 2006). In surface sediments at a water depth of 69 m just above the sulphide zone in the Black Sea, the sulphur isotopic values associated with early diagenetic sulphide minerals are around -20‰ (Hiscott et al., 2007b; Murray et al., 2007). In the study area, a decrease in the ratio of heavier ^{34}S to lighter ^{32}S (i.e. more negative $\delta^{34}S$ values) likely indicates the reduction of sulphate by anaerobes, a process which promotes dysoxia in bottom water because organic matter and free oxygen are also consumed. Water-column stratification accentuates the bottom-water dysoxia and the rate of sulphate reduction, as took place in the Marmara Sea following the establishment of two-way flow across the Bosphorus Strait (Hiscott et al., 2007b). Watanabe et al. (2003) demonstrated that in the deep waters of Lake Baikal TS values of less than 1% represent oxic conditions while typical freshwater sediment TS/TOC ratio values are 0.003-0.187. The ratio of total sulphur to total organic carbon (TS/TOC) may act as a

paleo-redox proxy due to production of excess sulphur in euxinic conditions (Watanabe et al., 2003).

2.4 Palynology Sample Preparation

The MAR02-89P core was sampled at 10 cm intervals and 2 – 5 cm^3 volume of sediment was used for palynomorph extraction. Extraction of organic palynomorph residues from sediment was done by Helen Gillispie, using slight modification of standard methods for Quaternary marine sediments (Rochon et al., 1999). Samples were wetted with distilled water and then sieved at 10 μm mesh size. The sediment residue >10 μm was then digested in cold 15% hydrochloric acid (HCl) to remove carbonates, and exotic spores (*Lycopodium* sp.), totaling 55,749 ± 764 spores per 3 tablets (batch number 483216), were added to each sample to obtain estimates of the number of palynomorphs per gram (concentration). After removal of HCl by repeated washing and centrifuging the samples were digested in 52% hydrofluoric acid (HF) for 24 – 48 hours at room temperature to remove silicates. After washing, any residual minerals were swirled off and the residues were mounted on slides with glycerine gelatine.

Palynological analysis was done on each processed slide (or two slides if required). Palynomorphs were routinely counted at x160 – 250 magnification, using a Zeiss Photomicroscope III (Phomi III) configured for transmitted light with interference contrast, until a minimum of 300 exotic spores was reached whenever possible. Detailed

taxonomic identification was made at a magnification of x400 and specimens were photographed using an Infinity1 microscope camera.

2.4.1 Palynomorph Identification

Various references were used to aide in determining the pollen and dinoflagellate cysts that were found in core MAR02-89P. The second edition of Pollen Analysis (Moore et al., 1991), along with How to Know Pollen and Spores (Kapp, 1969) were two useful sources for determining pollen palynomorphs. Dinoflagellate cyst indentification sources were focused towards modern North Hemisphere cysts using the monograph of Rochon et al. (1999), photoplates from published works within the Marmara and Black Sea region (Londeix et al., 2009; Mudie et al., 2001, 2004), and teaching posters of Dr. Fabienne Marret at the University of Liverpool, UK. The taxonomy and nomenclature of the dinocysts taxa is based on Fensome et al. (1990), Fensome and Williams (2004), and Marret et al. (2004). Recognition of the non-pollen palynomorphs was done using Kapp (1969), photoplates from Londeix et al. (2009) and Mudie et al. (2011), and identifications of Dr. Petra Mudie. A list of all the taxa is given in Appendix II. Reworked pre-Quaternary cysts were recognized from the morphological characteristics and/or yellow to brown or black colour.

2.4.2 Palynological Diagrams and Statistical Analyses

Palynological diagrams for this study were plotted using the software Psimpoll 4.27 (Bennett, 2007; Leroy et al., 2010). All pollen taxa (Appendix III) were totaled together in the percentage diagram to add up to 100%; however, only the most abundant and key indicator species are represented in the graphs. The same procedure was used for the dinoflagellate cysts (Appendix IV). Non-pollen palynomorphs that were recognized within the MAR02-89P core are shown as abundance/g, as estimated from the exotic spore count and sample sediment weight.

Zonation was determined using Psimpoll 4.27 (Bennett, 2007; Leroy et al., 2010). This program uses CONISS (Constrained Incremental Sums of Squares cluster analysis) after square-root transformation, and was made based on the taxa assigned to the categories "abundant" and "key indicator species" of pollen and dinoflagellate cysts. CONISS statistical cluster analysis allows for the division of palynomorphs into assemblage zones, which helps with the descriptions and correlations of microfossil data.

Pollen and dinocyst concentrations represent estimates of the number of these palynomorphs per gram weight of sediment, as determined from the known number of exotic *Lycopodium* spores added to each sample during laboratory processing (Traverse, 1988). The concentrations were calculated by multiplying the number of pollen grains or number of dinocysts counted on a slide by the number of *Lycopodium* spores (mean = 55,749) added to the sample, then dividing by the number of *Lycopodium* counted for the

slide, followed by division by weight of the sample:

Concentration of pollen or dinocysts/g =

(pollen or dinocysts counted x number of exotic spores added) / sample dry weight

number of added lycopodium counted

As explained by Traverse (1988), pollen and dinocyst influxes per cm^2 per year were determined by dividing the pollen or dinocysts per gram (1 gram ~ =$1cm^3$) and dividing by the years for vertical deposition of 1cm of sediment, as estimated from sedimentation rates that were calculated for MAR02-89P:

Pollen or dinocyst influx/cm^2/yr = number of pollen or cysts per cm^3

Number of years for deposition of 1cm (vertical) of sediment

Results

3.1 Age Model

Although the piston core MAR02-89P initially appeared to have a continuous sequence of glacial stage to lower Holocene (sapropel M1) sediments, the radiocarbon ages obtained from eight Accelerator Mass Spectrometry ages on shell samples revealed that there is a hiatus at a core depth of ~250 cm. The core description noted a sharp lithologic change and shell concentration at this depth. All figures displaying the results of sedimentological, geochemical and palynological analyses are shown in both depth and time domains. The depth domain diagrams show the down-core sample intervals together with the observed position of the Y2 ash layer and the location of the unconformity (Figure 3.1).

The data in time domain plots have been transformed using the Ager and Timer programs, assuming constant sedimentation between each 200 year age increment interval within the known age measurements, and can become less detailed due to averaging or interpolations between adjacent primary data values. The age domain diagrams also show significant climatic, oceanographic and volcanic events known from the region or from other parts of the Northern Hemisphere. These time intervals are used to compare data throughout the thesis and with other published palynological data (Mudie et al., 2002a,b; Caner and Algan, 2002; Londeix et al., 2009; Vidal et al., 2010), and are consistent with the Greenland ice core-calibrated time-scale of Fletcher and Sánchez

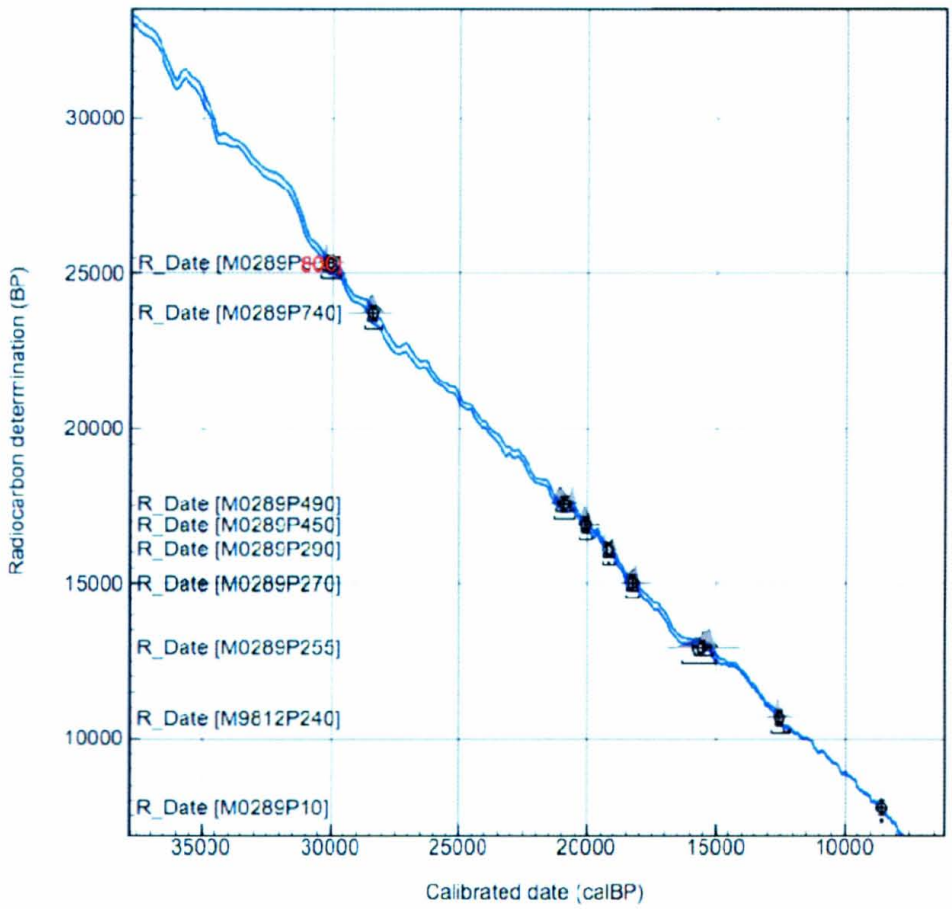

Figure 3.1: Radiocarbon determined ages (BP) vs. calibrated ages (cal. yr BP) of core MAR02-89P from OxCal Marine 09 program, marine reservoir value of zero years. The last data R_Date [M0289P800] is partially highlighted in red because the label is obstructed by the graph.

Goñi (2008). Known time events used are: the Younger Dryas (12,800 – 11,500 cal. yr BP), Bølling-Allerød (15,000 – 13,000 cal. yr BP), Heinrich stadial intervals (HS1 and HS2 at 18,000 – 15,600 cal. yr BP and 26,500 – 24,400 cal. yr BP, respectively), the Y2 ash layer (21,780 cal. yr BP), the end of the last glacial maximum (23,500 – 19,000 cal. yr BP), and Marine Isotope Stage boundaries MIS 3/2 (27,800 cal. yr BP) and MIS 2/1 (14,700 cal. yr BP). Obbink et al. (2010) have suggested a revised age for the Bølling-Allerød (~14,650 – 12,900 cal. yr BP), which may explain why there are no major changes in palynomorphs during this time interval, which is represented by 1 sample (250 cm) in core MAR02-89P. Core MAR02-89P represents a large section of upper Pleistocene and lower Holocene sediments (dated ~30,000 – 8,000 cal. yr BP); however, the most recent sediments were not collected in this piston core because of core-top loss.

Table 3.1 shows the eight ^{14}C AMS dates that were determined for core MAR02-89P, and two ^{14}C AMS dates for core MAR02-88P and their respective calibrated ages using Oxcal Marine 09 software. There are no shells present in MAR02-89P to constrain the age of the base of the M1 sapropel and the top of the assumed hiatus; therefore, a known date for the assumed base of the M1 sapropel was extrapolated from Aksu et al. (2002a). This age was reported as 10,660 ± 130 yrBP and was calibrated by Aksu et al. (2002a) to be ~11,850 cal. yr BP. Londeix et al. (2009) also used this date to represent the base of the M1 sapropel in core MD01-2430 and those authors calibrated the date to ~12,003 cal. yr BP. For this study, the ^{14}C AMS date of the *Nuculacea* spp. was calibrated using the same reservoir age as was used for the ^{14}C AMS dates for MAR02-

89P and MAR02-88P shown in Table 3.1 and was determined to have an age of ~12,535 cal. yr BP, which will be used for this thesis.

Table 3.1. Accelerator Mass Spectrometry (AMS) radiocarbon ages for Core MAR02-89P, reported as uncalibrated conventional ^{14}C ages and calibrated Oxcal Marine09 dates (cal. yr BP) using a marine reservoir correction of zero years. Dating was done by ULA (Radiocarbon Dating Laboratory, Université Laval) and TO (IsoTrace Radiocarbon Laboratory, Accelerator Mass Spectrometry Facility, University of Toronto). Errors are one standard deviation.

Core # and Depth (cm)	Dated Material	^{14}C age (yrBP)	cal. yr BP (Oxcal Marine09)	Sample #
MAR02-89P 10	Bivalve fragments	7,775 ± 15	8,663 ± 48	ULA -173 6
MAR02-89P 255	Bivalve fragments	12,920 ± 110	15,567 ± 348	TO-11147
MAR02-89P 270	*Dreissena polymorpha*	15,005 ± 30	18,258 ± 153	ULA-173 7
MAR02-89P 290	*Dreissena polymorpha*	16,085 ±30	19,207 ± 153	ULA-173 8
MAR02-89P 450	*Dreissena polymorpha*	16,895 ± 35	20,079 ± 137	ULA-173 9
MAR02-89P 490	*Dreissena polymorpha*	17,570 ± 35	20,914 ± 233	ULA-174 0
MAR02-89P 740	*Dreissena polymorpha*	23,690 ± 70	28,412 ± 169	ULA-174 1
MAR02-89P 800	*Dreissena polymorpha*	25,320 ± 90	30,091 ± 229	ULA-174 2
MAR02-88P 43	*Dreissena polymorpha*	1,065 ± 15	1,011 ± 33	ULA-174 3
MAR02-88P 663	*Dreissena polymorpha*	5,935 ± 15	6,804 ± 38	ULA-174 4

Tie points for the Ager and Timer programs were selected based on known ages from the core (shell radiocarbon data, ash layer) and three extrapolated dates indicated in Table 3.2. The Y2 ash layer occurs between 563 and 568 cm in the core. This volcanic eruption and the associated ash deposition are considered geologically instantaneous events; therefore, only one additional year was assumed to elapse for the deposition of the 5 cm-thick ash layer in the core. Two additional points were determined using linear extrapolation to better constrain the hiatus; i.e., the jump between the inferred age for the base of M1 and the radiocarbon date at 255 cm. This calculation was done (a) using the known ages from 10 and 240 cm to extrapolate down to the unconformity determined from core description to lie at 249 cm, and (b) using the calculated sedimentation rate for shell ages at 255 and 270 cm to extrapolate up to the unconformity at 251 cm. Based on these calculated values, the hiatus spans approximately 14,849 to 12,686 cal. yr BP, and given the sharp lithologic break in the core is probably associated with an erosional event.

Table 3.2. Tie-points used for Age-Depth conversion for core MAR02-89P. The 240 cm depth tie-point is an extrapolated age imported from core MAR98-12P. * = extrapolated points used to better define the hiatus determined by linear extrapolation, $ = interpolated age for the top of the Santorini ash.

Depth (cm)	10	240	249*	251*	255	270	290	450	490	563[5]	568	740	800
Cal. yr BP	8663	12535	12686	14849	15567	18258	19207	20079	20914	21781	21780	28412	30091

3.2 Core Location and Bottom Topography

Core MAR02-89P was collected from the edge of a perched basin on the upper continental slope of the southeastern Marmara Sea (Figure 2.1). The bathymetric map (Figure 3.2) also shows the locations of other cores MAR98-12P and MAR97-11P (Table 2.1), which have been previously described by Aksu et al. (2002b) and were used for late Pleistocene – Holocene palynological studies by Mudie et al. (2002a,b), Mudie et al. (2004), Mudie et al. (2007). The deep-water core MAR98-12P has a radiocarbon date (on the mollusk *Nuculacea* spp.) at the base of the Marmara Sea M1 sapropel layer with an age of ~12,535 cal. yr BP; this age was also used by Londeix et al. (2009) to date the base of the sapropel in their deep water core (MD01-2430). The shelf core MAR97-11P (-111 m water depth; Table 2.1) has four ages from ~12,240 cal. yr BP to ~18,540 cal. yr BP that overlap those of MAR02-89P and were used to help interpret the hiatus in MAR02-89P.

The core MAR02-88P (Figure 3.2) was collected on the floor of the upper-slope perched basin about 3 km south of the location of MAR02-89P. MAR02-88P comprises 682 cm of Holocene sediments, and two shell ages show that it includes the part of sapropel M1 younger than ~6,804 cal. yr BP and a younger sapropelic mud layer that is missing from MAR02-89P. The sample from the top of MAR02-88P contains *Ambrosia* weed pollen and provides a reference for modern assemblages (see Plate I). Although

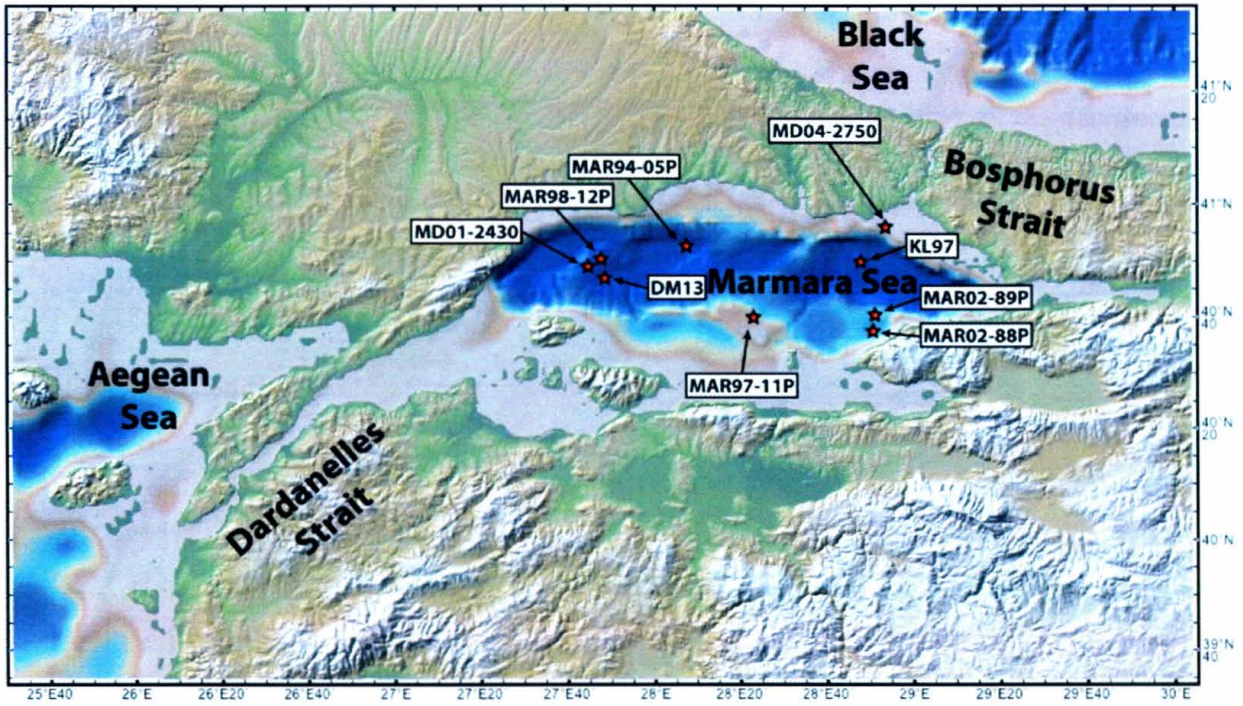

Figure 3.2: Global Multi-Resolution Topography (GMRT) map of the Aegean, Marmara, and Black Seas; brown shading marks approximate water depths of 100 m; darkest blue shading marks basin depths greater than 1000 m, and red stars mark core locations discussed in this study (www.geomapapp.org)

beyond the scope of this thesis, it should eventually be possible to splice data from both core sites to create an almost complete picture of sedimentation in the Marmara Sea for the past ~30,000 years.

3.3 MAR02-89P Lithology

Figure 3.3 shows the lithology of core MAR02-89P and indicates the depths of shells extracted for radiocarbon dating. Three sedimentary units are present, all consisting of silty muds. Unit 3 (from 810 – 249 cm) comprises mildly bioturbated silty muds with shell fragments throughout; it has an age of ~30,091 – 14,850 cal. yr BP. The colour is primarily olive gray, but there is almost a meter of greenish gray silt at the base. The Y2 ash layer occurs within Unit 3: here the sediment colour changes from dark greenish/olive gray to a dark to pale yellowish brown. There is also a small amount of lamination at 410 cm (~19,800 cal. yr BP), and a dark gray band at ~450 cm (~20,000 cal. yr BP). The colour changes to grayish green just below the top of the unit, which is capped by a shelly horizon.

Units 3 and 2 are separated by a ~2,160 year hiatus in sedimentation from ~14,850 – 12,700 cal. yr BP at a depth of ~250 cm (Figure 3.3). This hiatus is contemporaneous with most of the Bølling/Allerød event (~15,000 – 13,000 cal. yr BP, as per the age-model of Fletcher and Sánchez- Goñi, 2008) and the beginning of the Younger Dryas at

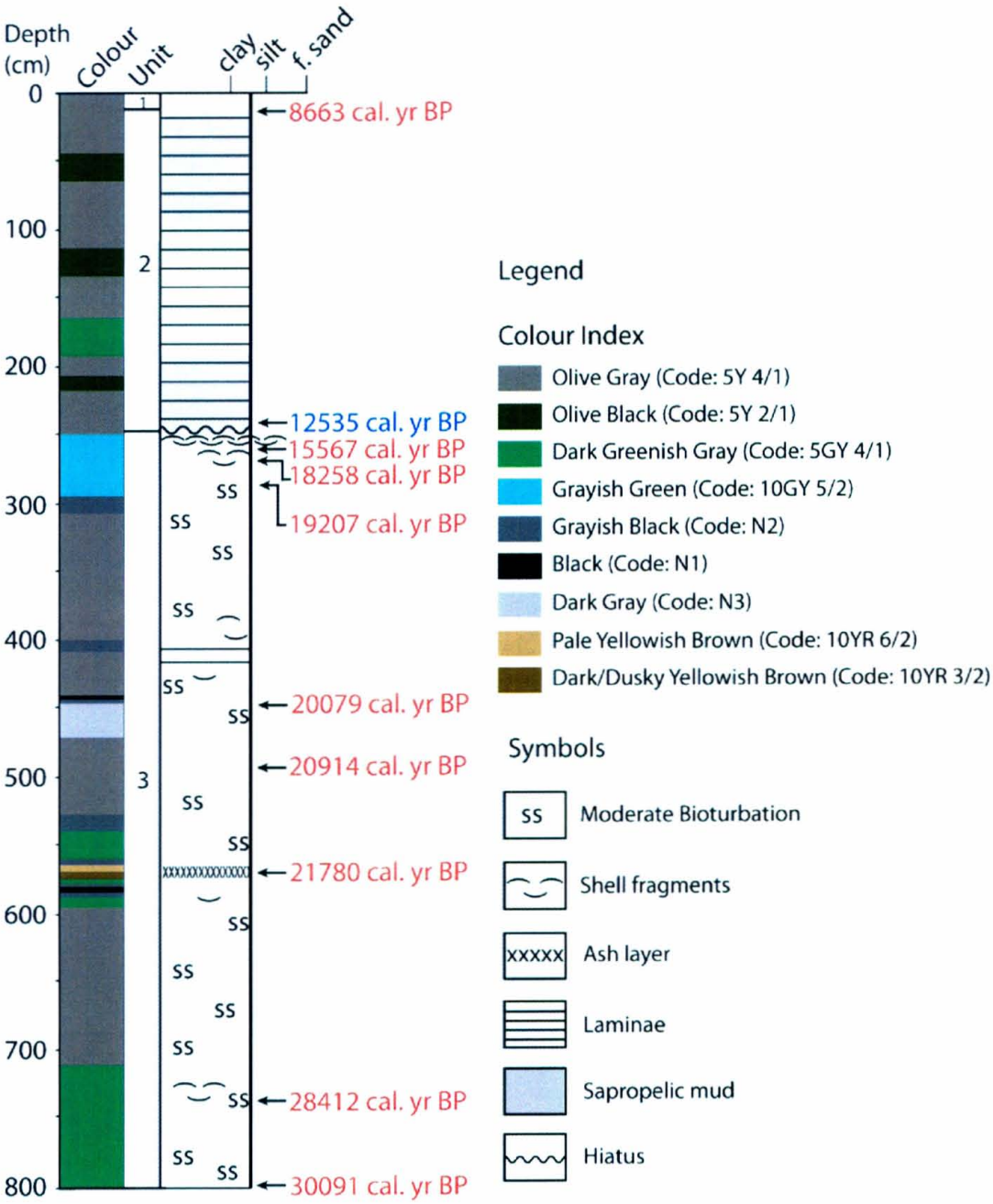

Figure 3.3: Summary lithostratigraphy of core MAR02-89P. Also shown are calibrated radiocarbon dates (red) listed in Table 3.1. One of the dates (12,535 cal. yr BP, blue) is imported from core MAR98-12P as an age for the base of the sapropel.

~12,800 cal. yr BP. Unit 2 (249 – 23 cm) with an age of ~12,686 – 8,874 cal. yr BP, is laminated silty mud throughout, except for a 1 cm-thick shell lag at the base. There are two sapropel layers: one at the base from ~249 – 190 cm (12,686 – 11,700 cal. yr BP) and one at the top, from 100 – 23 cm (10,000 to 8,600 cal. yr BP) separated by sapropelic silty mud. The colour of Unit 2 is generally olive gray with some bands of olive black and dark greenish gray within or between the sapropel layers (Figure 3.3). The base of the lowest sapropel of Unit 2, 1 cm above the hiatus is assumed to be the base of the Marmara Sea M1 sapropel. No date could be obtained from MAR02-89P for the base of Unit 2, so a previously determined Accelerator Mass Spectrometry age (Aksu et al., 2002b) for *Nuculacea* shells at the base of M1 in core MAR98-12P (Figure 3.2) was used. This extrapolated date of ~12,535 cal. yr BP from MAR98-12P is believed to represent the base of the M1 sapropel and has been used for other published core data in the Marmara Sea region (Londeix et al., 2009).

Unit 1 in MAR02-89P is very thin, extending from 23 cm to 0 cm. It has an estimated age of ~8,874 – 8,000 cal. yr BP and shows a change in lithology from the laminated silty muds of Unit 2 to non-laminated silty mud (Figure 3.3). Unit 1 is strongly bioturbated olive-gray mud with echinoderm shell fragments and spines, and a few small mollusk shell fragments. An Accelerator Mass Spectrometry age of 8,663 cal. yr BP from echinoderm shell fragments at 10 cm depth, the high organic content (Section 3.5) and olive-gray colour are not the expected characteristics of the youngest brownish, more oxidized sediments of Unit 1B (Aksu et al., 2002b) seen elsewhere in the Marmara Sea. It

is therefore concluded that Unit 1B is missing from the core because of incomplete recovery of the uppermost deposits. This youngest unit is present at the top of adjacent core MAR02-88P where it has an Accelerator Mass Spectrometry age of ~1,011 cal. yr BP for echinoderm shell at 43 cm depth.

Figure 3.4 shows the sedimentation rates of MAR02-89P which vary from the base of the core to the unconformity: ~28 cm/ka from 800 – 750 cm (~30,000 – 28,700 cal. yr BP), ~30 cm/ka from 740 – 520 cm (~28,700 – 22,100 cal. yr BP) during the Heinrich HS2 stadial, ~43 cm/ka from 510 – 500 cm (~22,100 – 21,700 cal. yr BP), ~21 cm/ka from 490 – 460 cm (~21,700 – 20,300 cal. yr BP), ~5 cm/ka from 450 – 300 cm (~20,300 – 19,300 cal. yr BP), and ~47 cm/ka from 290 – 249 cm (~19,300 – 14,849 cal. yr BP) contemporaneous with the Heinrich HS1 stade in the North Atlantic Ocean.

From the unconformity to the top of the core, 249 – 0 cm (~12,700 – 8,000 cal. yr BP), sedimentation rates are ~17 cm/ka throughout the represented Younger Dryas time interval and sapropel development.

3.4 Seismic Data

The seismic profile shown in Figure 2.1 indicates the positions of cores MAR02-88P and MAR02-89P that have lengths of 682 and 813 cm, respectively. These cores are from the floor and seaward side of a perched upper-slope basin. The seismic-reflection

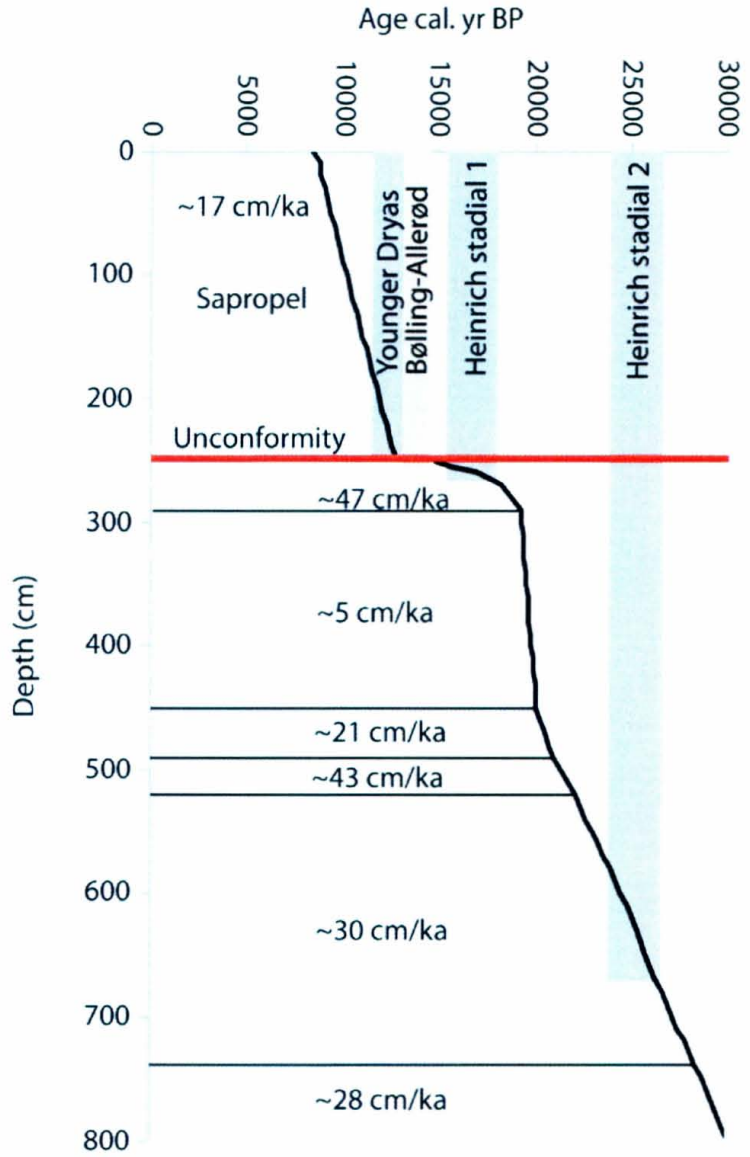

Figure 3.4: Sedimentation rates (cm/ka) of core MAR02-89P, determined using calibrated radiocarbon dates. The unconformity is highlighted with a red line at 250 cm and significant time events recognized elsewhere in the Northern Hemisphere are shown: Younger Dryas, Bølling-Allerød, Heinrich stadial events HS1 and HS2. Ages of HS events are from Fletcher and Sanchez-Goñi (2008; Table 1).

profile (Figure 2.1) shows that sediments are thicker within the basin and becomes thinner on the ridge where the reflections converge. Two Accelerator Mass Spectrometry radiocarbon ages from a *Dreissena* shell at 663 cm (~6,804 cal. yr BP) and from an echinoderm shell at 43 cm (~1,011 cal. yr BP) for core MAR02-88P (Table 3.1) show that the prominent reflector at the MAR02-88P site corresponds approximately to the top of the Holocene sapropel M1, indicating that there is an extended section of upper Holocene sediments in the deepest part of the perched basin. This thick sedimentary section pinches out as it approaches the ridge at MAR02-89P. The thinning of sediments on the ridge at the seaward edge of the basin means that this is a good site for possible recovery of a hemipelagic section with continuous sedimentation from the Late Pleistocene to Present. It is unfortunate that the loss of the gravity corer earlier in the cruise made it impossible to obtain a trigger-weight core that would have recovered the upper Holocene section at the site. Detailed inspection of the radiocarbon ages for core MAR02-89P has also revealed that Late Pleistocene sedimentation at this site was not continuous throughout the postglacial – Holocene time period and that while the pleniglacial and last glacial maximum sediments are well represented, accumulation from ~18,260 to 14,850 cal. yr BP was very condensed and terminated with a ~2,160 year hiatus.

3.5 MAR02-89P Geochemistry Data

As explained in Chapter 2, this thesis employs data for total organic carbon (TOC,

excluding carbonate carbon), total sulphur (TS) and the stable carbon isotopic signature of the organic carbon ($\delta^{13}C$). Sulphur isotopic data ($\delta^{34}S$) are plotted and can be compared with Black Sea Holocene core data of Hiscott et al. (2007b), but the MAR02-89P data are not discussed because the dynamics of isotopic fractionation in lakes and during early diagenesis are complex (Jørgensen and Kasten, 2006; Thode, 1991) and beyond the scope of this thesis. The geochemical data obtained for core MAR02-89P (Figures 3.5 and 3.6, Appendix I) show that from the base of the core to the unconformity, the TOC is relatively low (~0.5 – <1%) but it is much higher above the unconformity at ~250 cm and ranges from >1.5% – >2.5% from there to the top of the core. Above the unconformity there are two intervals that are sapropels with estimated ages of ~12,535 to 11,700 cal. yr BP and ~10,000 to 8,663 cal. yr BP.

The $\delta^{13}C$ ratios are minimal (-28‰) at the base, then remain around -26 to -26.5‰ up to ~250 cm, just below the unconformity (Figures 3.5 and 3.6). There is then a shift to slightly lighter (more negative) values of -27.5‰ from just below the unconformity to ~200 cm, followed by a gradual transition to heavier values of -25‰ between 200 cm (~12,000 cal. yr BP) and the core top at ~8,000 cal yr BP, with a conspicuous small peak in the middle of the upper sapropel. Total sulphur (TS) for the MAR02-89P core has an average value of ~0.5%, with three peaks of 1 to 2% (Figures 3.5 and 3.6). The stratigraphically lowest peak centers on the tephra layer from about 650 – 500 cm and is on average 1%. The second peak of ~1% occurs from about 450 – 400 cm. The third peak is much larger, with values initially increasing below the unconformity (300 cm,

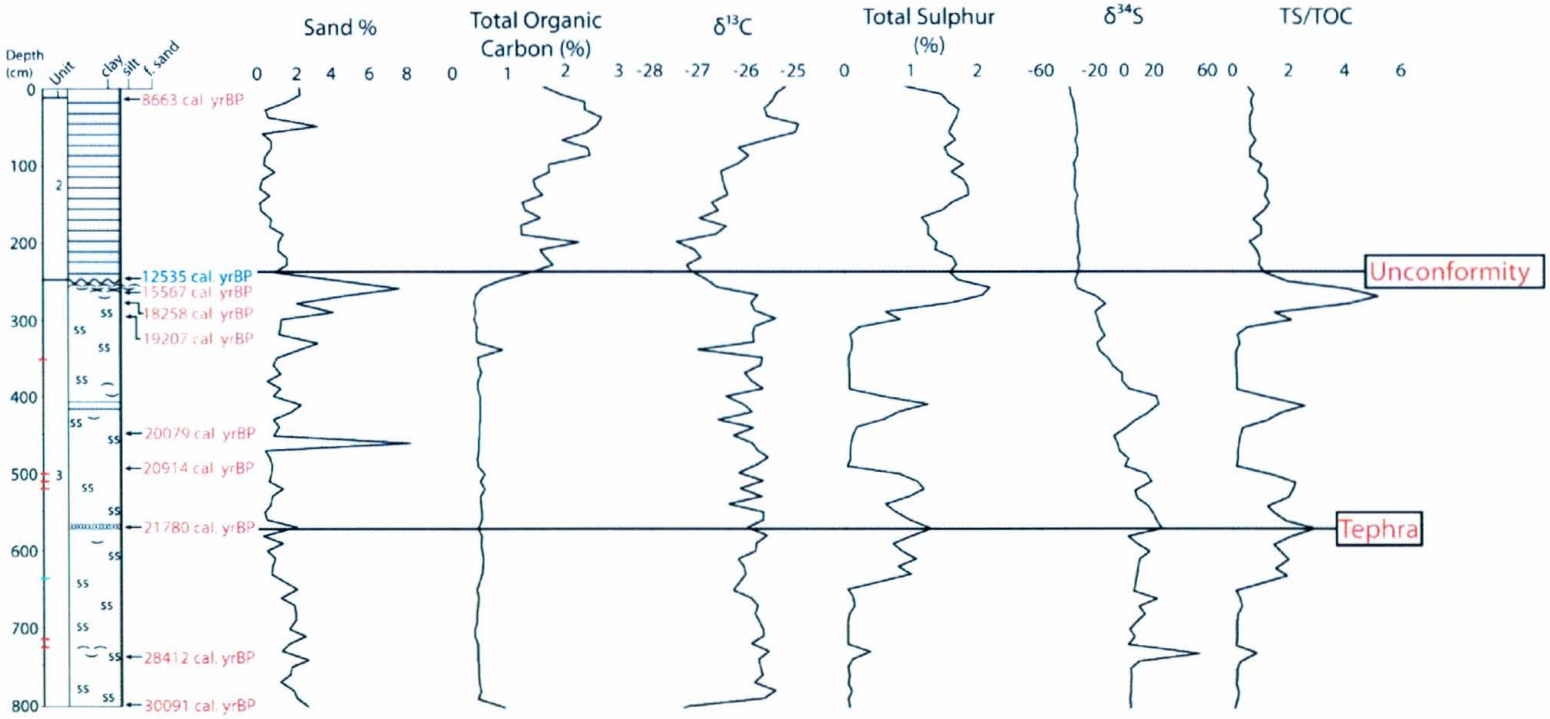

Figure 3.5: Geochemistry of core MAR02-89P in depth domain showing sand percent, total organic carbon (TOC), $\delta^{13}C$, total sulphur (TS), $\delta^{34}S$, the ratio of total sulphur to total organic carbon, calibrated radiocarbon dates (red) and core lithology. No sample was taken at 640 cm – that depth is flagged with a blue dash.

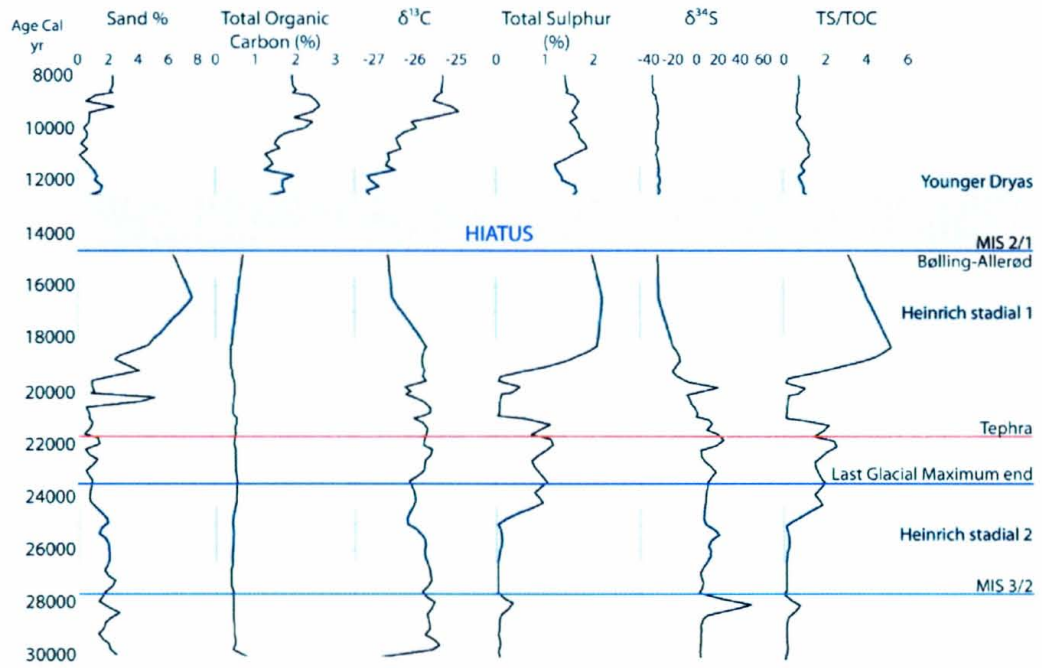

Figure 3.6: Geochemistry of core MAR02-89P in age domain showing sand percent, total organic carbon (TOC), $\delta^{13}C$, total sulphur (TS), $\delta^{34}S$, the ratio of total sulphur to total organic carbon. Significant time events recognized elsewhere in the Northern Hemisphere are shown: Younger Dryas, Bølling-Allerød, Heinrich stadial events (HS1 and HS2), the Y2 ash layer (tephra), last glacial maximum, Marine Isotope Stages (MIS 3/2 and MIS 2/1), and a hiatus (brown) indicates a break in sedimentation.

~19,000 cal. yr BP) to the top of the core, attaining the highest value of >2% just below the unconformity (~250 cm).

The ratio of total sulphur to total organic carbon shows three large peaks in core MAR02-89P. The first peak occurs from 650 – 500 cm and has an age of ~25,000 – 23,000 cal. yr BP; the second smaller peak is from 450 – 400 cm (~20,000 cal. yr BP), and the final third peak is just below the unconformity from 310 – 249 cm, with an age of ~18,000 – 14,850 cal. yr BP.

There is a smaller peak from 750 – 730 cm (~28,600 – 27,700 cal. yr BP) and a gradual decrease in TS/TOC from the unconformity to the top of the core, 250 – 0 cm (~12,700 – 8,000 cal. yr BP).

3.6 MAR02-89P Pollen Data

The full set of pollen data for MAR02-89P is shown in Appendix III and the concentrations, total pollen influxes and percentages of selected pollen taxa are shown in Figures 3.7 and 3.8. There are three almost barren zones in core MAR02-89P: from 730 – 720 cm, 520 – 500 cm, and 350 cm. The limited counts that came from these slides were excluded from the data. Also, there are no data at the 640 cm level because there was no sediment sample collected from that depth. Variable amount of reworked grains

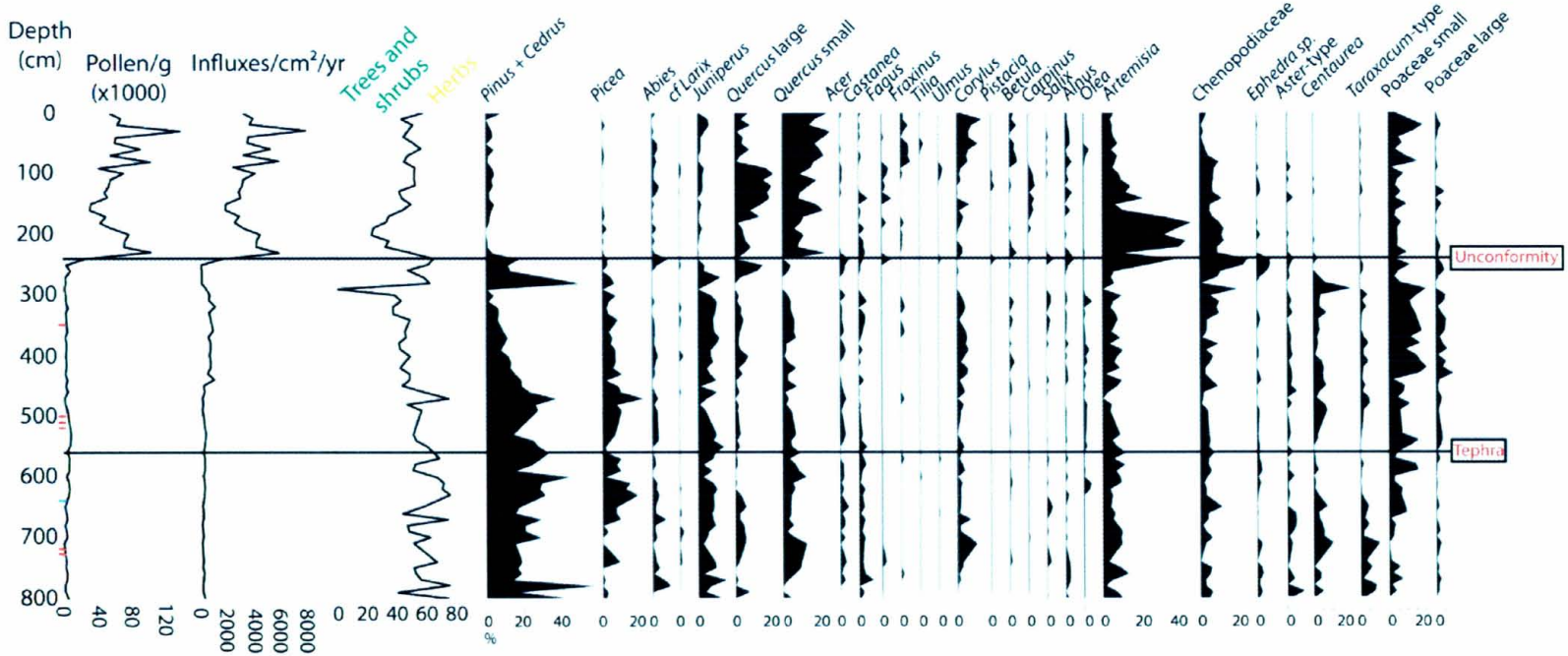

Figure 3.7: Pollen percentage diagram for core MAR02-89P in depth domain, also showing concentrations per gram and influxes. Almost barren zones are denoted by red dashes at corresponding depths, and no sample was taken at 640 cm – that depth is flagged with a blue dash.

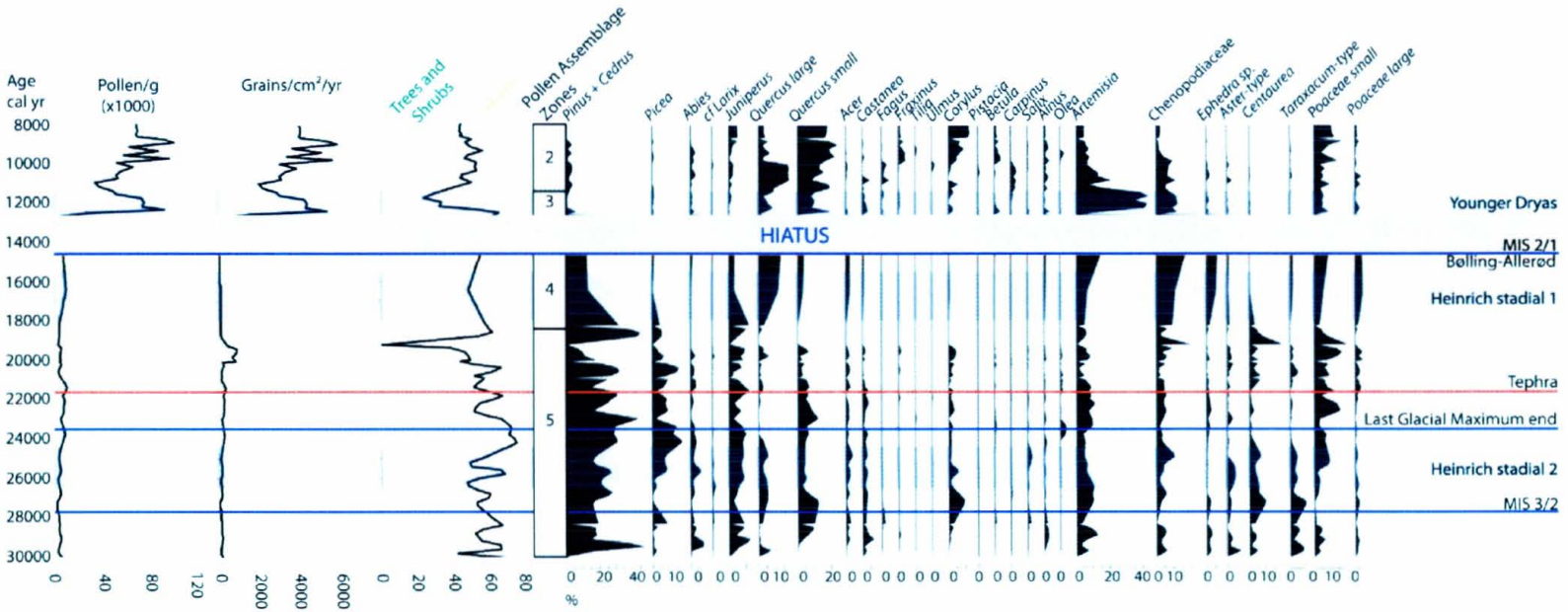

Figure 3.8: Pollen data from Figure 3.5 converted to age domain and showing pollen assemblage zones determined from CONISS (Constrained Incremental Sums of Squares cluster analysis). Significant time events recognized elsewhere in the Northern Hemisphere are shown: Younger Dryas, Bølling-Allerød, Heinrich stadial events (HS1 and HS2), the Y2 ash layer (tephra), last glacial maximum, Marine Isotope Stages (MIS 3/2 and MIS 2/1), and a hiatus (brown) indicates a break in sedimentation.

were found throughout the core and were identified based on appearance of strongly oxidized, poorly preserved grains, and known pre-Quaternary taxa.

The pollen concentrations are relatively low (less than 40,000 grains/g) from ~800 – 250 cm, ~30,000 to 14,850 cal. yr BP (Figures 3.7 and 3.8). From ~249 – 0 cm depth in the core (~12,700 – 8,000 cal. yr BP) there is an increase in pollen concentrations to values ranging between ~45,000 to 130,000 grains/g. Total pollen influxes are also low towards the base of the core but increase slightly from 450 cm to 290 cm (~22,200 – 18,800 cal. yr BP). From the unconformity to the top of the core, the concentrations and pollen influxes increase six-fold and their fluctuations show coincident peaks (Figures 3.7 and 3.8).

From the base of the core (800 cm) to ~300 cm (~30,000 – 19,200 cal. yr BP) the pollen assemblages are mainly dominated by tree and shrub taxa (~40 – 65%) with peaks up to 75% at 770 cm (~26,000 cal. yr BP), 730 cm (~23,300 – 24,500 cal. yr BP), and 450 cm (~20,200 – 20,800 cal. yr BP; Figures 3.5 and 3.6). At 300 cm (~19,200 cal. yr BP) there is an abrupt peak in herbs (~95%) but from ~285 – 250 cm (18,500 – 14,850 cal. yr BP), arboreal pollen (AP = tree and shrub taxa) are again ~60%. Non-arboreal herb taxa (NAP) increase to approximately 70% from ~220 – 180 cm (~12,300 – 11,500 cal. yr BP), and from ~180 – 0 cm (~11,500 – 8,000 cal. yr BP) the percentage ratios of trees and shrubs (AP) to herbs (NAP) vary between 40–60% (Figures 3.7 and 3.8).

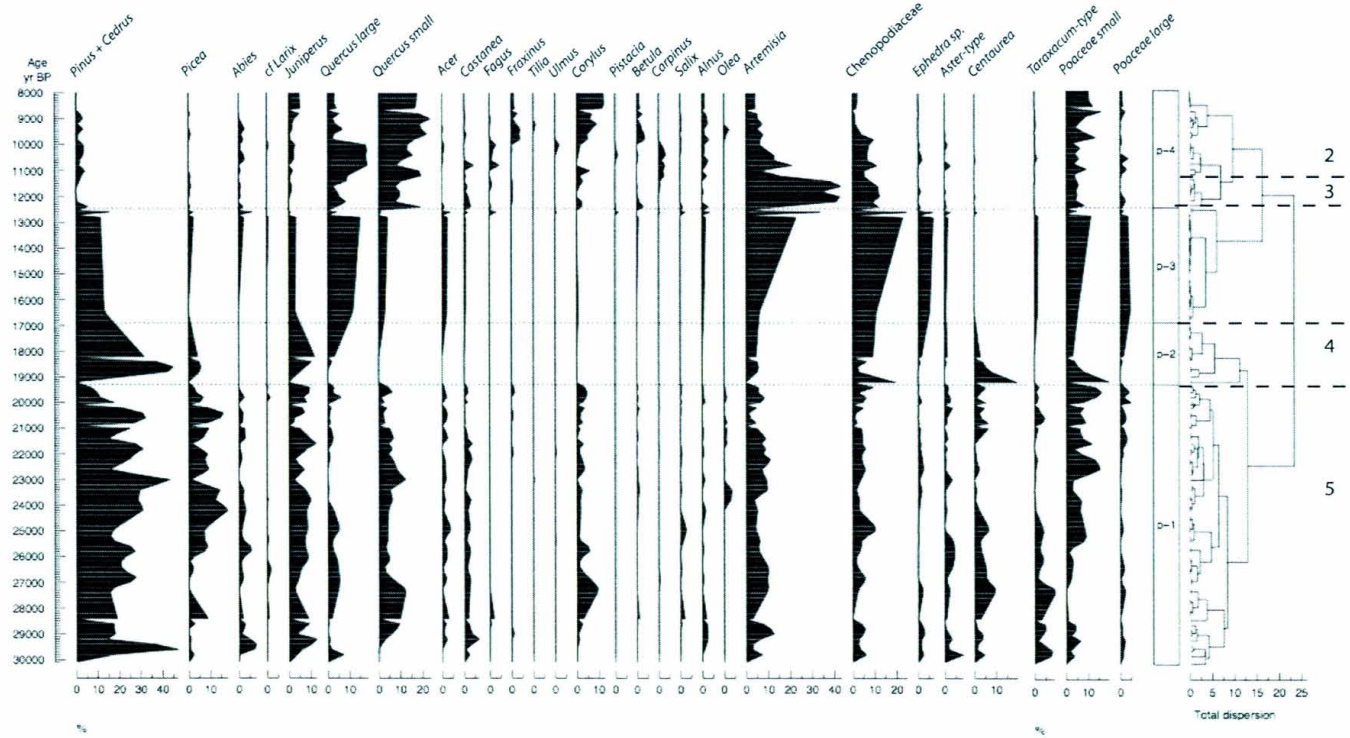

Figure 3.9: Relative abundances (percentages) of the main pollen taxa represented in age domain with zonations determined by CONISS (Constrained Incremental Sums of Squares cluster analysis) and assemblage zones indicated by dashed lines. Full list of pollen taxa given in Appendix III.

Pollen assemblage zones (Figure 3.7) were determined using constrained incremental sums of squares cluster analysis and choosing boundaries at similarity levels of 0.2 (Figure 3.9). Four pollen assemblage zones were determined for the MAR02-89P core and are numbered zones 5 – 2 based on similarity to previously defined regional pollen stratigraphies (Caner and Algan, 2002; Mudie et al., 2002b, 2007). The regional pollen zone 1 (Caner and Algan, 2002; Mudie et al., 2002b, 2007) that includes a decline in tree pollen concentrations and an increase in herbaceous and weed pollen is missing from the top of MAR02-89P (Figure 3.9).

Pollen Assemblage Zone 5 (800 – 290 cm; ~30,000 – 18,500 cal. yr BP) predominantly comprises very low influxes of tree and shrub pollen (~45 – 65 grains/cm^2/yr) with *Pinus* (Plate I-A) + *Cedrus* dominating (~20 – 40%) and relatively large percentages of evergreen *Quercus* (small grains, Plate I-B). *Corylus* (Plate I-D) shrub pollen has a peak around 28,000 cal. yr BP at the MIS 3/2 boundary, and *Artemisia*, *Centaurea*, *Taraxacum* and diverse chenopod genera (Plate I-E, -F, -G, -H to -J) are the most abundant herbs (~5 – 10%) in the lower half, followed by increased proportions of small Poaceae grains (Figure 3.8).

Pollen Assemblage Zone 4 (290 – 250 cm, ~18,500 – 14,850 cal. yr BP) is marked by a slight increase in ratio of trees and shrubs to herbs. *Pinus* and *Cedrus* continue to dominate (~15 – 35%) and there is a clear decrease in evergreen *Quercus* spp. with small grains less than 35 μm (<5%) and increase in deciduous summer green *Quercus* spp. with

larger grains (~5 – 10%; Figure 3.7). *Chenopodiaceae* (Plate I-H, -I, -J) taxa are the most abundant herbs (~10%), together with *Artemisia*, *Centaurea* (~5%) and Poaceae (Plate I-K, -L; ~5%). There is a peak in *Ephedra* pollen (~5%, Plate I-M) that marks the top of this pollen assemblage zone. Zone 4 is interrupted by an ~2,160 year hiatus beginning at ~14,850 cal. yr BP, below the MIS 2/1 boundary. It is possible that the transition from Zone 4 to Zone 3 occurred during the hiatus but the top of this zone is thought to be above the associated unconformity because of the continued high %AP and the high *Artemisia* values that characterize the Younger Dryas event (Figure 3.8).

Pollen Assemblage Zone 3 (249 – 170 cm, ~12,700 – 11,500 cal. yr BP) developed during the Younger Dryas event, where the pollen influxes rise strongly and there is an increase in NAP to ~60 – 80% (Figures 3.7 and 3.8). *Artemisia* has its highest peak (~40%) within core MAR02-89P in this assemblage zone. Chenopodiaceae comprise ~10% of total pollen and total percentages of the Asteraceae (*Aster*, *Centaurea* and *Taraxacum*) decrease. There is a noticeable decrease in *Pinus* and *Cedrus* relative abundances (<10%), while evergreen *Quercus* (~10%) and deciduous *Quercus* (Plate I-C) (<10%) dominate the AP (Figure 3.8).

Pollen Assemblage Zone 2 (170 – 0 cm, ~11,500 – 8,000 cal. yr BP) has high pollen influxes and an AP:NAP ratio of about 50% (Figure 3.7). *Quercus* is the dominant tree pollen, comprising ~20% evergreen *Quercus* and ~5 – 15% deciduous *Quercus*, respectively. *Artemisia* is the most abundant herb (~5 – 20%), with small Poaceae grains

(5 – 10%) and Chenopodiaceae (~5%) as the dominant herbs. Pollen of the arable field weeds *Centaurea* and *Taraxacum* are almost absent.

Figures 3.10 and 3.11 show the ratio of Chenopodiaceae to *Artemisia* pollen and the ratio of *Quercus* evergreen (small grains) to deciduous (large grains) pollen in both depth and age domain, respectively. The ratio of chenopod to *Artemisia* pollen is a rough index of aridity (El-Mosilmany, 1990). The Chenopodiaceae to *Artemisia* ratios generally show an upward tendency towards wetter conditions that is interrupted by four peaks that indicate drier periods. The first drought peak appears from 800 – 770 cm (~30,000 – 29,300 cal. yr BP), followed by a shift to wetter conditions until a level coincident with the end of the Heinrich HS2 stadial (660 – 640 cm; ~25,300 – 24,100 cal. yr BP) that lasted ~1000 cal. yr BP (Figures 3.10 and 3.11). The third drought peak occurs at 440 – 420 cm (~19,300 cal. yr BP). The fourth peak (closely spaced peaks at ~320 cm and 270 cm in depth domain Figure 3.10 are shown as one peak in Figure 3.11 because age domain is less detailed due to averaging or interpolations between adjacent primary data values) spikes just before the time of Heinrich HS1 stadial at 390 cm (~18,500 cal. yr BP). At ~10,000 cal. yr BP (80 cm) there is a smaller peak that falls in between the wetter vs. drier limits. The ratio of summer green deciduous to evergreen *Quercus* pollen is an index of summer moisture and winter cold (Kothoff et al., 2008). In core MAR02-89P, Chenopodiaceae:*Artemisia* ratios indicate wet and dry cycles, while fluctuations in the deciduous:evergreen *Quercus* ratios show intervals of warmer, drier summers corresponding to the Chenopodiaceae:*Artemisia* ratios drought peaks (more evergreens)

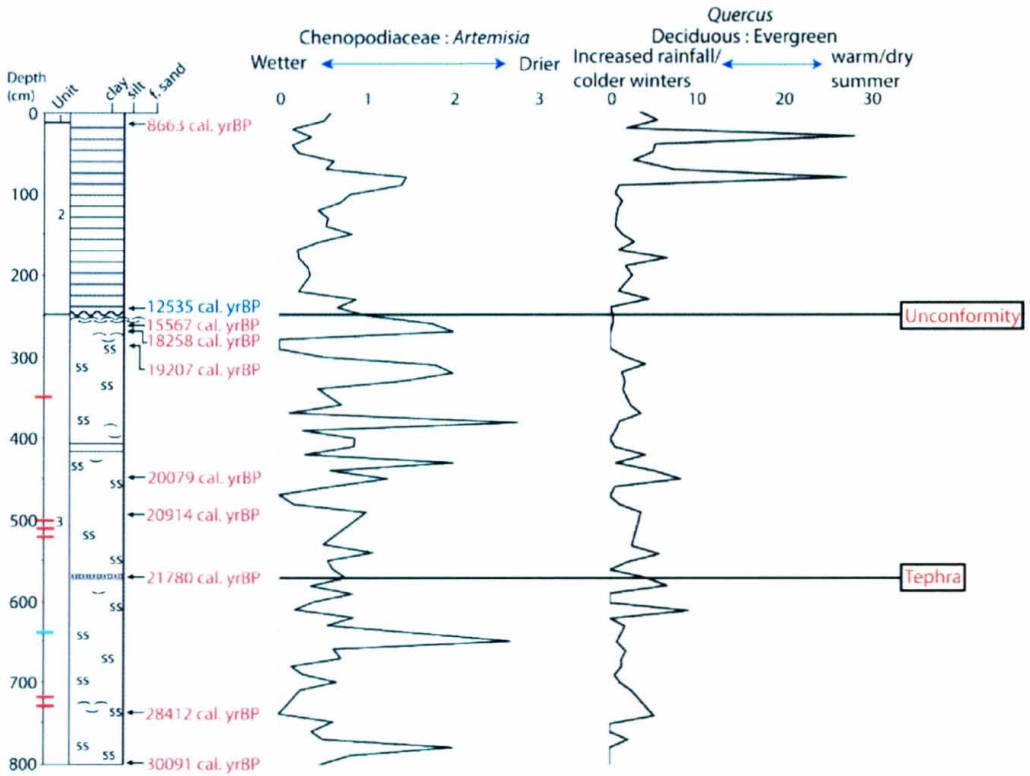

Figure 3.10: Ratio of Chenopodiaceae to *Artemisia* pollen and small evergreen to large deciduous *Quercus* pollen grains from core MAR02-89P in depth domain with core lithology. Almost barren zones are highlighted (red dashes at depth) and no sample was taken at 640 cm – that depth is flagged with a blue dash.

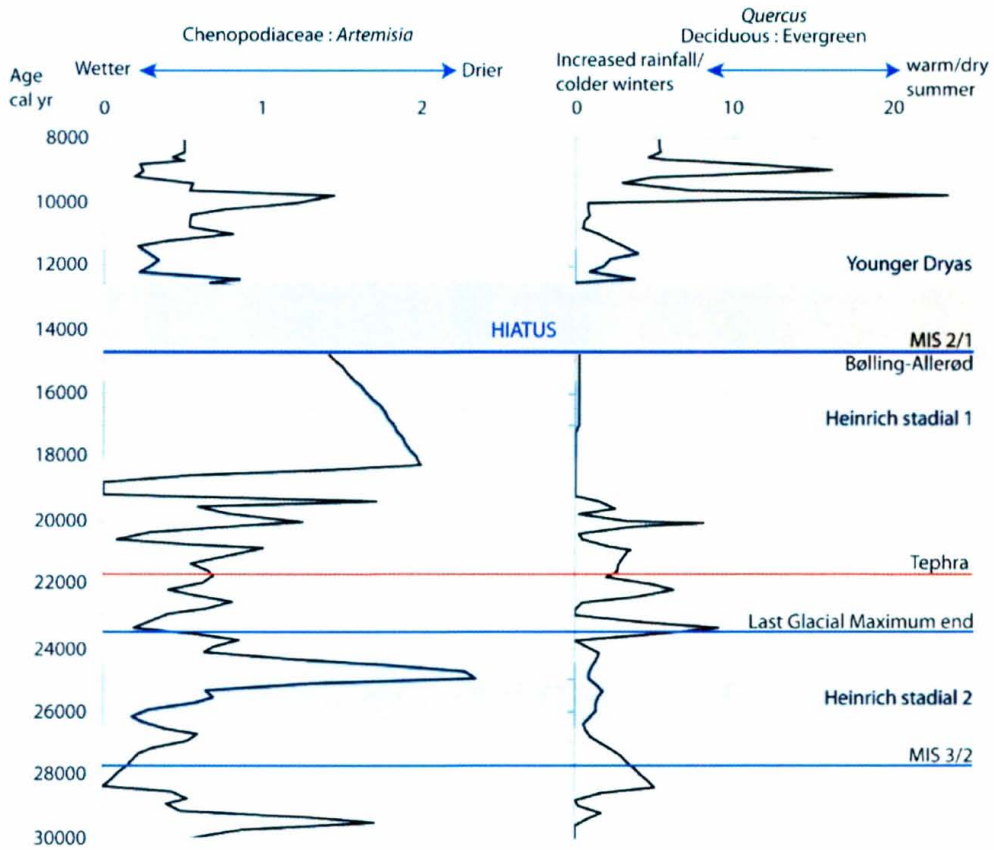

Figure 3.11: Ratio of Chenopodiaceae to *Artemisia* pollen and small evergreen to large deciduous *Quercus* pollen grains from core MAR02-89P in age domain. Significant time events recognized elsewhere in the Northern Hemisphere are shown: Younger Dryas, Bølling-Allerød, Heinrich stadial events (HS1 and HS2), the Y2 ash layer (tephra), last glacial maximum, Marine Isotope Stages (MIS 3/2 and MIS 2/1), and a hiatus (brown) indicates a break in sedimentation.

alternating with periods of increased cold and/or summer moisture (more deciduous *Quercus*). From 800 – 90 cm (~30,000 – 10,000 cal. yr BP), deciduous *Quercus* is dominant indicating increased rainfall and colder winters. There are two peaks from 90 – 70 cm (~10,000 – 9,500 cal. yr BP) and 40 – 20 cm (~9,200 – 8,800 cal. yr BP) showing an increase in evergreen *Quercus* indicating an increase in summer rainfall and drier summers (Figures 3.10 and 3.11).

Fern and moss spore data for MAR02-89P are presented in Figures 3.12 and 3.13 shown as number counted per slide. *Asplenium* is a forest fern genus that occurs from 660 – 645 cm (~25,800 – 24,800 cal. yr BP). *Equisetum* (horse-tail fern) is a fern-like primitive vascular plant that reproduces by spores and, in MAR02-89P, and it has peaks at 700 – 645 cm (~27,000 – 24,800 cal. yr BP), 260 – 250 cm (~16,500 – 14,850 cal. yr BP) and 140 – 95 cm (~11,000 – 9,900 cal. yr BP; Figures 3.12 and 3.13). Polypodiaceae fern spores (Plate I-DD, -EE) are found throughout core MAR02-89P but are only preserved with an intact perine (outer wall layer) in the sapropelic sediments from 249 – 0 cm (~12,700 – 8,000 cal. yr BP). *Dryopteris*-type (Plate I-FF) woodland fern spores are also present from 110 – 90 cm (~10,600 – 9,700 cal. yr BP). *Pteridium* fern spores occur at 280 – 250 cm (~18,900 – 14,850 cal. yr BP) and 140 – 90 cm (~11,000 – 9,900 cal. yr BP). Mosses and lycopod clubmoss spores peak at 700 – 750 cm (~27,000 – 24,900 cal. yr BP), and 120 – 110 cm (~10,800 – 10,200 cal. yr BP). Spore of the liverwort *Anthoceros* (Plate I-HH) that characterize wet stream banks are found from 670 – 660 cm (~25,800 – 24,800 cal. yr BP; Figures 3.12 and 3.13).

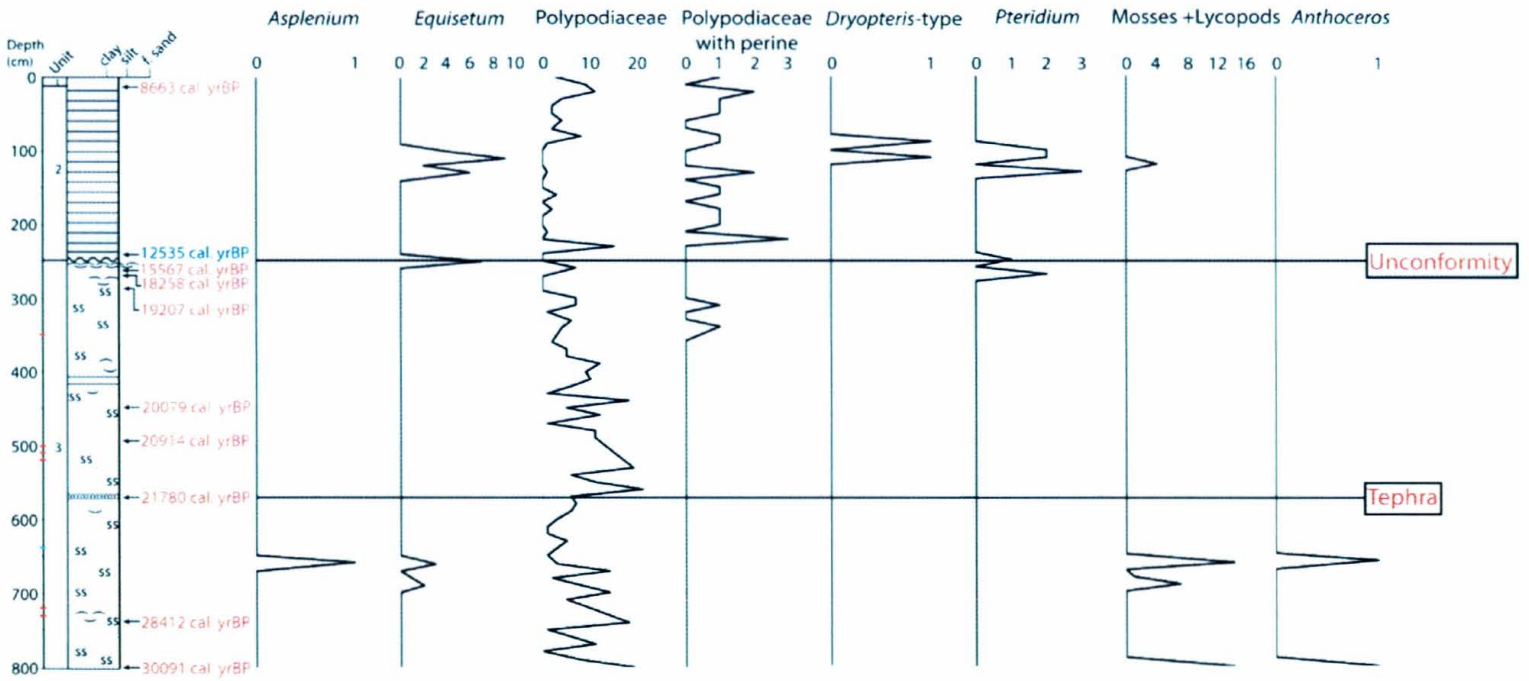

Figure 3.12: Fern, moss and liverwort count per slide data of core MAR02-89P in depth domain with lithology. Almost barren zones are highlighted (red dashes at depth) and no sample was taken at 640 cm – that depth is flagged with a blue dash.

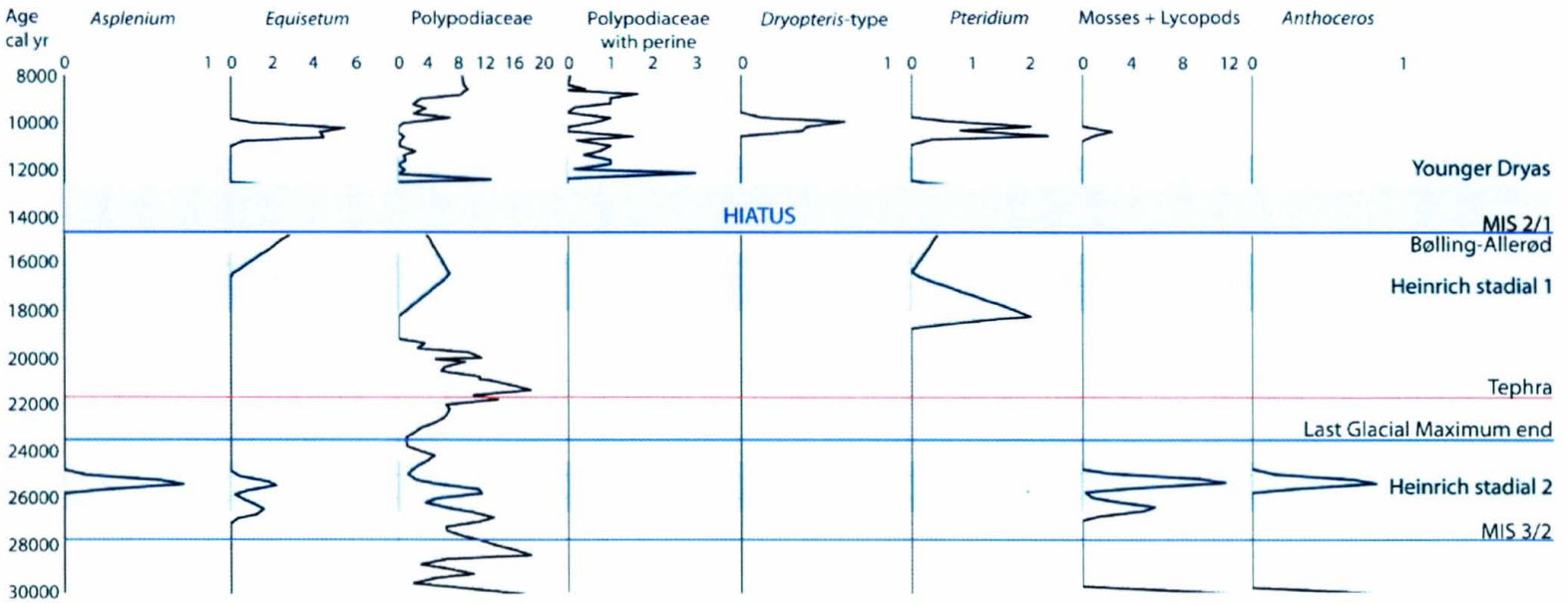

Figure 3.13: Fern, moss and liverwort count per slide data of core MAR02-89P in age domain. Significant time events recognized elsewhere in the Northern Hemisphere are shown: Younger Dryas, Bølling-Allerød, Heinrich stadial events (HS1 and HS2), the Y2 ash layer (tephra), last glacial maximum, Marine Isotope Stages (MIS 3/2 and MIS 2/1), and a hiatus (brown) indicates a break in sedimentation.

3.7 MAR02-89P Dinoflagellate Cyst Data

The abundance of dinoflagellate cyst (dinocysts) is relatively low throughout core MAR02-89P compared to other published Marmara and Black Sea core data, with a moderate diversity of ~30 species as listed in Appendix IV. When present, the preservation of dinoflagellate cysts usually appears to be good, as shown for the key taxa that are illustrated in Plate II, but pyrite and fine particulate organic matter in sapropel samples sometimes made identification difficult. Recognizable pre-Quaternary reworked cysts are common in some intervals.

The percentages of dinoflagellate cysts, abundances and influxes per cm^2 per year are shown in Figures 3.14 and 3.15, in depth and time domains, respectively. From the base of the core to 160 cm (~30,000 – 11,000 cal. yr BP), most dinocyst concentrations are less than 10,000 cysts/g with a small peak of ~20,000 cysts/g at ~12,700 cal. yr BP. The dinocyst influxes mostly vary synchronously with changes in abundances, but there are some notable minor influx peaks in the late glacial interval between the tephra layer and the unconformity. The dinocyst concentrations peak at 150 cm (~60,000 cysts/g) and slowly decrease upwards to ~25,000 cysts/g. Reworked dinoflagellate cysts (Figures 3.14 and 3.15) have two small peaks at 770 – 750 cm (~29,400 – 29,00 cal. yr BP) and 580 – 540 cm (~22,200 – 21,000 cal. yr BP) with ~400 cysts/g. There is a large peak of ~1400 pre-Quaternary cysts/g from 290 – 270 cm (~19,000 – 18,400 cal. yr BP) and above the unconformity, there is a peak of ~600 cysts/g from 230 – 160 cm (~12,200 – 11,200 cal. yr BP). At the top of the core there are three short-lived spikes of ~1200

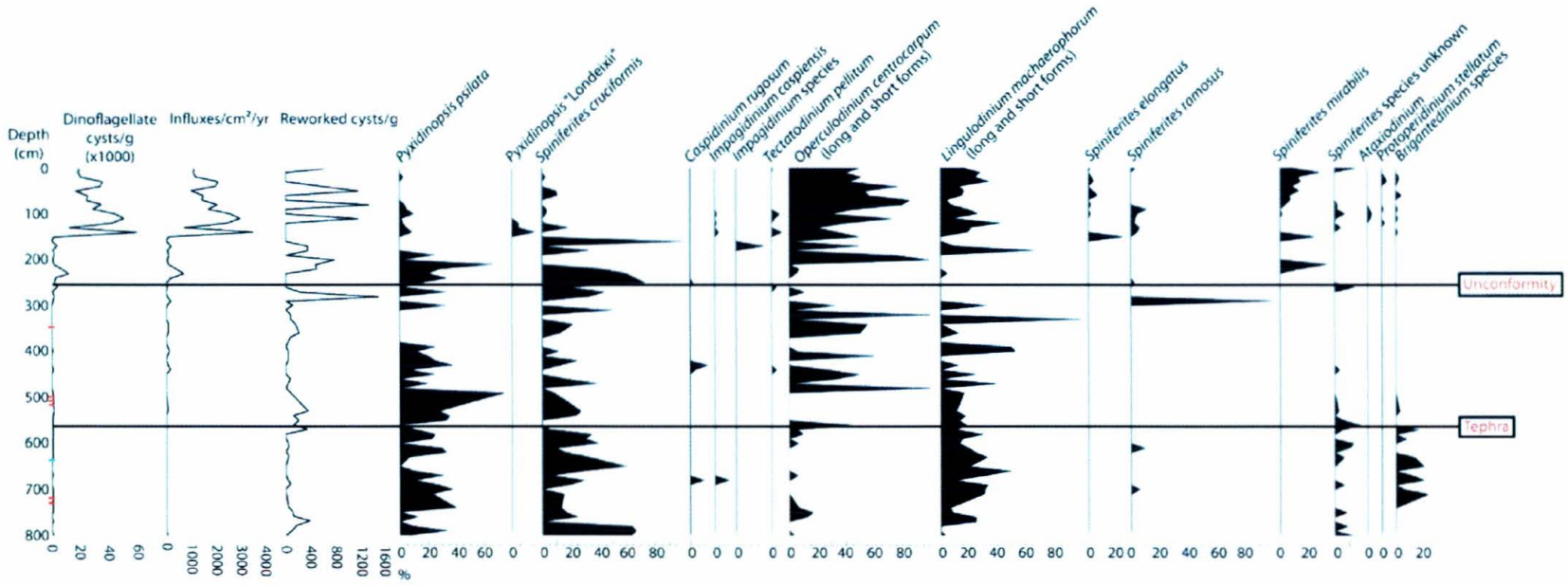

Figure 3.14: Dinoflagellate cyst data of core MAR02-89P in depth domain. Almost barren zones are highlighted (red dashes at depth) and no sample was taken at 640 cm – that depth is flagged with a blue dash.

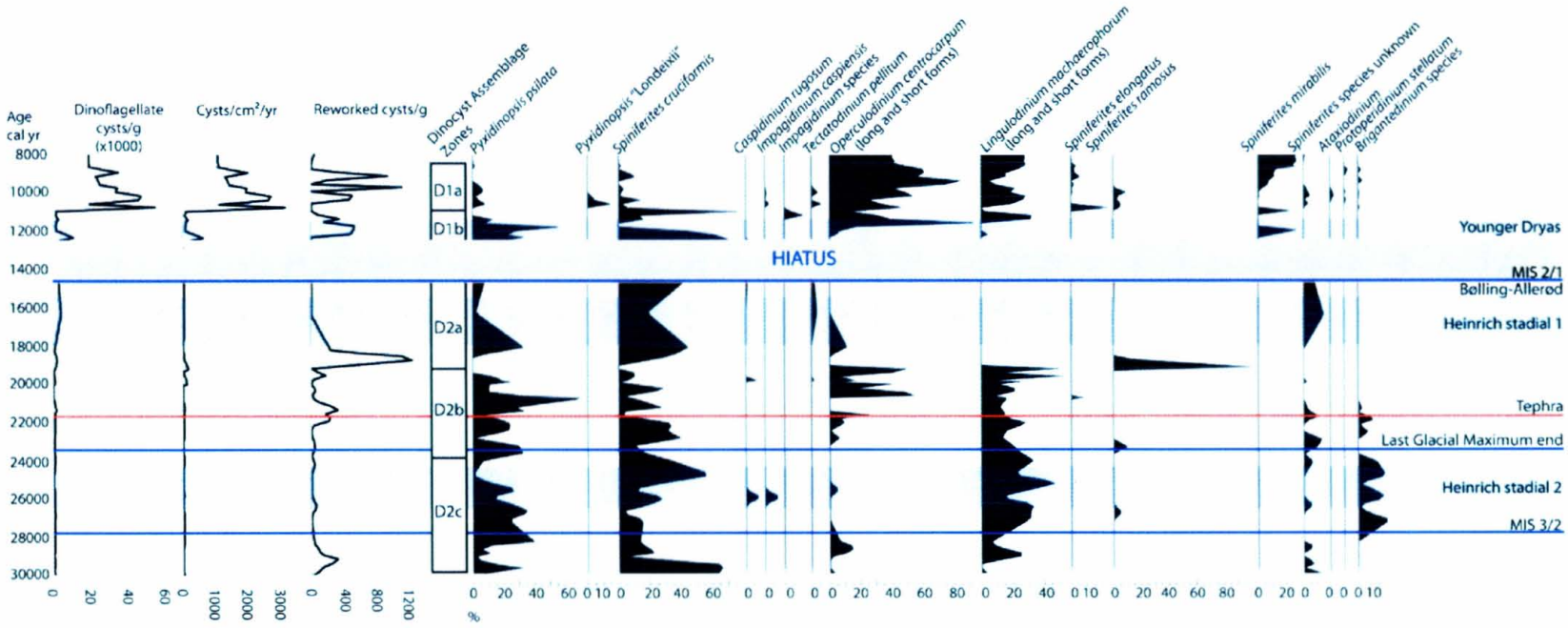

Figure 3.15: Dinoflagellate cyst data of Figure 3.12 converted to age domain, dinocyst assemblage zones are determined based on CONISS (Constrained Incremental Sums of Squares cluster analysis). Significant time events recognized elsewhere in the Northern Hemisphere are shown: Younger Dryas, Bølling-Allerød, Heinrich stadial events (HS1 and HS2), the Y2 ash layer (tephra), last glacial maximum, Marine Isotope Stages (MIS 3/2 and MIS 2/1), and a hiatus (brown) indicates a break in sedimentation.

pre-Quaternary cysts/g at 110 cm (~10,600 – 10,200 cal. yr BP), 80 cm (~9,800 cal. yr BP) and 50–40 cm (~9,200 – 9,000 cal. yr BP).

Constrained incremental sums of squares cluster analysis was used to determine two dinoflagellate cyst assemblage zones for the core MAR02-89P data and to delimit subzones within each zone (Figure 3.16). Dinocyst Zone D2, characterized by *Spiniferites cruciformis*, *Pyxidinopsis psilata*, and *Lingulodinium machaerophorum*, occurs in the pleniglacial and late glacial interval from 800 – 250 cm (~30,000 – 14,850 cal. yr BP), and can be subdivided into three subzones.

D2c. *S. cruciformis-P. psilata-L. machaerophorum-Brigantedinium* spp. subzone (800 – 630 cm, ~30,000 – 24,000 cal. yr BP). *S. cruciformis* (Plate II-A1, -A2, -B1, -B2) is the most common species with an average of ~35% throughout the subzone during the pleniglacial interval, with a maximum of ~65%. *Pyxidinopsis psilata* (Plate II-C) and *L. machaerophorum* (Plate II-D, -E) are co-dominant at ~5 – 40% and 10 – 45%, respectively. *Brigantedinium* spp. (Plate II-F) is present in lower percentages (5 – 15%), throughout most of this subzone. Subzone D2c has restricted occurrences of *Operculodinium centrocarpum* (Plate II-G1, -G2) before the MIS 3/2 boundary (~28,000 cal. yr BP) and again during the Heinrich HS2 time interval (~25,000 – 26,500 cal. yr BP). The Heinrich HS2 time interval also has sporadic occurrences of *Caspidinium rugosum* (Plate II-H) and *Impagidinium caspiensis* (Plate II-I).

D2b. *S. cruciformis-P. psilata-L. machaerophorum-O. centrocarpum-Spiniferites*

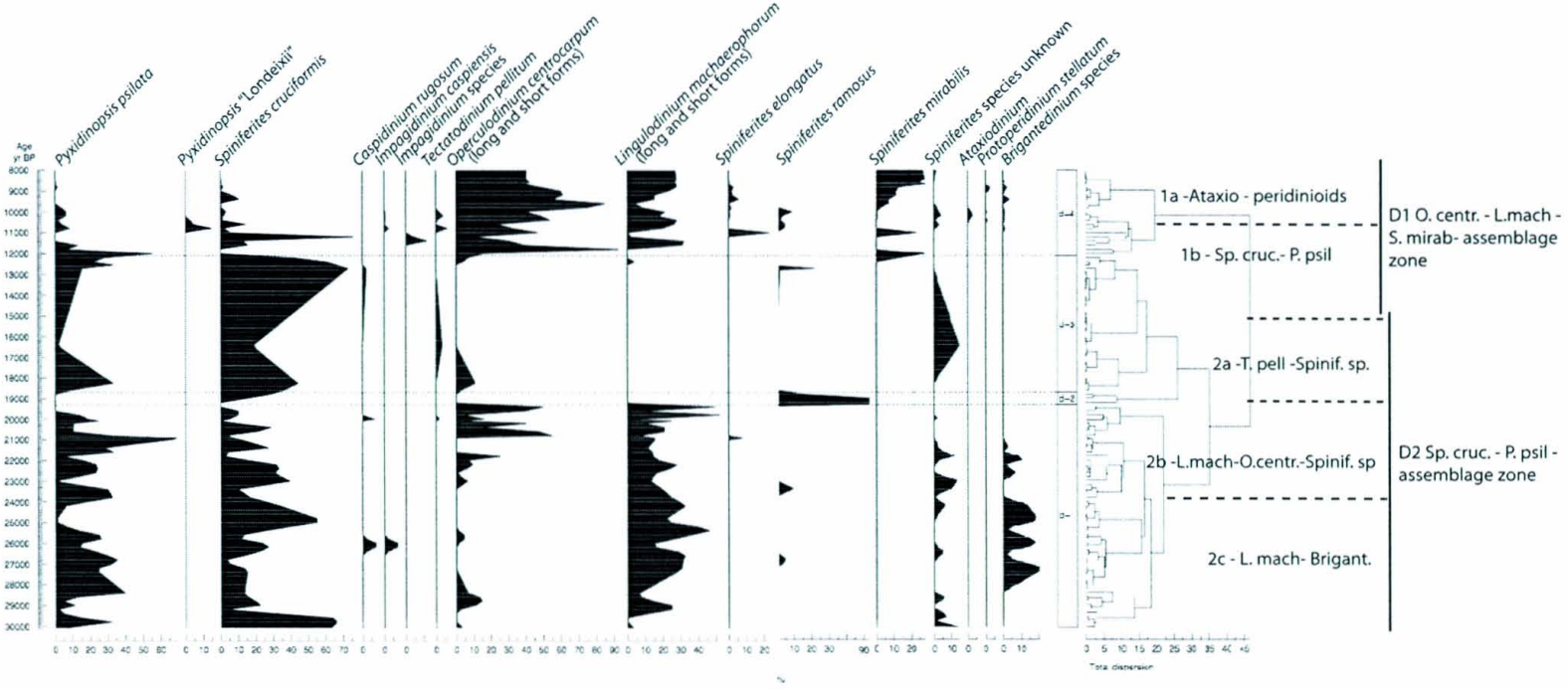

Figure 3.16: Dinocyst taxa (percentages) represented in age domain with zonations determined by CONISS (Constrained Incremental Sums of Squares cluster analysis) and dinocyst assemblage zones indicated by dashed lines and labelled.

spp. subzone (630 – 360 cm, ~24,000 – 19,500 cal. yr BP). *S. cruciformis* continues to dominate this last glacial maximum subzone (up to 40%), together with high percentages of *P. psilata* (up to 35%) that reaches its peak of ~60% at ~21,000 cal. yr BP. *Lingulodinium machaerophorum* is also common (~10 – 35%) with two large peaks (~50%) at the top of the subzone. *Operculodinium centrocarpum* is less common and not continuously present throughout the subzone but increases from ~5 – 30% until the tephra bed (dated ~21,800 cal. yr BP) where it disappears temporarily but returns strongly at ~21,000 cal. yr BP, varying between ~10 – 55% to the top of the subzone (Figure 3.15). Subzone D2b is marked by an increase in *Spiniferites* spp. above the tephra layer. Near the top of the subzone there are restricted occurrences of *C. rugosum* and *Tectatodinium pellitum* (Plate II-J). The zone has several unknown *Spiniferites* spp. that include unusual morphotypes of *Spiniferites ramosus* (cf. Mudie et al., 2004) and *Spiniferites belerius* (Marret et al., 2009) in various orientations, making it difficult to distinguish *Spiniferites* species level with certainty.

D2a. *S. cruciformis-P. psilata-L. machaerophorum-T. pellitum- Spiniferites* spp. subzone (360 – 250 cm; ~19,500 – 14,850 cal. yr BP). This subzone of D2 spanning the Heinrich HS1 glacial stade and the start of the interstadial Bølling-Allerød interval continue to have high relative abundances of *S. cruciformis* (~20 – 45%) and *P. psilata* (up to 35%); however, *L. machaerophorum* is almost absent in this subzone. *T. pellitum* (~5%) is present during the Heinrich HS1 and one sample (250 cm) for the start of the Bølling-Allerød time intervals (~18,000 – 14,850 cal. yr BP), as well as unknown

Spiniferites spp. (~10%). At the base of the subzone there is a peak (95%) of *S. ramosus* (Plate II-K1, -K2) in one sample where only a small number of dinoflagellate cysts were present (300 cm; ~19,000 cal. yr BP).

Dinocyst Assemblage zone D1. *O. centrocarpum-L. machaerophorum-Spiniferites mirabilis* (249 – 0 cm, ~12,700 – 8,000 cal. yr BP) is characterized by much higher percentages of *O. centrocarpum* with a decrease in previously dominant *S. cruciformis* and with two recognizable subzones (Figure 3.15). It is assumed that the transition between Dinocyst Assemblage Zone D2 and Dinocyst Assemblage Zone D1 occurs within the hiatus because there is a notable increase in dinocyst concentrations immediately above the unconformity. Zone D1 generally shows an abrupt decline of the dominant Pleniglacial species and a switch to dominance of the species *O. centrocarpum* with high nutrient requirements (*O. centrocarpum*) and high temperature-salinity tolerances (*S. mirabilis*; Marret and Zonneveld, 2003; Londeix et al., 2009).

Subzone D1b. *O. centrocarpum-L. machaerophorum-S. mirabilis-S. cruciformis- P. psilata* subzone (249 – 150cm, ~12,700 – 11,000 cal. yr BP). *Operculodinium. centrocarpum* (~90%) and *L. machaerophorum* (~40%) are the most abundant dinocyst species (Figure 3.15). The subzone is marked by peaks of *S. mirabilis* (~25%) (Plate II-L), together with *S. cruciformis* (65%) and *P. psilata* (10 – 55%), which peak during the Younger Dryas. *S. cruciformis* has an additional peak of 75% at the top of subzone D1-a (~11,000 cal. yr BP). This subzone also shows restricted occurrences of *Impagidinium spp.* (~10%), *S. elongatus* (~20%), and *S. ramosus* (~5%) that all appear at the top of the

pre-boreal subzone above the Younger Dryas time interval.

Subzone D1a. *O. centrocarpum-L. machaerophorum-S. mirabilis-Ataxiodinium choanum-Protoperidinium* subzone (150 – 0 cm, ~11,000 – 8,000 cal. yr BP) is dominated by *O. centrocarpum* (~30 – 85%), *L. machaerophorum* (~10 – 30%) and *S. mirabilis* (~10 – 25%; Figure 3.15). This early Holocene subzone is marked by a large increase in cyst influxes, and by the reoccurrences and first occurrence in core MAR02-89P of several cyst-types of *Protoperidinium* taxa. This includes *Brigantedinium* spp. (cysts of *Protoperidinium conicum* and other *Protoperidinium* spp.) and *Protoperidinium stellatum* (Plate II-M); it also includes the marine gonyaulacoid taxon *Ataxiodinium* spp. (<5%). Peaks in concentration (~11,000 – 10,000 cal. yr BP) show restricted occurrences (5%) of the *Pyxidinopsis* species of Londeix et al., (2009), here informally labeled *Pyxidinopsis Londeixii* (Plate II-N1, -N2), *I. caspiensis* (<5%), *T. pellitum* (~5%), *S. ramosus* (~5 – 10%), and some unknown *Spiniferites* spp. (~5%). *Spiniferites elongatus* (~5%) occurs towards the top of the subzone (~9,500 – 8,000 cal. yr BP).

3.8 MAR02-89P Non-Pollen Palynomorph (NPP) Data

For the most part preservation of non-pollen palynomorphs is good, although all samples of *Pediastrum* specimens seem to be thin walled and very transluscent. This can be seen in Plate III-A, -B and may be characteristic of the genus as it is the same in both the sapropelic sediments and sediments with low TOC.

Figure 3.17 shows the non-pollen palynomorphs of core MAR02-89P in depth domain, with the core lithology. The non-pollen palynomorphs (Figures 3.17 and 3.18) are represented in abundance/g rather than percentages used for the pollen and dinocysts.

The colonial fresh-brackish water algae *Pediastrum* spp. (*Pediastrum boryanum* and *Pediastrum simplex*; Plate III-A, -B) have three major peaks (Figures 3.17 and 3.18). The oldest peak at 650 – 620 cm (~25,000 – 23,400 cal. yr BP), corresponds to the second moisture peak in the Chenopodiaceae to *Artemisia* ratios and deciduous:evergreen *Quercus* ratios. The second peak at 580 – 490 cm (~22,600 – 19,900 cal. yr BP) corresponds to the moist interval before the last glacial maximum drought peak. The third peak occurs from 290 cm to the onset of the hiatus (~18,800 – 14,850 cal. yr BP). The other colonial alga, *Botryococcus* (Plate III-C) that is common in eutrophic fresh or brackish water, has two peaks flanking the time of the Heinrich HS2 stadial, at 700 – 685 cm (~26,900 – 26,000 cal. yr BP) and 670 – 650 cm (~25,800 – 24,800 cal. yr BP). There are also *Botryococcus* peaks just before the upper *Pediastrum* peak (280 – 260 cm; ~18,800 – 16,500 cal. yr BP), and at 130 – 120 cm (~10,500 – 11,000 cal. yr BP).

Another alga, the desmid, *Staurastrum tetracerum* (Plate III-D, -E) first appears from approximately 230 – 30 cm (~12,000 – 9,900 cal. yr BP; Figures 3.15 and 3.16). The *Multiplicasphaeridium*-type acritarch species (Plate III-F, -G) of uncertain biological affinity (possibly a dinocyst) is abundant from 800 – 250 cm (~30,000 – 14,850 cal. yr BP), and peaks at ~670cm (~25,500 cal. yr BP). This non-pollen palynomorph taxon associated with cool, low SSS conditions is briefly absent from 280 – 260 cm (~18.700 –

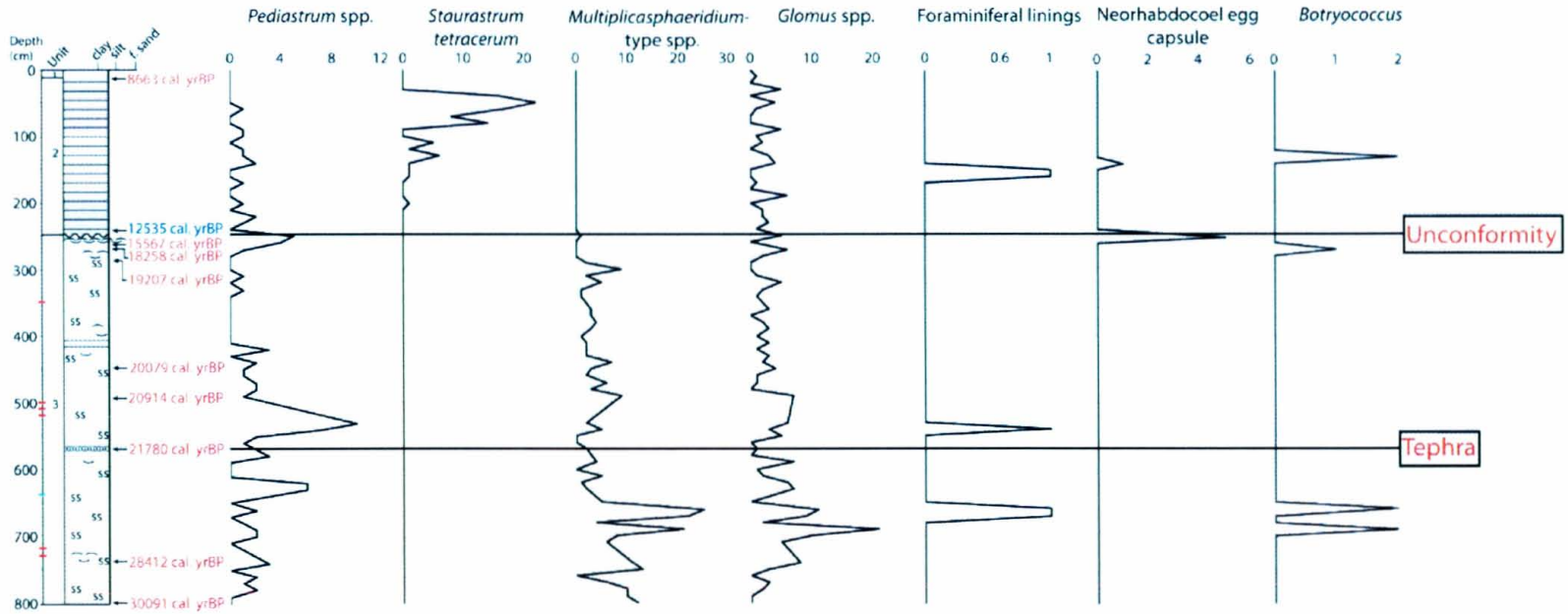

Figure 3.17: Abundance of non-pollen palynomorphs for core MAR02-89P in depth domain with lithology. Almost barren zones are highlighted (red dashes at depth) and no sample was taken at 640 cm – that depth is flagged with a blue dash.

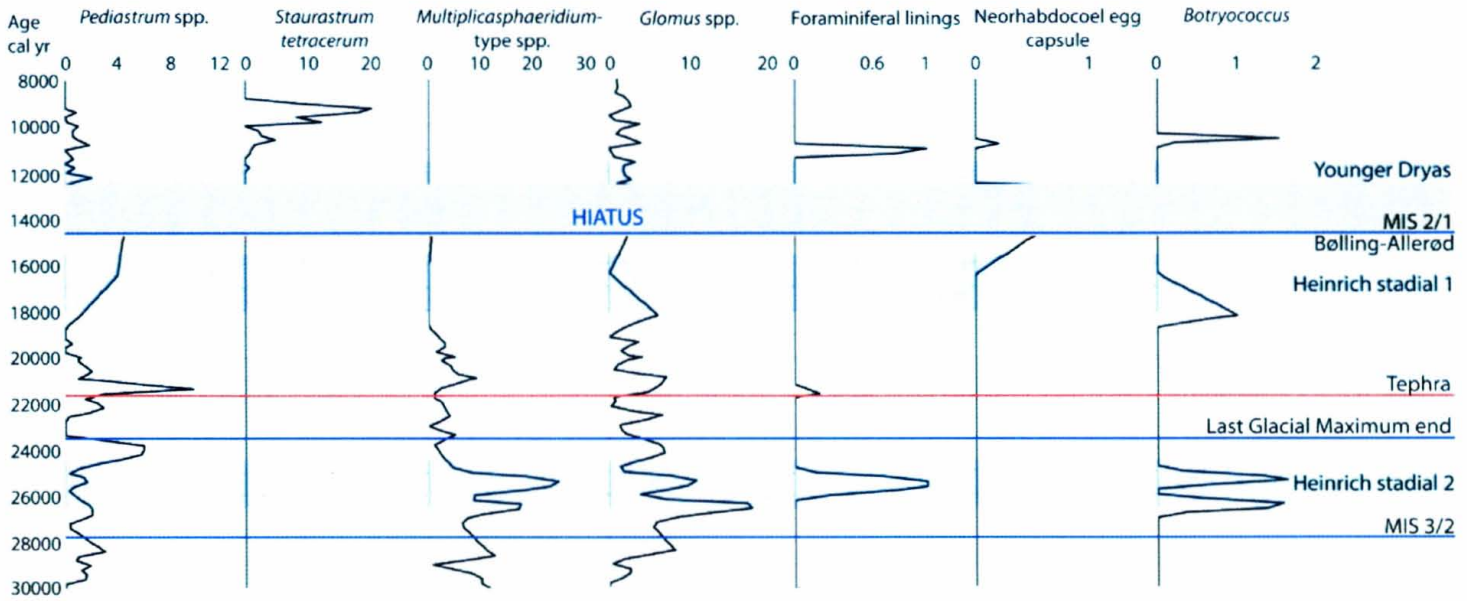

Figure 3.18: Abundance of non-pollen palynomorphs data for core MAR02-89P in age domain. Significant time events recognized elsewhere in the Northern Hemisphere are shown: Younger Dryas, Bølling-Allerød, Heinrich stadial events (HS1 and HS2), the Y2 ash layer (tephra), last glacial maximum, Marine Isotope Stages (MIS 3/2 and MIS 2/1), and a hiatus (brown) indicates a break in sedimentation.

16,000 cal. yr BP), and reoccurs in low numbers from 260 – 250 cm (~16,000 – 14,850 cal. yr BP). This taxon also occurs in low numbers in lower Holocene sediments of the Black Sea (P. Mudie, personal communication, 2011.)

The fungal spore *Glomus* (Plate III-H, -I) is present throughout the core, with greatest abundance from 690 – 700 cm (~26,300 – 26,800 cal. yr BP; Figures 3.15 and 3.16). Organic microforaminiferal linings (Plate III-J, -K) are rare and occur at only three intervals: at 780 – 760 cm (~24,800 – 26,200 cal. yr BP), 550 – 530 cm (~21,200 – 21,800 cal. yr BP), and above the unconformity at 170 – 150 cm (~11,300 – 10,900 cal. yr BP). Egg capsules of Neorhabdocoel-type flatworms (Plate III-L) are also found at 260 cm just below the unconformity (~16,000 – 16,500 cal. yr BP), and at 130 cm (~10,600 – 11,000 cal. yr BP). These are common in surface sediments of Marmara Sea and on the Black Sea shelf but not in the anoxic basins (P. Mudie, personal communication, 2012).

Interpretation and Discussion

4.1 MAR02-89P Core Location

The Marmara Sea core MAR02-89P described in this thesis is from a perched basin on the upper SE slope at a depth of -257 m which is about 180 m deeper than the sill connecting the Marmara Sea and Aegean Sea so it should not have been exposed to subaerial erosion even at maximum global sea level lowering of ~-125 m below present level, nor when the Marmara Sea itself was drawn down by evaporation to ~100 m in the Late Pleistocene (Aksu et al., 1999b; Hiscott et al., 2007a). This location is much deeper than the only other long sediment core from the eastern Marmara Sea: MD04-2750 at ~-80 m below sea level in a prodelta succession near the Bosphorus Strait exit into the Marmara Sea (Eriş et al., 2007, 2011). Sediment deposition is thicker on the floor of the perched basin and thinner on the ridge, resulting in an Upper Pleistocene – Holocene section at the site of core MAR02-89P, and an extended Holocene section at site of core MAR02-88P (Figure 2.1).

4.2 MAR02-89P Lithology

The assumption of constant sedimentation rates between dated intervals (Figure 3.4) indicates an average sedimentation rate of ~30 cm/ka, with high sedimentation rates

occurring from ~21,800 – 21,300 cal. yr BP (~43 cm/ka) and lower sedimentation rates occurring from ~20,000 – 19,200 cal. yr BP (~5 cm/ka) and during sapropel development from ~12,700 – 8,000 cal. yr BP (~17 cm/ka). During sapropel deposition there is a marked increase in TOC (Figures 3.3 and 3.4), which is not observed in the older sediments that accumulated at higher sedimentation rates in core MAR02-89P.

The small variations in amount of sand in core MAR02-89P (Figures 3.5 and 3.6) show that late glacial maximum, Heinrich stadial HS1, and early interstadial Bølling-Allerød peaks of slightly higher sand content did not obviously dilute the deposition of palynomorphs (Figures 3.7 and 3.8). Throughout the Late Pleistocene, pollen influxes remain less than 1000 grains/cm^2/yr, (Figures 3.7 and 3.8), i.e., from ~30,000 – 14,850 cal. yr BP, at the base of the unconformity. Subsequently, after ~12,700 cal. yr BP (i.e., above the unconformity), influxes are higher at 3,000 – 8,000 grains/cm^2/yr. However, dinoflagellate cyst influxes did not rise greatly until around 11,000 cal. yr BP. This difference in the timing of the increased influxes of organic-walled microfossils implies that the rise in pollen influx is not only because of improved palynomorph preservation accompanying the increased %TOC (Figure 3.6) after 12,700 cal. yr BP. The offset in influx increases at this continental shelf location implies that in the Marmara Sea region, the forest vegetation responded more rapidly to the climate changes at the end of MIS 2/1 than did the phytoplankton.

4.3 MAR02-89P Geochemistry Data

Relatively high TOC percentages mark the Younger Dryas and Holocene sediments in core MAR02-89P with two broad peaks corresponding to the upper and lower sapropels with TOC >2% (Figure 3.6). There is a gradual upward enrichment in the $\delta^{13}C$ values from 12,700 – 8,000 cal. yr BP, suggesting an increase in marine biological production over terrigenous supply, in agreement with results reported by Abrajano et al. (2002) and Vidal et al. (2010). The second peak in TOC roughly coincides with the rise in dinocyst influxes, also indicating increased primary productivity in Marmara Sea.

The TS percentages in core MAR02-89P show a broad peak of ~1% from ~25,000 to 21,000 cal. yr BP (Figures 3.5 and 3.6). There is a rise in TS to ~2% beginning ~19,000 cal. yr BP, possibly indicating a transition to more dysoxic conditions resulting from enhanced water-column stratification. After ~19,000 cal. yr BP, there is an increase in pyrite grains that might indicate an increase in bacterial sulphate reduction at the core site. Alternatively, the changes in sulphur chemistry might have been caused by a phase of Black Sea outflow during which previously isolated deep bottom waters from the Black Sea were mixed into the outflow plume, assuming that those brackish waters contained excess hydrogen sulphide. This is contrary to Major et al. (2006) who indicate full mixing in the deep water of the Black Sea lacustrine phase.

The ratio of TS to TOC can be used as an index of water stratification (Watanabe et al., 2003). The ratio shows two large peaks (at ~24,000 – 21,000 cal. yr BP and 19,500 – 14,850 cal. yr BP), and three smaller peaks (~28,500 – 28,000, 20,000 – 19,500, and 12,700 – 8,000 cal. yr BP) possibly indicating periods of flooding of the Black Sea into the Marmara Sea. Chepalyga (2007) describes megafloods from the Ponto-Caspian region spilling over into the Black Sea from ~19,800 – 11,000 cal. yr BP, with the main flooding event occurring ~19,800 – 16,800 cal. yr BP. The main Chepalyga (2007) megaflood interval is correlative with the large peak in TS/TOC during the Heinrich HS1 stadial time interval and one of the small peaks prior to the Heinrich HS1 stadial in MAR02-89P.

4.4 MAR02-89P Pollen Data

Pollen concentrations and influxes (Figure 3.8) are relatively low from the base of the core through the Heinrich HS2 and HS1 stadial time intervals and the start of the Bølling-Allerød time interval until the beginning of the hiatus at ~14,850 cal. yr BP. In the Younger Dryas sediments, there is an abundance peak that corresponds to the lower sapropel (Figure 3.8 compared with Figure 3.6) with an age of ~12,535 – 11,500 cal. yr BP; this is followed by a second pollen abundance peak corresponding to the thicker Holocene sapropel layer that accumulated from ~10,800 – 8,600 cal. yr BP. Pollen of trees and shrubs generally dominate core MAR02-89P from ~30,000 – 16,000 cal. yr BP after which there is an increase in herbs, followed by a relatively even distribution of

Arboreal Pollen:Non-Arboreal Pollen from ~13,000 – 8,000 cal. yr BP.

It is interesting to note a near absence of *Pinus* from ~16,000 cal. yr BP through the Younger Dryas, because normally *Pinus* is greatly over represented in marine and lake cores (Traverse, 1988; Mudie et al., 2002a; Mudie and McCarthy, 2006) and it is rare to have such low amounts in a lacustrine or marine environment. This sparsity could indicate either a drastic change in climate or a reduction of inflow of river water to the Marmara Sea, which has been suggested by Vidal et al. (2010) for the Younger Dryas. Studies of Black Sea cores have indicated a high water level during the Younger Dryas (Major et al., 2006; Vidal et al., 2010), with overflow through the Bosphorus Strait. Caner and Algan (2002) have also reported a notable decrease in *Pinus* in their Pollen Zone B (~13,500 – 6,200 cal. yr BP) of their western basin core, and Tzedakis et al. (2004) show a big decrease in % *Juniperus* + *Pinus* in Kopais east of the Pindus Mountains of western Greece from ~17,800 – 13,400 cal. yr BP. Previous studies in cores that recovered late glacial through Younger Dryas successions in northern Anatolia and Greece (Bottema, 1995) do not report a big fluctuation in *Pinus* but show that there are large variations in AP:NAP ratios throughout the region.

Quercus (oak) pollen occurs throughout core MAR02-89P, with higher percentages as pollen concentrations and %TOC increase, thus possibly indicating some diagenetic influences for this oxidation-sensitive pollen type (Traverse, 1988). There are 18 *Quercus* species in Turkey today (Urğulu et al., 2012). The severe landscape changes that have accompanied land clearance and overgrazing makes it difficult to relate the

modern distribution of these species to climate conditions (Urğulu et al., 2012). However, small *Quercus* pollen grains mark evergreen oak shrubs and generally indicate warm and dry Mediterranean summers, while the large *Quercus* grains are from deciduous oak trees that indicate higher rainfall and colder winters (Mudie et al., 2002b; Urğulu et al., 2012). Evergreen *Quercus* are tolerant to drought, while deciduous *Quercus* are more moisture demanding; the ratio of deciduous to evergreen pollen species can provide information about relative amounts of moisture (Caner and Algan, 2002; Mudie et al., 2002b; Kotthof et al., 2008). Use of the ratio also avoids the issue of possible diagenetic influences if it is assumed that both small and large *Quercus* grains have the same sensitivity to oxidation.

There is also a prominent amount of Chenopodiaceae and *Artemisia* pollen throughout core MAR02-89P, which are important herbaceous pollen markers of arid and semi-arid regions (El-Moslimany 1990; Li et al., 2010). The percentages of these pollen in modern surface sediments have been calibrated against temperature and moisture conditions to show that in general, *Artemisia* needs more soil moisture than Chenopodiaceae, so the ratio can be used as an indicator of net moisture accumulation (precipitation-evaporation = P-E) within the region where the vegetation grows (El-Moslimany 1990; Li et al., 2010).

In Pollen Assemblage Zone 5 (~30,000 – 18,500 cal. yr BP; Figure 3.8) AP are approximately 40 – 60%, with *Pinus* as the dominant taxon, and strong representation of *Abies* (Plate I-Q), *Juniperus* (Plate I-X) and both evergreen and deciduous *Quercus*. The

winter-green (evergreen) small *Quercus* pollen tend to dominate and there is a notable drop in summer green (deciduous) *Quercus* pollen percentages in the Heinrich HS2 cold stadial time interval. *Picea* (Plate I-P) pollen also increases after the Heinrich HS2 stadial time interval, perhaps indicating a southward expansion of more northerly cold forest vegetation. There are also variable small amounts of *Acer* (Plate I-R) and *Castanea* (Plate I-N) tree pollen, but a near absence of other temperate deciduous tree pollen taxa. The presence of *Castanea* pollen in core MAR02-89P is interesting because this temperate tree is normally associated with warmer conditions suitable for *Fagus* and *Tilia* (Plate I-V) (Krebs et al, 2004), but its occurrence in MAR02-89P is consistent with other data indicating a glacial refugium for *Castanea sativa* (sweet chestnut) in the western Pontic Mountains (Caner and Algan, 2002; Krebs et al., 2004). *Corylus* shrub pollen has its maximum in this zone. Minor amounts of *Salix* and *Alnus* (Plate I-O) pollen indicate conditions wet enough to support gallery forest in river valleys. NAP has *Artemisia*, chenopods, and Asteraceae species in almost equal amounts but low percentages. Chenopodiaceae:*Artemisia* ratios indicate several drought events (Figures 3.10 and 3.11). The NAP values of ~40% or less indicate the presence of steppe or steppe-forest environments interspersed between larger areas of forest, and the AP taxa indicate a mixture of oro-Mediterranean forest environments (with dry summers, approximately 600 mm of annual rain), and warmer, wetter coastal areas supporting thermophilous trees like *C. sativa* that cannot tolerate spring frost and that require 700 – 800 mm of precipitation throughout the year.

Pollen Assemblage Zone 4 (~18,500 – 14,850 cal. yr BP; Figure 3.8) occurs during the Heinrich HS1 stadial and the early interstadial Bølling-Allerød time intervals, and is terminated by the hiatus. The AP comprise ~50 – 60% of the low pollen concentrations, with *Pinus* continuing to dominate, but there are decreases in the temperate – cold climate trees *Picea*, *Abies*, as well as the summer-drought-resistant evergreen *Quercus*. The Heinrich HS1 stadial and early Bølling-Allerød time intervals display a transition from predominately evergreen *Quercus* to deciduous *Quercus*, suggesting higher rainfall to the region and colder winters (Mudie et al., 2002b). Not all temperate species from Zone 5 occur in Zone 4 and *C. sativa* pollen disappears, perhaps indicating cooler temperatures within the region. Deciduous *Acer* reaches a maximum during the Heinrich HS1 stadial and the early Bølling-Allerød time intervals, consistent with cooler conditions, as this taxon is found presently in northern regions of the Marmara Sea (Caner and Algan, 2002). The NAP are dominated by *Artemisia* and Chenopodiaceae in equal amounts with a decrease of Asteraceae. There is a maximum of *Ephedra* (Plate I-M) during the Heinrich HS1 and early Bølling-Allerød intervals, indicating areas with very dry conditions, and Chenopodiaceae:*Artemisia* ratios indicate drier conditions as well. The AP taxa indicate a continuing presence of oro-Mediterranean forest with relatively high summer precipitation, while the NAP taxa indicate an expansion of steppe environments with <600 mm of annual rainfall.

Pollen Assemblage Zone 3 (~12,700 – 11,500 cal. yr BP; Figure 3.8) corresponds to the Younger Dryas event in core MAR02-89P and is dominated by non-arboreal pollen.

AP comprise ~30% of the total pollen and there is a significant decrease in *Pinus* and reciprocal increase in evergreen *Quercus* (signifying warmer and drier summers). *Corylus* along with *Salix* and *Alnus* reappear in low amounts during the Younger Dryas, perhaps indicating the return of wet conditions and gallery forest in river valleys. There is a small percentage of coniferous forest taxa (*Betula*, *Abies*, and *Acer* (Plate I-R)), which also indicates wet conditions (Mudie et al., 2002b). *Castanea* pollen returns during the Younger Dryas, possibly indicating the presence of coastal refugia with wetter and warmer conditions within the region. However, NAP comprise ~70% of the total pollen and are dominated by *Artemisia*, with a strong presence of Chenopods and Poaceae (Plate I-K, -L), and low amounts of *Ephedra*. The Chenopodiaceae:*Artemisia* ratios indicate wetter conditions than during the Heinrich HS1 time interval. Overall, the large amount of NAP indicates expanded steppe land, while the limited AP represent smaller amounts of oro-Mediterranean woodland characterized by ~300 – 600 mm annual rain (Mudie et al., 2002b).

Pollen Assemblage Zone 2 (~11,500 – 8,000 cal. yr BP; Figure 3.8) has approximately 50% AP, with evergreen and deciduous *Quercus* being the dominant taxa, along with some components of a mesic euxinian forest vegetation, including *Fagus, Fraxinus*, *Ulmus* (Plate I-T), and *Carpinus* (Plate I-U) (Mudie et al. 2002b). *Castanea* pollen is found in association with *Fagus* and *Tilia*, indicating warm and wet conditions (Krebs et al, 2004). The increasing percentages of *Corylus*, *Salix*, and *Alnus* suggest locally wet conditions and additional development of gallery forests. Caner and Algan

(2002) consider that the upland broad-leaved conifers and deciduous trees found in this zone combined with *Olea* (Plate I-BB) are indicative of a Mediterranean climate consisting of mild and humid winters with warm and dry summers, and they interpret the presence of *Alnus*, *Acer*, and *Tilia* as indicating Black Sea inflow, whereas Mudie et al. (2002b) conclude that the early Holocene Marmara Sea environment supported mesic temperate forest. Low percentages of coniferous forests (*Pinus*, *Betula*, *Abies*, *Acer*) as reflected in the pollen from core MAR02-89P also indicate wet conditions within pollen zone 2. NAP are present in approximately equal amounts to AP with a strong presence of *Artemisia*, Chenopodiaceae, and Poaceae, which indicate some areas of steppe grassland within the region. The Chenopodiaceae:*Artemisia* ratios indicate that this was a wetter period than during the development of pollen zone 3, which seems to be in agreement with the increased quantity of AP taxa occurring within this zone. This pollen assemblage zone could indicate a broad leaf deciduous mesic euxinian forest receiving greater than 600 mm of annual rainfall, interspersed with drier steppe areas. In this zone pollen grains are filled with high amounts of organic matter, and pyrite, the latter indicating strongly reducing bottom conditions associated with increased stratification and/or TOC accumulation.

Caner and Algan (2002) determined zones representing the last glacial and interglacial paleoclimate changes for sparsely-dated cores from both eastern (core KL97) and western basins (core DM-13; Figure 3.2). Last glacial Zone D spanning the Y2 tephra layer (Caner and Algan, 2002) showed increasing steppe-herbs such as *Artemisia*

in core KL97 and Chenopods in core DM13, indicating cold and arid conditions, similar to assemblage zone 4 of core MAR02-89P. Holocene zone B of Caner and Algan (2002) contains temperate Mediterranean scrub pollen taxa indicating a warmer and more humid in winter climate similar to the zone 3 identified in core MAR02-89P for the Younger Dryas. Total abundance of pollen was found to be at its maximum during the development of sapropels in both core MAR02-89P and cores studied by Caner and Algan (2002).

In core MAR02-89P, the presence of *Asplenium*, *Equisetum*, Polypodiaceae, *Anthoceros* and mosses and lycopods during the Heinrich HS2 stadial time interval indicate wet, open and relatively mild conditions for this pleniglacial period, in agreement with data from core MAR94-05 (Figure 3.2; Mudie et al, 2002b). A peak in Polypodiaceae fern spores at the end of the last glacial maximum indicates prevailing wet and temperate conditions that decrease during the Heinrich HS1 stadial and early Bølling-Allerød intervals. There is a peak of *Pteridium* during the Heinrich HS1 stadial interval, which may indicate a period of fires. During the start of the Bølling-Allerød time interval, the appearance of *Equisetum* supports the presence of wet and sandy soils (Figure 3.13). Polypodiaceae spores are present in the Younger Dryas with and without a perine (expanded outer wall layer), indicating moist conditions and better preservation of these palynomorphs. The early Holocene record with a peak of *Dryopteris* ferns is indicative of high rainfall supporting deciduous forest, and interspersed open, cleared, sandy soils supporting *Equisetum*, *Pteridium*, *Polytrichum*-type mosses and lycopods.

There is no unequivocal indication of Neolithic influence in core MAR02-89P. The presence of *Pteridium* could indicate cleared land from man-made fires and/or grazing, but the low occurrence of bracken fern spores and absence of fungal spores indicating animal herding most likely implicates forest fires as the controlling environmental factors (Figure 3.13). Pollen data do not show high percentages of walnuts (*Juglans*), olives (*Olea*), and pistachios (*Pistacia*, Plate I-W) that indicate arboriculture. Percentages of large Poaceae grains that might indicate cereal-growing are sporadic and low. On the other hand, the reduced amount of AP compared to the average for the pleniglacial zone 5 could indicate the start of some forest/woodland clearance by the Holocene.

4.5 MAR02-89P Dinoflagellate Cyst (Dinocyst) Data

Dinoflagellate cyst concentrations were quite low from ~30,000 – 18,000 cal. yr BP, and were highest during accumulation of the sapropel layers, while peaks in the number of reworked cysts were common during the last glacial maximum, prior to the Heinrich HS1 stadial time interval, and during the Holocene increases in dinocyst concentrations (Figure 3.15). The dominant Quaternary species throughout core MAR02-89P are *S. cruciformis*, *P. psilata*, *O. centrocarpum*, and *L. machaerophorum* (both long and short spine forms have been combined in the graphs; Figures 3.14, 3.15 and 3.16). *S. cruciformis* is an endemic Caspian-Pontic Sea species that generally characterizes lower salinities in the Marmara Sea region and when found in association with *P. psilata*

without *L. machaerophorum* is considered to indicate brackish water with a salinity of <7 – 10 psu (Mudie et al., 2001; Mudie et al., 2004; Mertens et al., 2012). *O. centrocarpum* is considered a cosmopolitan species and is most common in cold to temperate regions with nutrient-enriched surface waters (Marret and Zonneveld, 2003). This species prefers sea surface temperatures (SST) ranging from -2.1°C (winter) to 29.6°C (summer) and sea surface salinities (SSS) of 16.1 psu (spring) to 36.8 psu (summer), but is not restricted to these conditions. *O. centrocarpum* can live in lower salinities where reduced development of its processes is expressed as shorter length (Marret and Zonneveld, 2003), and many specimens in core MAR02-89P show this feature. *L. machaerophorum* is a temperate to tropical, coastal euryhaline species, most commonly found in brackish to marine SSS of 16.9 psu (spring) to 36.7 psu (summer) and a SST of -1.5°C (winter) and 29.1°C (summer) but is most common in regions with summer temperatures exceeding 12°C. Similar to *O. centrocarpum*, *L. machaerophorum* can survive in lower salinities with a reduction in process length also being observed, e.g. in the Caspian Sea with SSS of 7 – 13 psu (Marret et al., 2004).

Two major dinocyst assemblage zones were determined from the dinocyst data in core MAR02-89P (Figure 3.15). The lower zone (D2) is dominated by *S. cruciformis* and *P. psilata* indicating low salinities but with a consistent presence of *L. machaerophorum*. This most likely means that *S. cruciformis* and *P. psilata* are present at their upper salinity limits, while *L. machaerophorum* is present at the lower end of its preferred salinity range and has reduced process lengths (~4 – 7 μm). The SSS must be at least >7 – 10 psu for *L.*

machaerophorum to survive (Mertens et al., 2012). The winter temperature of this zone is most likely cool due to the presence of *S. cruciformis* and *P. psilata*. The upper dinocyst assemblage zone D1 is dominated by *O. centrocarpum* with a strong presence of *L. machaerophorum* most likely indicating an increase in salinity and more eutrophic surface waters (Figure 3.15; cf. Marret and Zonneveld, 2003). Zone D1 also includes several other warm water taxa *Tectatodinium pellitum*, *S. mirabilis* and *P. stellatum* indicating an increase in surface water temperatures as well as salinity (Marret and Zonneveld, 2003).

The pleniglacial dinocyst assemblage subzone D2c (Figure 3.15) has a strong presence of *S. cruciformis*, *P. psilata*, and *L. machaerophorum*, that together indicate surface salinities of minimum 7 to maximum ~13 psu (Mertens et al., 2012) in contrast to values of around 15 psu estimated for planktonic foraminifers in a deeper water core MAR94-05P from the central Marmara Sea (Mudie et al., 2007). It is interesting to note the presence of heterotrophic *Brigantedinium* spp. with *C. rugosum* in deposits contemporaneous with Heinrich HS2 stadial time interval: *C. rugosum* may indicate a period of spill over from the Black Sea into the Marmara Sea. The main dinocyst taxa are today restricted to the Caspian and Black Seas and most likely represent cool to temperate conditions (~0 – 10˚C) (Marret et al., 2009), possibly with high seasonal temperature contrasts (Londeix et al., 2009).

The last glacial maximum dinocyst assemblage zone D2b (Figure 3.15) has the same dominant species as Zone D2c, but also a strong presence of *O. centrocarpum*. *S.*

cruciformis and *P. psilata* indicating lower salinities (up to ~13 – 17 psu; Mudie et al., 2001; Mertens et al., 2012), with the upper salinity range for these species coinciding with the lower salinity range for the cosmopolitan species in this zone. The sporadic presence of *C. rugosum* may indicate periodic additional inflow from the Black Sea. Temperatures appear similar to zone D2c, ranging from cool to temperate conditions (Marret et al., 2009), and *Nematosphaeropsis labyrinthus* (Plate II-R) is present. There are common pre-Quaternary cysts of *Homotryblium plectilum* (Plate II-Q), *Apteodinium*, and *Wetzeliella* sp. (Plate II-P) possibly of Oligocene age similar to those described by Bati and Sancay (2007). These might be associated with melt water from advancing glaciers in the western Pontic Mountains ~24,000-19,000 cal. yr BP (Sarıkaya et al., 2009). Presence of *Tuberculodinium vancampoae* (Plate II-O) and *Polyspheridium zoharyi* in D2b is therefore interpreted as the result of reworking. This is in contrast to Londeix et al. (2009) who described *T. vancampoae* and *P. zoharyi* as in place for core MD01-2430 inferring warm climatic conditions during the Marmara Sea last glacial maximum, in contrast to globally reported cool climatic conditions.

Dinocyst assemblage subzone D2a correlating with the Heinrich HS1 stadial and early Bølling-Allerød time intervals (Figure 3.15) is dominated by *S. cruciformis* and *P. psilata* with a noticeable disappearance of *L. machaerophorum* and a low occurrence of *O. centrocarpum* at the base of the zone; absence of these taxa during the early Bølling-Allerød interval indicates a decrease in salinity to less than ~7 – 10 psu. All taxa within the subzone D2a have broad temperature requirements and most likely SST within the

region was temperate (Marret and Zonneveld, 2003). The decrease in marine dinocyst species from ~19,500 – 14,850 cal. yr BP might indicate increased inflow of low-salinity water from the Black Sea into the Marmara Sea. Londeix et al. (2009) also indicate a strong presence of *S. cruciformis* and a decrease in *O. centrocarpum*, with a continued presence of *C. rugosum*; they interpreted continued presence of tropical *T. vancampoae* as indicating warm SST in the core MD01-2430 during the Heinrich HS1 stadial; this interpretation stands in contrast to the colder, drier climate conditions recorded in the core MAR02-89P pollen assemblage zone 4.

The Younger Dryas dinocyst assemblage subzone D1b (Figure 3.15) shows a transition to *O. centrocarpum* being the dominant species and a return of *L. machaerophorum*. Both taxa have similar living requirements and occur with *S. mirabilis*, which is found in marine environments with SSS exceeding ~28.5 psu (Marret and Zonneveld, 2003). This suggests an increase in salinity and most likely indicates well established Mediterranean water inflow into the Marmara Sea. However, *S. cruciformis* and *P. psilata* are still present (in low abundance) within this zone indicating SSS was ~13 – 17 psu (Mudie et al., 2001; Mertens et al., 2012), and some species indicate cold to temperate conditions (*Spiniferites elongatus*, *O. centrocarpum*). In the western basin, core MD01-2430 shows *S. cruciformis* and *O. centrocarpum* in equal amounts (~20%) and the reappearance of *L. machaerophorum* in the Younger Dryas interval, along with a strong presence of *Pyxidinopsis* species. At this deep water site, Londeix et al. (2009) see the reappearance of heterotrophic taxa during the Younger Dryas interval but this does

not occur in the shallower location of core MAR02-89P until the subzone D1a in the early Holocene although sapropelic sediments are favorable for preservation of thin-walled peridinioids.

In the early Holocene dinocyst assemblage subzone D1a (Figure 3.15) *S. cruciformis* and *P. psilata* percentages continue to decrease while *O. centrocarpum* increases. The presence of brackish to fully marine taxa *S. elongatus*, S. *mirabilis* and *Protoperidinium stellatum* indicate Aegean Sea sources. This assemblage change indicates increasing SSS (~13 – 17 psu) becoming similar to present day surface waters at ~17 – 20 psu (Figure 1.2), and SST was most likely increasing from temperate to subtropical because of the presence of some thermophilic species (*Protoperidinium stellatum*, *S. mirabilis*, *T. pellitum*; Marret and Zonneveld, 2003). Occurrence of *S. ramosus*, *S. elongatus*, *T. pellitum*, *P. stellatum*, *O. centrocarpum*, and *L. machaerophorum* are all often related to eutrophic surface water conditions (Marret and Zonneveld, 2003). *O. centrocarpum* dominates the early Holocene of core MD01-2430, with a strong presence of *L. machaerophorum*, *S. ramosus*, and *Spiniferites belerius* and with continued strong occurrence of heterotrophic taxa.

Using geochemical proxies, Vidal et al. (2010) determined a maximum of dinoflagellate production (as dinosterol) as well as TOC occurring at ~10,000 cal. yr BP. The maximum abundance of dinocysts occurs at ~10,800 cal. yr BP in MAR02-89P, with maximum TOC values (~2.5%) occurring from ~10,000 – 8,800 cal. yr BP. Menot and Bard (2010) suggest a huge methane release that lasted ~3000 years during the last

deglaciation, as revealed by depleted carbon isotopic values. They also found an increase in bacteria (hopanoid) concentrations within the Marmara Sea associated with deep temperature changes indicating the dissociation of methane hydrates during the last deglaciation. At the onset of the Heinrich HS1 stadial and early Bølling-Allerød intervals (~18,000 – 14,850 cal. yr BP), core MAR02-89P begins to show a small increase in dinocyst abundance until the hiatus, potentially influenced by a release of methane causing a decline in bottom-water oxygen contents and leading to better preservation in the Marmara Sea over this period of time.

4.6 MAR02-89P Non-Pollen Palynomorph (NPP) Data

Pediastrum is a common non-pollen palynomorph in core MAR02-89P (Figures 3.17 and 3.18). Blooms of *Pediastrum* can be triggered by increases of phosphate and their development is commonly attributed to inflow of river water and wetter climates (Londeix et al., 2009; Mudie et al., 2011). *Pediastrum* levels in core MAR02-89P peak after the Heinrich HS2 stadial time interval (~24,000 cal. yr BP) and after the accumulation of the Y2 ash layer (~21,500 cal. yr BP). Throughout the Heinrich HS1 stadial and early Bølling-Allerød intervals (~18,500 – 14,850 cal. yr BP) there is a continuous presence of freshwater *Pediastrum* spp. although the Chenopodiaceae:*Artemisia* ratio indicates regionally drier conditions (Figure 3.11). This suggests the *Pediastrum* was transported into Marmara Sea from the Black Sea in

overflow of fresh water resulting from discharge of melt water from distant Eurasian icesheets. However, there may also have been some periodic melting of Pontic Mountain glaciers that resulted in increased river water flow directly into the Marmara Sea. *Pediastrum boryanum* characterizes salinities up to 6 – 8 psu. *Pediastrum* is present throughout the core with *P. boryanum* dominating from the base of the core to the unconformity (~30,000 – 14,850 cal. yr BP). *P. simplex* is dominant from ~12,700 cal. yr BP until its disappearance at ~9,000 cal. yr BP. *Pediastrum* is also found throughout the western basin core MD01-2430 of Londeix et al. (2009), with highest peaks occurring during the Heinrich HS1 stadial, Bølling-Allerød and beginning of the Younger Dryas time intervals in contrast to the earlier peaks found in core MAR02-89P. In core MAR98-12P (Mudie et al., 2002a) from the southwestern Marmara Sea at -549 m water depth, *Pediastrum* is also found throughout most of the core down to ~18,000 cal. yr BP with its highest peaks occurring at ~11,000 cal. yr BP at the end of the Younger Dryas time interval.

Staurastrum tetracerum (a desmid, green algae) is an indicator of fresh water (Bellinger and Sigee, 2010). *Cymatiosphaera*, a prasinophyte, is found today in brackish to low salinity marine water, and appears to be a euryhaline organism (Mudie et al., 2011). The presence of *S. tetracerum* indicates outflow of low salinity Black Sea water, with an initial appearance during the Younger Dryas at ~12,000 cal. yr BP, followed by a large increase in abundance at ~10,000 cal yr BP. *Cymatiosphaera* first appears in the low salinity interval ~24,000 – 22,000 cal. yr BP in MAR02-89P but disappears after

~22,000 cal. yr BP. Londeix et al. (2009) reported that this taxon occurs in the western basin during the Bølling-Allerød (which is very incomplete in core MAR02-89P), and it is ubiquitously present throughout the Younger Dryas interval and shortly after, reappearing in the late Holocene, which is missing from the MAR02-89P core. The *Multiplicasphaeridium*-type acritarch is characteristic of glacial stage sediments of the Black Sea region and also occurs in Holocene to Recent sediments of channels in the Canadian Arctic (Pienkowski et al., 2011). This taxon is present from the base of core MAR02-89P with highest peaks during the Heinrich HS2 stadial time interval and almost complete absence at the beginning of the Heinrich HS1 stadial and early Bølling-Allerød interstadial time intervals, with only a small peak occurring just before the hiatus. Londeix et al. (2009) found a continuous presence of *Multiplicasphaeridium*-type spp. from the last glacial maximum until the Bølling-Allerød, absence during the Younger Dryas, and a small peak at the beginning of the Holocene.

Glomus spp. is an indicator of soil erosion and records periods of river runoff (Mudie et al., 2002, 2004). *Glomus* is found throughout core MAR02-89P, with highest peaks during the Heinrich HS2 stadial, possibly due to glacial melt waters increasing erosion. Foraminiferal linings are limited in core MAR02-89P, occurring during the Heinrich HS2 stadial time interval, just after the Y2 ash layer, and toward the end of the Younger Dryas event. Planktonic foraminifera may indicate a sustained marine connection but foraminiferal linings are very susceptible to oxidation (Kotthoff et al., 2008) and they have a variable occurrence in core MAR02-89P although Londeix et al.

(2009) found them throughout the Younger Dryas and Holocene sections of their deep water core MD01-2430 from the western basin. Foraminiferal lining abundance varies throughout the M1 sapropel of core MAR02-89P and then increases, most likely indicating a sustained marine connection in addition to less oxidizing bottom water conditions. Neorhabdocoel worm egg capsules are sporadically present in sediments deposited during the Heinrich HS2 stadial and toward the end of the Heinrich HS1 stadial, early Bølling-Allerød interstadial interval, and at the end of the Younger Dryas interval. Some of these are freshwater organisms, which may be present due to pulses of Black Sea water spilling over the Bosphorus Strait into the Marmara Sea; others, however are marine and are quite common in modern surface sediments of the Marmara Sea (Mudie et al., 2011). *Botryococcus* is present during time intervals coincident with the Heinrich HS2 and HS1 stadial time intervals, and the end of the Younger Dryas interval (10,500 cal. yr BP) and could indicate periods of high organic-matter deposition during intervals of low salinity.

Figure 4.1 summarizes the environmental and oceanographic changes that have been interpreted for the Late Pleistocene – early Holocene using selected pollen ratios (Figures 3.10 and 3.11), Caspian-Pontic indicator dinocysts (Figures 3.14 and 3.15) and the colonial aquatic algae, *Pediastrum* and *Botryococcus* (Figures 3.17 and 3.18) data. The Chenopodiaceae to *Artemisia* ratios provide a humidity index (wetter versus drier) for core MAR-02-89P, and the deciduous to evergreen *Quercus* ratios provide a climate

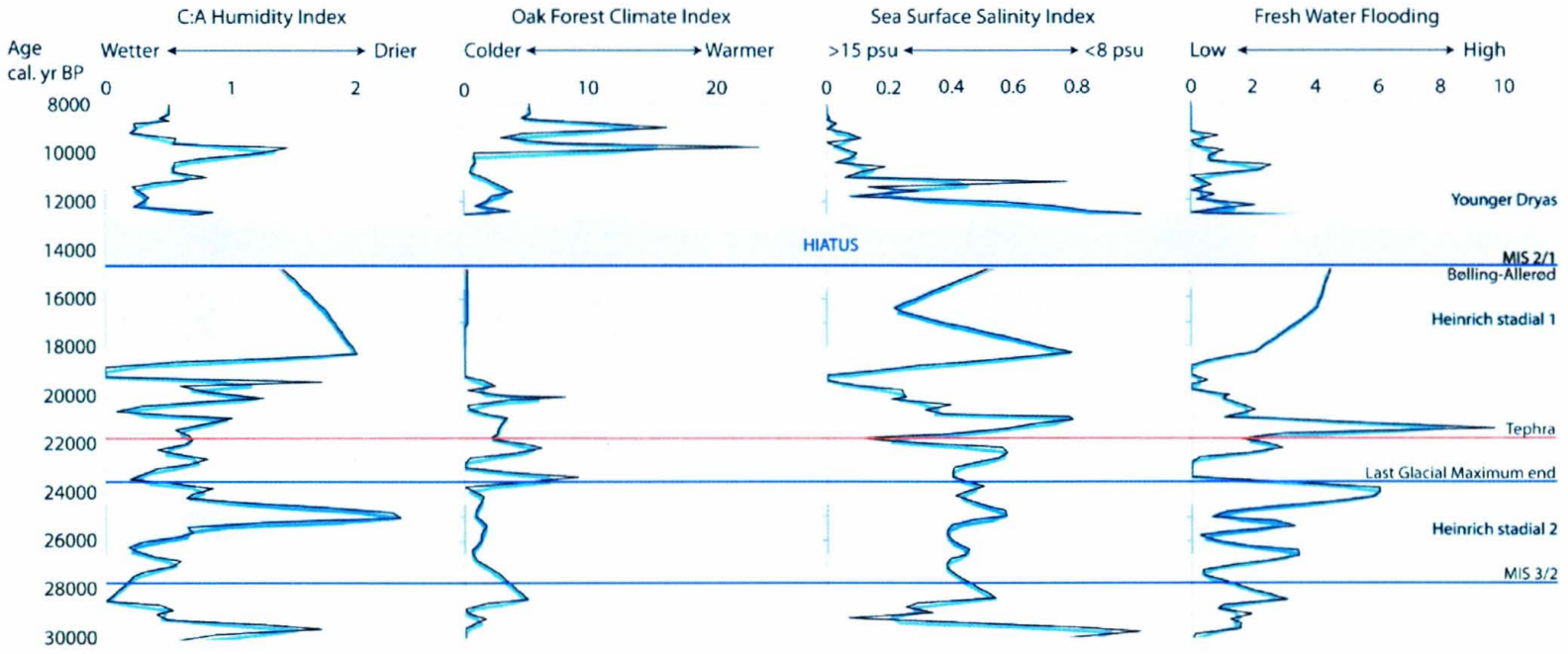

Figure 4.1: Summary of environmental and oceanographic changes (black) for core MAR02-89P with two point running averages also shown (blue). Significant time events recognized elsewhere in the Northern Hemisphere are shown: Younger Dryas, Bølling-Allerød, Heinrich stadial events (HS1 and HS2), the Y2 ash layer (tephra), last glacial maximum, Marine Isotope Stages (MIS 3/2 and MIS 2/1), and a hiatus (brown) indicates a break in sedimentation.

index (colder versus summer warmer). Sea surface salinity (SSS) is qualitatively determined by combining the *P. psilata* and *S. cruciformis* percentages: high percentages indicate lower salinities (~8 psu) and lower percentages indicate higher salinities (~15 psu). Fresh water flooding is determined by combining the abundance of *Pediastrum* spp. and *Botryococcus*, with increased abundance indicating higher amounts of flooding.

4.7 Correlation

Both pollen and dinocyst assemblages zones, along with known time events from the North Atlantic and Mediterranean regions are shown to allow comparison of core MAR02-89P with the Marmara Sea cores from Caner and Algan (2002), Londeix et al. (2009), and Mudie et al. (2004) (Figure 4.2). The Y2 ash layer can be correlated from the core DM13 (~21,100 cal. yr BP) to core MD01-2430 (~21,400 cal. yr BP) to core MAR97-11 (~21,000 cal. yr BP) and core MAR02-89P (~21,800 cal. yr BP). Apparent age differences are ascribed to analytical, calibration and interpolation errors.

Mudie et al. (2004) determined two dinocyst assemblage zones for the Marmara Sea: zones D2 and D1. Their D2 has similar dominant species and can be correlated to similarly named zone D2 of MAR02-89P (this thesis). The dominant species are *S. cruciformis* and *P. psilata*, with presence of *O. centrocarpum* and *L. machaerophorum*. Subzone D1a of MAR02-89P can be correlated with Mudie et al. (2004) subzone D1a

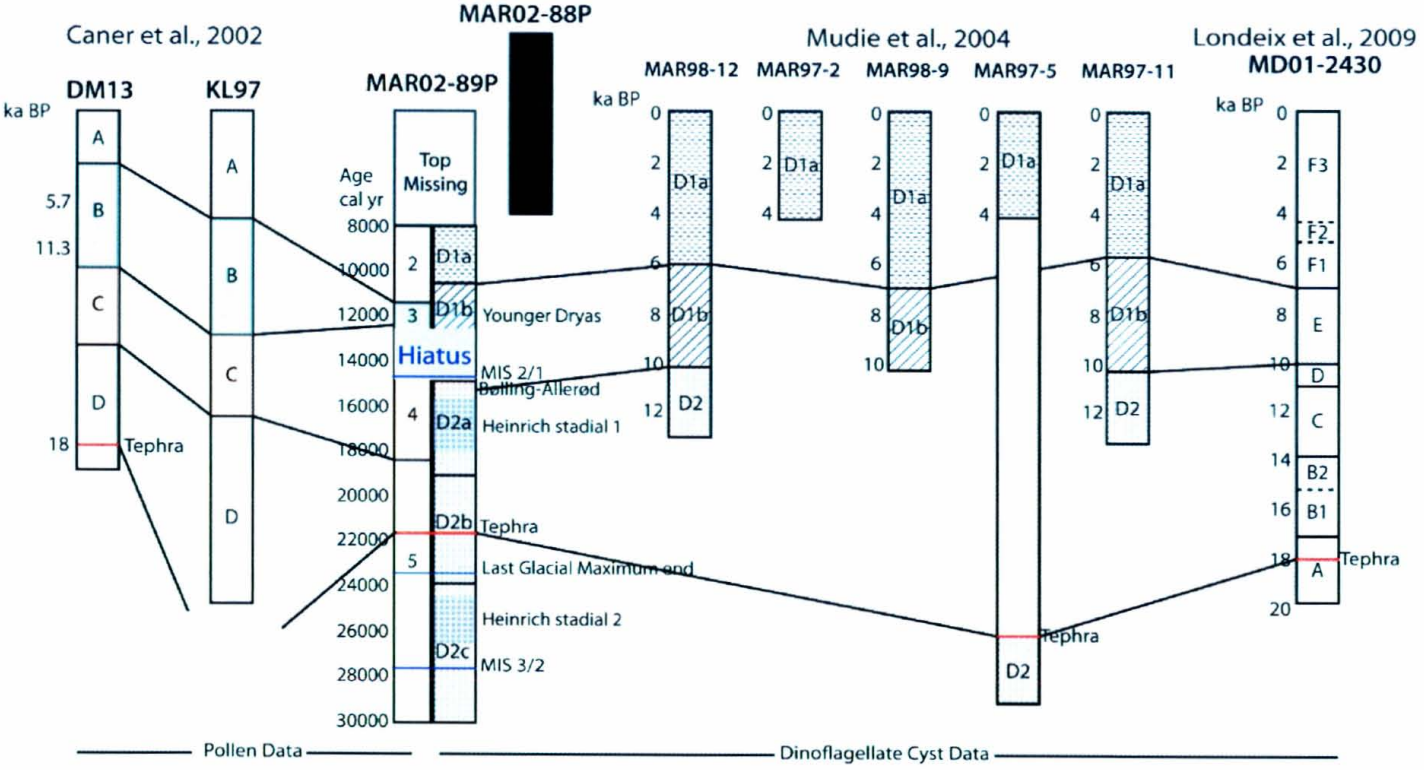

Figure 4.2: Correlation of cores in the Marmara Sea from Caner and Algan (2002), Londeix et al. (2009), Mudie et al. (2004), MAR02-89P. Published core ages are shown in conventional radiocarbon years (= ka BP), MAR02-89P shown in calibrated ages with zero reservoir age (=cal. yr BP), with colours used to correlate pollen assemblage zones and similar gradient styles for dinocyst assemblage zones.

which has a transition to *L. machaerophorum* and *O. centrocarpum* as dominant species along with low amounts of *S. cruciformis*, *P. psilata*, *S. ramosus*, *Brigantedinium* spp., and *S. mirabilis.*

Pollen zone C of Caner and Algan (2002) is correlated to zone 4 of core MAR02-89P. In core MAR02-89P, this zone is represented by an increase in *Artemisia* and chenopods indicating cold and arid conditions during the Heinrich HS1 stadial time interval. Caner and Algan (2002) determined their zone B to be represented by a warm and humid climate with temperate Mediterranean pollen taxa similar to those found in zone 3 of core MAR02-89P. Dinocyst zone B1 and A of Londeix et al. (2009) occur during the last glacial maximum and contain assemblages indicating SSS of ~7 – 14 psu that can be correlated to subzone D2b of core MAR02-89P. Zone E of Londeix et al. (2009) comprises Holocene assemblages similar to but more diverse than those in dinocyst subzone D1 of core MAR02-89P.

4.8 MAR02-89P Timing of Marmara Gateway Reconnection

Comparison of results from geochemistry, dinocysts and selected non-pollen palynomorphs in core MAR02-89P (Figure 4.3) makes it possible to estimate the sources of water flowing into the Marmara Sea from ~30,000 to 8,000 cal. yr BP. The TS/TOC data suggest five Black Sea outflow events from ~28,500 – 8,000 cal. yr BP. The

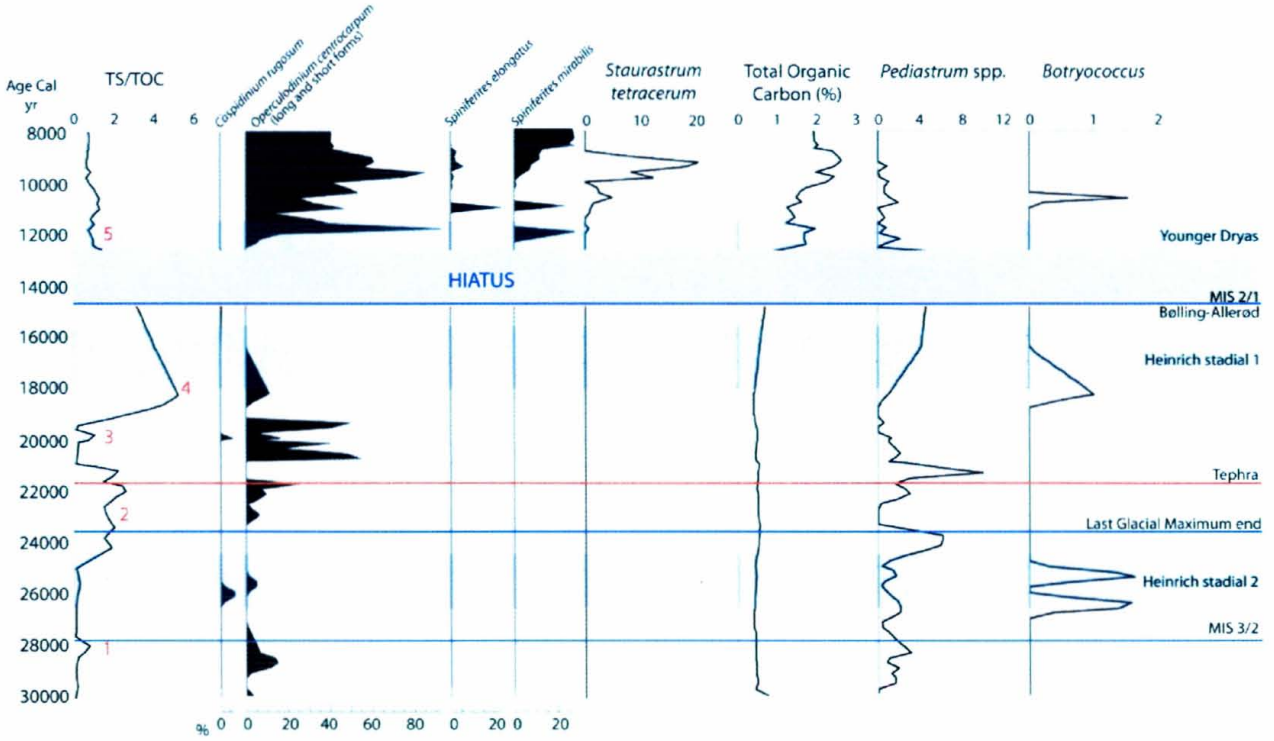

Figure 4.3: Summary diagram of core MAR02-89P using geochemistry, dinocyst data, and non-pollen palynomorph data to determine Aegean and Black Sea influence on the Marmara Sea with red numbers (1-5) indicating Black Sea flooding events. Significant time events recognized elsewhere in the Northern Hemisphere are shown: Younger Dryas, Bølling-Allerød, Heinrich stadial events (HS1 and HS2), the Y2 ash layer (tephra), last glacial maximum, Marine Isotope Stages (MIS 3/2 and MIS 2/1), and a hiatus (brown) indicates a break in sedimentation.

presence of large, sustained outflow of Black Sea water could also coincide with the presence of Caspian-Pontic dinocysts (*C. rugosum* and *I. caspiensis*) during the Heinrich HS2 stadial and around 20,000 cal yr BP. *O. centrocarpum* is present from ~29,000 – 17,000 cal. yr BP and appears to occur during TS/TOC peaks 1 through 4 (Figure 4.3). The presence of *Pediastrum* spp. and low salinity *Botryococcus* most likely indicate Black Sea water inflow to the Marmara Sea.

After the hiatus from ~14,850 – 12,700 cal. yr BP, the perched basin experienced the development of sapropelic sediments and sapropels. This event coincides with a decrease in low salinity dinocyst taxa (*S. cruciformis*, *P. psilata*) and increase in the marine dinocyst taxa and foraminiferal linings from the Younger Dryas interval to the top of the core at 8,000 cal. yr BP. The presence of freshwater *S. tetracerum* from ~11,500 – 8,000 cal. yr BP may indicate local river water inflow or Black Sea inflow. The appearance of heterotrophic dinocyst taxa (*Brigantedinium* spp. and *P. stellatum*) from ~11,000 – 8,000 cal. yr BP indicates increased inflow of Mediterranean waters into the Marmara Sea, accompanied by increased presence of dissolved organic matter and phytoplankton, e.g. diatoms that are the food sources of heterotrophic dinoflagellates. By the end of the Younger Dryas interval, it appears that the Marmara Sea was receiving water from both the Aegean and the Black seas.

Palynomorphs and %TOC values in core MAR02-89P appear to record periodic Black Sea outflow to the eastern Marmara Sea from ~30,000 – 14,850 cal. yr BP. This

interpretation is in agreement with Vidal et al. (2010) who used alkenone geochemistry to suggest the presence of Black Sea water in the western Marmara Sea from ~ 23,000 cal. yr BP until the Bølling-Allerød (~14,650 – 12,900 cal. yr BP). Aksu et al. (1999b) speculated that there was no connection between the Aegean, Marmara, and Black Seas during the last glacial maximum (~23,000 cal. yr BP), but did not have a sediment record older than ~18,000 cal. yr BP. Eriş et al. (2011) indicate a pleniglacial disconnect between the Aegean, Marmara, and Black seas from ~30,000 to 18,000 cal. yr BP, followed by Black Sea inflow into the Marmara Sea from ~18,000 to 15,700 cal. yr BP and then disconnection again at the onset of the Younger Dryas interval (~13,800 cal. yr BP). McHugh et al. (2008) determined the Marmara Sea to be a lake from ~15,500 – 12,000 cal. yr BP with cold and dry conditions that warmed during the Bølling-Allerød, leading to a drawdown of both Black Sea and Marmara Sea waters (to -85 m below sea level) and a rapid marine incursion into the Marmara Sea at ~12,000 cal. yr BP. Eriş et al. (2011) record an exchange between the Marmara and Aegean seas and Black Sea inflow from ~13,400 – 12,400 cal. yr BP. Data from core MAR02-89P is in agreement with Vidal et al. (2010), and Eriş et al. (2011) that Black Sea inflow occurred from ~18,000 – 14,850 cal. yr BP. Aksu et al. (1999b), Vidal et al. (2010), and Eriş et al. (2011) are all in agreement that Mediterranean water penetrated the Dardanelles Strait during the MAR02-89P hiatus (~14,850 – 12,700 cal. yr BP). The Younger Dryas interval of core MAR02-89P appears to start with Aegean Sea inflow, concurrent with Black Sea inflow similar to what was determined by Londeix et al. (2009) and Vidal et al.

(2010).

Aksu et al. (1999b) determined that the Aegean Sea breached the Dardanelles Strait during the late Bølling-Allerød (~13,500 cal. yr BP). Vidal et al. (2010) found Sr isotopic evidence for an earlier incursion of the Mediterranean Sea into the Marmara Sea during the Bølling-Allerød (~14,700 cal. yr BP). Mediterranean water penetrated into the Marmara Sea increasing SSS until ~ 9,000 cal. yr BP when a significant amount of Black Sea outflow began, apparently indicating a late full and open connection of the Aegean, Marmara, and Black Seas between ~9,000 – 8,000 cal yr BP. McHugh et al. (2008) recorded a Marmara Sea still stand at -65 m below the present-day sea level during the Younger Dryas soon after the marine incursion. Subsequent to the still stand, they interpreted inflow of Black Sea water at ~9,400 – 9,200 cal. yr BP, resulting in strong stratification.

The Eriş et al. (2011) model provides for no Black Sea inflow into the Marmara Sea from ~12,400 – 9,800 cal. yr BP, with the Aegean Sea filling the Marmara Sea and then entering the Black Sea at ~9,800 cal. yr BP. In core MAR02-89P pinstripe-laminated sapropel deposits rest directly on the unconformity and are dated to approximately 12,700 cal. yr BP, which is approximately the age assigned to the base of the M1 sapropel by Hiscott et al. (2007b) and is the accepted timing proposed by Londeix et al., (2009). Sediments in core MAR02-89P first reached TOC values >2% at ~12,000 cal. yr BP. Vidal et al. (2010) indicate the deposition of sapropels occurring from ~11,500 to 7,000 cal. yr BP, and Eriş et al. (2011) also associate sapropel development with the end of the

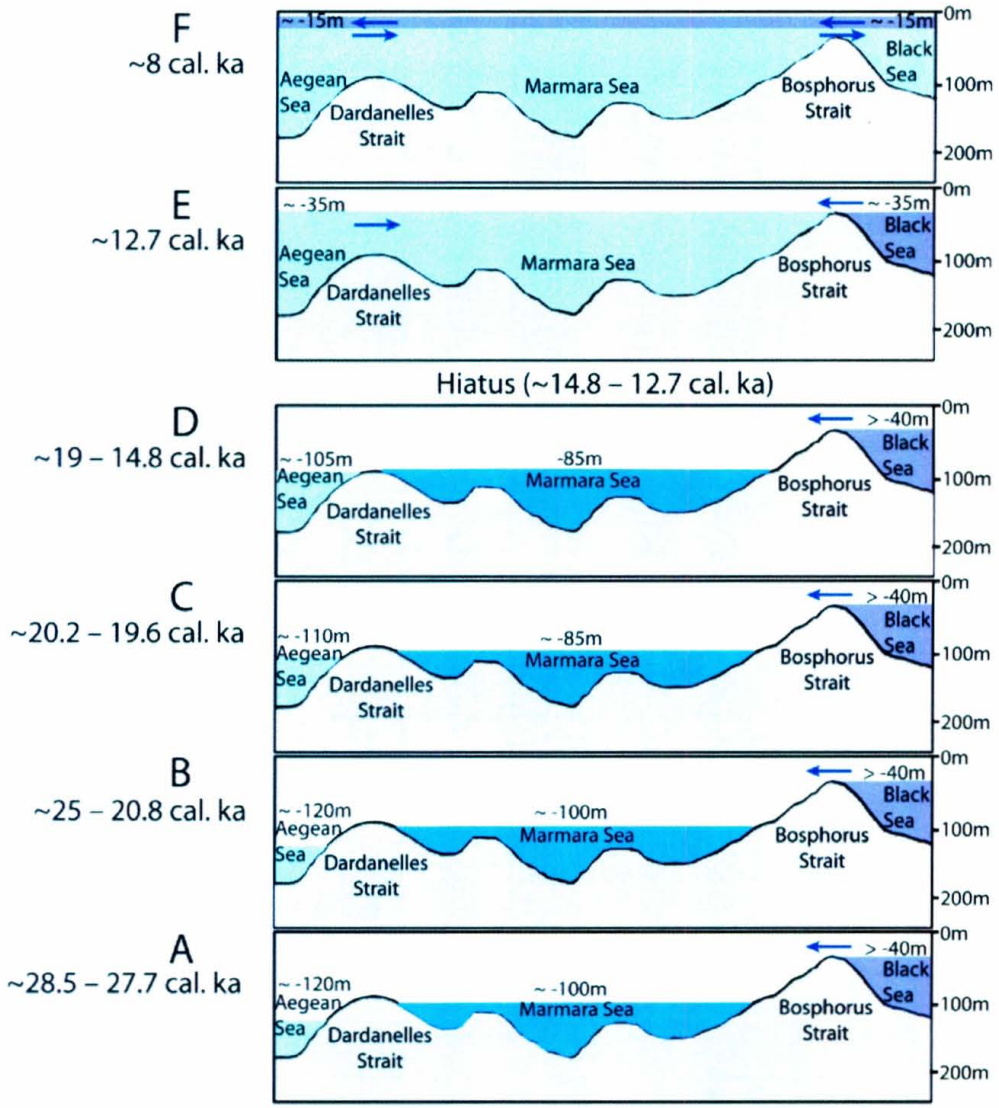

Figure 4.4: Cartoon reconnection diagram of Aegean (AS), Marmara (MS), and Black Seas (BS) determined from data of MAR02-89P, with arrows indicating water inflow. Aegean Sea water levels are from Peltier and Fairbanks (2006) and the Black Sea and Marmara Sea levels (A-D) are taken from Eriş et al. (2011), and Black Sea level in E is from Londeix et al. (2009).

Younger Dryas interval.

Figure 4.4 is a series of cartoons showing the reconnection of the Aegean, Marmara, and Black Seas based on the results of data collected from core MAR02-89P which are combined with Marmara Sea depth estimates of Eriş et al. (2011), the global relative sea level record of Peltier and Fairbanks (2006), and some salinity estimates from Londeix et al. (2009), and Vidal et al. (2010). Phase A represents the first Black Sea flood from ~28,500 – 27,700 cal. yr BP, with the Black Sea level >-40 m to permit spillover across the Bosphorus Strait into the Marmara Sea with a water level of ~-100 m (Eriş et al., 2011). There was no influence of Mediterranean water because global sea level was ~-120 m (Peltier and Fairbanks, 2006). Phase B represents the next Black Sea flood recorded in core MAR02-89P at ~25,000 – 20,800 cal. yr BP, with global sea level remaining at ~-120 m. The next inferred flooding phase (C) was shorter (~20,200 – 19,600 cal. yr BP), possibly contributing to a rise in Marmara Sea level which rose to ~-85 m (Eriş et al., 2011) when global sea level was at ~-110 m, still below the Dardanelles sill. Phase D may be a final Black Sea flood event recorded in core MAR02-89P, which occurred ~19,000 – 14,850 cal. yr BP when Marmara Sea level was still around ~-85 m (Eriş et al., 2011), and global sea level was at ~-105 m (Peltier and Fairbanks, 2006). However, the high TS/TOC ratio used to recognize this final proposed event might be an artifact created by a diagenetic overprint that could have affected TS in the first 100 cm below the unconformity. For example, when the unconformity was exposed at the seabed under sulphate-rich marine waters introduced by the reconnection with the Aegean Sea,

sulphate-reducing anaerobes could have colonized the older Upper Pleistocene sediments, fixing sulphur extracted from the overlying water column as iron monosulphide minerals. Therefore, it is possible that the sulphur in sediments dated to ~19,000 – 14,850 cal. yr BP is significantly younger than the detrital matrix fixed by diagenesis after the ~13,500 cal. yr BP reconnection of the Marmara Sea with the Aegean Sea. An expanded, conformable sedimentary section with detailed dinocyst and non-pollen palynomorph paleoceanographic data is needed to help decide which of these two interpretations is more reasonable.

Sediments with ages ~14,850 – 12,700 cal. yr BP are missing at the MAR02-89P core site, so the next phase E is assigned to an interval of time beginning at the end of the MAR02-89P hiatus at ~12,700 cal. yr BP, by which time the Aegean and Marmara seas were connected by a rise in global sea level to ~-35 m (Peltier and Fairbanks, 2006). Annual inflow from the Black Sea is estimated by Londeix et al. (2009) and Vidal et al. (2010) to have been about the same as the inflow of saline water from the Mediterranean Sea water. Phase F represents the youngest events recorded in core MAR02-89P at ~ 8,000 cal. yr BP, with a well established two-way flow between the Marmara and Black seas and a global sea level of ~-15 m, well above the early Holocene Dardanelles sill depth of -70 m.

Conclusions

The extended Upper Pleistocene section makes core MAR02-89P a special and detailed storehouse of information regarding the paleoclimatic and paleoceanographic history of the Marmara Sea. This core site, at -257 m present water depth, was never subaerially exposed during glacial sea level lowering. The site has an almost continuous pleniglacial – Holocene record with the exception of an unconformity resulting in a hiatus from ~14,850 – 12,700 cal. yr BP, possibly created by local sediment sliding and/or erosion under bottom currents. Because of this hiatus most of the Bølling-Allerød time interval (~15,000 – 13,000 cal. yr BP) is not recorded in core MAR02-89P and the earliest part of the Younger Dryas interval is absent. Palynological studies of pollen and terrestrial spores, dinoflagellate cysts and other non-pollen spores or plant remains have led to the following conclusions regarding six objectives set for this thesis.

1. Pollen-spore diagrams from core MAR02-89P provide the first detailed, well-dated, largely continuous high resolution record of vegetation changes for late pleniglacial (MIS 3 and 2) and late glacial stage (MIS 2/1) time intervals in the Marmara Sea up until the end of the Heinrich HS1 cold stadial and early part of the Bølling-Allerød time interval. The results give further insight into the question of whether the eastern Marmara Sea area might have been a last glacial maximum refugium for temperate European trees (cf. Caner and Algan, 2002). Palynomorph concentrations/g are low but pollen is fairly well preserved throughout the pre-Holocene sections of the core, with

abundance increasing at the onset of the MIS 2/1 transition when warmer summers coincided with development of sapropel layers. High TOC concentrations account for good pollen preservation during the Younger Dryas and early Holocene.

2. Four pollen assemblage zones were determined for core MAR02-89P. These record fluctuations in amount of pollen representing three vegetation types: oro-Mediterranean forests or woodland, steppe grassland, and mesic euxinian forests. These four pollen zones are correlative with other pollen records available for the Marmara Sea. Pollen zone 5 (~30,000 – 18,500 cal. yr BP) includes much of the Late Weichselian Pleniglacial interval (from MIS 3/2 at 27,800 to 14,700 cal. yr BP) and shows low influxes of pollen representing fluctuating oro-Mediterranean and steppe grassland or woodland corresponding to alternating wetter and drier cycles during the Heinrich HS2 stadial and the last glacial maximum (~23,000-19,000 cal. yr BP). These conditions were locally favourable for growth of the temperate tree *Castanea sativa* in refugia. Zone 4 (~18,500 – 14,850 cal. yr BP) spans the Heinrich HS1 stadial and the beginning of the Bølling-Allerød interstadial time intervals, and is also characterized by pollen indicating oro-Mediterranean-type forest or open woodland dominated by pine and evergreen scrub oak, with an increase in steppe vegetation. The climate was too dry/cold to support *C. sativa*. Pollen zone 3 (~12,700 – 11,500 cal. yr BP) includes the Younger Dryas event (from 12,800-11,500 cal. yr BP) and pollen indicates a cold interval of predominately steppe grassland with some presence of oro-Mediterranean forests persisting in montane areas. The pre-boreal to Holocene pollen assemblages in zone 2 (~11,500 – 8,000 cal. yr

BP) mainly indicate the establishment of broad-leaved mesic euxinian forests interspersed with areas of steppe or steppe forests persisting in drier valleys. Overall, the pollen records in the continuous MIS 3 through last glacial maximum marine sediments in core MAR02-89P provide proxy-records of refugia and tree migrations that are not available from most regional lakes of the Marmara Sea region.

3. From ~30,000 – 28,500 cal. yr BP, before the start of the late pleniglacial interval, the Marmara Sea was an isolated basin receiving pollen exclusively from local drainage. However, pollen assemblages do not change significantly during a number of inferred early post-glacial outflow events (floods) from ~18,000 – 14,850 cal. yr BP bringing meltwater from high-latitude drainage networks that filled the Black Sea to a point of overflow. Only *Picea* and *Abies* pollen appear to have increased with Black Sea overflow events, suggesting that most of the pollen at the site of core MAR02-89P is of local origin on the shores of the Marmara Sea and/or the Pontic Mountains.

4. Pollen assemblages in core MAR02-89P correspond to cold, wet climate conditions during the pleniglacial and last glacial maximum, but persistence of *Quercus* and *Castanea* leads to interpretation of warmer last glacial maximum conditions than those found in short cores by Mudie et al. (2002b). Colder, more arid conditions are indicated during the Heinrich HS1 stadial and Bølling-Allerød time intervals, by increased *Artemisia*, Chenopods, and *Ephedra*. The Younger Dryas interval consisted of relatively warmer conditions and more winter rainfall as marked by the expansion of *Artemisia* steppeland and a large increase in tree pollen influxes dominated by evergreen

Quercus woodland, similar to the findings of Caner and Algan (2002). Warm and humid conditions characterize the early Holocene with the expansion of broadleaf deciduous forests similar to the records of Mudie et al. (2007).

5. Dinoflagellate cyst abundance in core MAR02-89P is low throughout the Late Pleistocene and productivity does not start to increase markedly until the Younger Dryas. Two assemblage zones and several subzones are present. Dinocyst assemblage zone D2 occurs from ~30,000 to 14,850 cal. yr BP and generally consists of assemblages that mark low SSS (average ~10 psu) and cool to temperate SST and a large seasonal temperature range, but the last glacial maximum D2b subzone (24,000 – 19,500 cal. yr BP) has slightly elevated SSS (~13 – 17 psu). TS/TOC indicate two Black Sea floods occurring within this D2b subzone with *Caspidinium rugosum* present and spikes in *Pediastrum* spp. Most likely the increased SSS is due to evaporative conditions because of the freshwater palynomorphs indicating runoff both locally and from the Black Sea. There are relatively high percentages of several pre-Quaternary reworked species within this subzone that includes traces of the tropical-subtropical taxa *T. vancampoaeae* and *P. zoharyi*, which Londeix et al. (2009) described as in place in the western basin, hence in their interpretation of a warm climate during the last glacial maximum and Heinrich HS1 stadial in contrast to the published pollen evidence for a cold climate (Caner and Algan, 2002; Mudie et al., 2002b). In MAR02-89P, the occurrence of some well-preserved pre-Quaternary reworked dinocysts leads to the conclusion that the tropical spp. *Tuberculodinium* and *Polysphaeridium* are also reworked. The second dinocyst zone

(D1) represents the interval from ~12,700 to 8,000 cal. yr BP where presence of Mediterranean species indicates higher SSS (~13 – 17 psu), increasing upwards towards present day conditions. Greater diversity of heterotrophic species indicates higher nutrient availability and diatom food sources. Select dinocysts within this zone indicate SST ranging from cool to temperate, with some subtropical taxa occurring in subzone D1a following the Younger Dryas event during a decrease in dinocyst influxes.

6. Geochemical data, specifically TS/TOC ratios, suggest that five Black Sea flooding events are recorded in core MAR02-89P: one occurs just before the MIS 3/2 boundary, three are between the Heinrich HS2 and HS1 stadial time intervals, and the last flood event occurs during the Younger Dryas and extends into the early Holocene. Development of sapropels began during the Younger Dryas, just after the hiatus and continues into the early Holocene. There was an increase in marine production seen in the gradual increase of $\delta^{13}C$. The combined MAR02-89P palynological and geochemical data support the notion that melt waters transiting the Black Sea from farther north and east crossed the Bosphorus Strait in flood events from ~28,500 to 14,850 cal. yr BP. By the end of an ~2,160 year hiatus which ended at ~12,700 cal. yr BP, Mediterranean and Black Sea water masses were both influencing the Marmara Sea. The joint influence presumably began during the hiatus, but cannot be constrained by data from core MAR02-89P.

Future work to complement this research could involve completing the geochemical and palynological analysis of the neighboring 6.8 m-long core MAR02-88P from the

floor of the perched basin on the southeastern Marmara Sea slope that has Accelerator Mass Spectrometry shell ages of ~6,804 – 1,011 cal. yr BP. The extended Holocene section in core MAR02-88P would provide insight not available from core MAR02-89P. Splicing these records with results from other cores covering the time interval from 8,200 cal. yr BP to the Late Pleistocene Bølling-Allerød event would result in a high resolution, comprehensive picture of the Marmara Sea from the Late Pleistocene (~30,000 cal. yr BP) to the Present.

Bibliography

Abrajano, T., Aksu, A.E., Hiscott, R.N., and Mudie, P.J., 2002. Aspects of carbon isotope biogeochemistry of late Quaternary sediments from the Marmara Sea and Black Sea. Marine Geology 190:151 – 164.

Aksu, A. E., Abrajano, T., Mudie, P.J., Yaşar, D., 1999a. Organic geochemical and palynological evidence for terrigenous origin of the organic matter in Aegean Sea sapropel S1. Marine Geology 153:303 – 318.

Aksu, A.E., Hiscott, R.N., Yaşar, D., 1999b. Oscillating Quaternary water levels of the Marmara Sea and vigorous outflow into the Aegean Sea from the Marmara Sea-Black Sea drainage corridor. Marine Geology 153:275 – 302.

Aksu, A.E., Calon, T.J., Hiscott, R.N., 2000. Anatomy of the North Anatolian Fault Zone in the Marmara Sea, Western Turkey: Extensional basins above a Continental transform. Geological Society of America 10(6): 3 – 7.

Aksu, A.E., Hiscott, R.N., Mudie, P.J., Rochon, A., Kaminski, M.A., Abrajano, T., Yaşar, D., 2002a. Last glacial-Holocene sea surface temperature and salinity

variations in the Black and Marmara Sea: stable isotopic, planktonic foraminiferal and coccolith evidence. Marine Geology 190:119 – 149.

Aksu, A.E., Hiscott, R.N., Mudie, P.J., Gillespie, H., Yaşar, D., 2002b. Persistant Holocene outflow from the Black Sea to the eastern Mediterranean contradicts Noah's Flood hypothesis. GSA Today 12:4 – 9.

Aksu, A.E., Jenner, G., Hiscott, R.N., Işler, E.B., 2008. Occurrence, stratigraphy and geochemistry of Late Quaternary tephra layers in the Aegean Sea and the Marmara Sea. Marine Geology 252(3-4):174 – 192.

Alavi, S.N., 1988. Late Holocene deep-sea benthic foraminifera from the Sea of Marmara. Marine Micropaleontology 13:213 – 237.

Algan, O., Yalçin, M. N., Özdoğan, M., Yilmaz, İ., Sarı, E., Kirci-Elmas, E., Ongan, D., Bulkan-Yesiladalı, Ö., Yılmaz, Y., Karamut, İ., 2009. A short note on the geo-archeological significance of the ancient Theodosius harbour (İstanbul, Turkey). Quaternary Research 72 (3):457 – 461.

Batı, Z., Sancay, R.H., 2007. Palynostratigraphy of Rupelian sediments in the Mus

Basin, Eastern Anatolia, Turkey. Micropaleontology 53:249 – 283.

Bellinger, E.G., and Sigee, D.C. Freshwater Algae: Identification and Use as Bioindicators. 2nd Ed. New York: John Wiley & Sons, 2010.

Bennett, K., 2007. Psimpoll and pscomn programs for plotting and analysis. Version psimpoll 4.10. http://www.chrono.qub.ac.ul/psimpoll/psimpoll.html (accessed December 2011).

Beşiktepe, S. T., Sur, H. İ., Özsoy, E., Latif, M. A., Oğuz, T., and Ünlüata, Ü., 1994. The circulation and hydrography of the Marmara Sea. Progress in Oceanography 34:285 – 334.

Bottema, S., Woldring, H., Aytuğ, B., 1995. Late Quaternary vegetation history of Northern Turkey. Paleohistoria 17:53 – 143.

Çağatay, M.N., Görür, N., Algan, O., Eastoe, C., Tchapalyga, A., Ongan, D., Kuhn, T. and Kuşcu, I., 2000. Late glacial-Holocene paleoceanography of the sea of Marmara: timing of connections with the Meditteranean and the Black Seas. Marine Geology 167:191 – 206.

Caner, H., and Algan, O., 2002. Palynology of sapropelic layers from the Marmara Sea. Marine Geology 190:35 – 46.

Chepalyga, A.L., 2007. The late glacial great flood in the Ponto-Caspian basin. In: V. Yanko-Hombach et al. (Eds.). The Black Sea Flood Question: Changes in Coastline, Climate and Human Settlement. Springer, New Jersey, pp.119 – 148.

Cohen, Andrew S. Paleolimnology:The history and evolution of lake systems. Oxford: New York, 2003.

Cordova, C.E., Harrison, S.P., Mudie, P.J., Riehl, S., Leroy, S.A.G., Ortiz, N., 2009. Pollen, plant macrofossil and charcoal records for palaeovegetation reconstruction in the Mediterranean-Black Sea Corridor since the Last Glacial Maximum. Quaternary International 97:12 – 26.

de Vernal, A., and Marret, F., 2007. Organic-walled dinoflagellate cysts: tracers of sea -surface conditions, In Hillaire-Marcel and de Vernal (eds.). Proxies in Late Cenozoic Paleoceanography, Elsevier, pp. 371 – 408.

Eimers, M.C., Paterson, A.M., Dillon, P.J., Schiff, S.L., Cumming, B.F., Hall, R.I., 2006.

Lake sediment core records of sulphur accumulation and sulphur isotopic composition in central Ontario, Canada lakes. Journal of Paleolimnology 35:99 – 109.

El-Moslimany, A.P., 1990. Ecological significance of common nonarboreal pollen: examples from drylands of the Middle East. Review of Palaeobotony and Palynology 64 (1-4):343 – 350.

Ergin, M., Kazancı, N., Varol, B., Ileri, O. and Karadenizli, L., 1997. Sea-level changes and related deopistional environments on the souther Marmara shelf. Marine Geology 140:391 – 403.

Ergin, M. and Bodur, M.N., 1999. Silt/clay fractionation in surficial Marmara sediments: implication for water movement and sediment transport paths in a semi-enclosed and two-layer flow system (northeastern Mediterranean Sea). Geo-Marine Letters 18:225 – 233.

Eriş, K. K., Ryan, W.B.F., Çağatay, M.N., Sancar, U., Lericolais, G., Menot, G., Bard, E., 2007. The timing and evolution of the post-glacial transgression across the Sea of

Marmara shelf south of Istanbul. Marine Geology 243:57 – 76.

Eriş, K. K., Çağatay, M.N., Akçer, S., Gasperini, L., Mart, Y., 2011. Late glacial to Holocene sea-level changes in the Sea of Marmara: new evidence from high-resolution seismics and core studies. Geo-Marine Letters 31:1 – 18.

Faure, G. Principles of Isotope Geology. New York: Wiley, 1986.

Fensome, R.A., Williams, G.I., Barss, S., Freeman, J.M., and Hill, J.M., 1990. Acritarchs and fossil prasinophytes: an index to genera, species and infraspecific taxa. American Association of Stratigraphic Palynology Foundation Contributions Series 25, 771p.

Fensome, R.A. and Williams, G.L., 2004. The Lentin and Williams Index of Fossil Dinoflagellates. American Association of Stratigraphic Palynologists Contributions Series 42, 909p.

Fletcher, W.J. and Sanchez-Goñi, M.F., 2008. Orbital- and sub-orbital-scale climate Impacts on vegetation of the western Mediterranean basin over the last 48,000 yr. Quaternary Research 70: 451 – 464.

Hiscott, R.N., Aksu, A.E., 2002. Late Quaternary history of the Marmara Sea and Black Sea from high-resolution seismic and gravity-core studies. Marine Geology 190:261 – 282.

Hiscott, R. N., Aksu, A. E., Mudie, P. J., Kaminski, M. A., Abrajano, T., Yaşar, D. and Rochon, A., 2007a. The Marmara Sea Gateway since ~16 Ky BP: Non-catastrophic causes of paleoceanographic events in the Black Sea at 8.4 and 7.15 Ky BP. In: Yanko- Hombach, V., Gilbert, A.S., Panin, N., Dolukhanov, P.M. (Eds.), The Black Sea Flood Question: Changes in Coastline, Climate, and Human Settlement. Springer pp 89 – 117.

Hiscott, R.N., Aksu, A.E., Mudie, P.J., Marret, F., Abrajano, T., Kaminski, M.A., Evans, J., Çakıroğlu, A.I., Yaşar, D., 2007b. A gradual drowning of the southwestern Black Sea shelf: evidence for a progressive rather than abrupt Holocene reconnection with the eastern Mediterranean Sea through the Marmara Sea gateway. Quaternary International 167 – 168:19 – 34.

Hopkins, J.A., McCarthy, F.M.G., 2002. Postdepositional palynomorph degradation in

Quaternary shelf sediments: a laboratory experiment studying the effects of progressive oxidation. Palynology 26:167 – 184.

Jansonius, J. & McGregor, D.C. 1996. Chapter 1. Introduction; in: Jansonius, J. & McGregor, D.C. (ed.), Palynology: principles and applications; American Association of Stratigraphic Palynologists Foundation, Vol.1, p.1 – 10, 227.

Jørgensen, B.B., Kasten, S., 2006. Sulfur cycling and methane oxidation. In: Schulz, H.D., Matthias, Z. (Eds.) Chapter 8: Marine Geochemistry. Springer-Verlag, New York, 271 – 309.

Kaminski, M. A., Aksu, A. E., Box, M., Hiscott, R. N., Filipescu, S. and Al-Salameen, M., 2002. Late glacial to Holocene benthic foraminifera in the Marmara Sea: implications for Black Sea-Mediterranean Sea connections following the last deglaciation. Marine Geology 190:165 – 202.

Kapp, Ronald O. How to Know Pollen and Spores. Dubuque, IA: W. C. Brown, 1969.

Kidd, R.B., Cita, M.B., Ryan, W.B.F., 1978. Stratigraphy of eastern Mediterranean sapropel sequences recovered during DSDP Leg 42A and their paleoenvironmental

significance. In Hsü, K., et al., (eds.), Init. Rep. Deep Sea Drill. Proj. 42:421 – 443.

Kotthoff, U., Pross, J., Muller, U.C., Peyron, O., Schmiedl, G., Schulz, H., Bordon, A., 2008. Climate dynamics in the borderlands of the Aegean Sea during formation of sapropel S1 deduced from a marine pollen record. Quaternary Science Reviews 27:832 – 845.

Krebs, P., Conedera, M., Pradella, M., Torriani, D., Felber, M., Tinner, W., 2004. Quaternary refugia of the sweet chestnut (Castanea sativa Mill.): an extended palynological approach. Vegetation History and Archaeobotany 13:145 – 160.

Lashin, G.M.A., 2012. Palynological studies of some species Aspleniaceae-Pteridophyta. American Journal of Plant Sciences 3:397 – 402.

De Leeuw, J. W., Versteegh, G.J.M. and Van Bergen, P. F., 2006. Biomacromolecules of algae and plants and their fossil analogues. Plant Ecology 182:209 – 233.

Leroy, S.A.G., Boyraz, S., Gürbüz, A., 2010. High-resolution palynological analysis in Lake Sapanca as a tool to detect recent earthquakes on the North Anatolian Fault. Quaternary Science Review 28:1 – 17.

Li, F., Sun, J., Zhao, Y., 2010. Ecological significance of common pollen ratios: A Review. Front. Earth Sci. Chine 4(3):253 – 258.

Londeix, L., Yannick, H., Turon, J.-L., and Fletcher, W., 2009. Last glacial to Holocene hydrology of the Marmara Sea inferred from a dinoflagellate cyst record. Review of Palaeobotany and Palynology 158:52 – 71.

Major, C.O., Goldstein, S.L., Ryan, W.B.F., Lericolais, G., Piotrowski, A.M., Hajdas, I., 2006. The co-evolution of Black Sea level and composition through the last deglaciation and its paleoclimatic significance. Quaternary Science Reviews 25 (17-18):2031 – 2047.

Marret, F., and Zonneveld, K., 2003. Atlas of modern organic-walled dinoflagellate cyst distribution. Review of Palaeobotany and Palynology 125:1 – 200.

Marret, F., Leroy, S.A.G., Chalié, F., Gasse, F., 2004. New organic-walled dinoflagellate cysts from recent sediments of Central Asian seas. Review of Palaeobotany and Palynology 129:1 – 20.

Marret, F., Mudie, P., Aksu, A.E., and Hiscott, R.N., 2009. A Holocene dinocyst record

of a two-step transformation of the Neoeuxinic brackish water lake into the Black Sea. Quaternary International 197 (1-2):72 – 86.

Mcglone, M.S., Wilmshurst, J.M., Leach, H.M., 2005. An ecological and historical review of bracken (*Pteridium esculentum*) in New Zealand, and its cultural significance. New Zealand Journal of Ecology (29) 2:165 – 184.

McHugh, C.M.G., Gurung, D., Giosan, L., Ryan, W.B.F., Mart, Y., Sancar, U., Burckle, L., Çağatay, M.N., 2008. The last reconnection of the Marmara Sea (Turkey) to the World Ocean: A paleoceanographic and paleoclimatic perspective. Marine Geology 255:64 – 82.

Menot, G., Bard, E., 2010. Geochemical evidence for a large methane release during the last deglaciation from Marmara Sea sediments. Geochimica et Cosmochimica 74:1537 – 1550.

Mertens, K.N., Ribeiro, S., and 29 others, 2009. Process length variation in cysts of a dinoflagellate, Lingulodinium machaerophorum, in surface sediments: investigating its potential as salinity proxy. Marine Micropaleontology 70:54 – 69.

Mertens, K.N., Bradley, L.R., Takano, Y., Mudie, P.J., Marret, F., Aksu, A.E., Hiscott, R. N., Verleye, T.J., Mousing, E.A., Smyrnova, L.L., Bagheri, S., Mansor, M., Pospelova, V., Matsuoka, K., 2012. Quantitative estimation of Holocene surface salinity variation in the Black Sea using dinoflagellate cyst process length. Quaternary Science Reviews 39:45 – 59.

Moore, P. D., Webb, J. A., Collinson, M.E. Pollen Analysis. 2nd ed. Oxford: Blackwell Scientific Publications, 1991.

Mudie, P. J., Aksu, A. E., and Yaşar, D., 2001. Late Quaternary dinocysts from the Black, Marmara, and Aegean Seas: variations in assemblages, morphology, and paleosalinity. Marine Micropaleontology 43:155 – 78.

Mudie, P. J., Rochon, A., Aksu, A. E. and Gillespie, H., 2002a. Dinoflagellate cysts, freshwater algae and fungal spores as salinity indicators in Late Quaternary cores from Marmara and Black Seas. Marine Geology 190:203 – 31.

Mudie, P. J., Rochon, A. and Aksu, A. E., 2002b. Pollen stratigraphy of Late Quaternary cores from Marmara Sea: land-sea correlation and paleoclimatic history. Marine

Geology 190:233 – 60.

Mudie, P.J., Rochon, A.E., Levac, E., 2002c. Palynological records of red tide-producing species in Canada: past trends and implications for the future. Paleogeography, Paleoclimatology, Paleoecology 180 (1):159 – 186.

Mudie, P. J., Rochon, A., Aksu, A. E. and Gillespie, H., 2004. Late glacial, Holocene and modern dinoflagellate cyst assemblages in the Aegean-Marmara-Black Sea corridor: statistical analysis and re-interpretation of the Early Holocene Noah's flood hypothesis. Review of Palaeobotany and Palynology 128:143 – 67.

Mudie, P.J., McCarthy, F.M., 2006. Marine palynoloy: potentials for onshore-offshore correlation of Pleistocene – Holocene records. Transactions of the Royal Society of South Africa 61(2):139 – 158.

Mudie, P. J., Marret, F., Aksu, A. E., Hiscott, R. N. and Gillespie, H., 2007. Palynological evidence for climatic change, anthropogenic activity and outflow of Black Sea water during the Late Pleistocene and Holocene: centennial- to decadal -scale records from the Black and Marmara Seas. Quaternary International 167-

168, 73 – 90.

Mudie, P.J., Marret, F., Rochon, A., and Aksu, A.E., 2010. Non-pollen palynomorphs In the Black Sea corridor. Vegetation History and Archaeobotany 19:531 – 544.

Mudie, P.J., Leroy, S.A.G., Marret, F., Gerasimenko, N., Kholeif, S.E.A., Sapelko, T., Filipova-Marinova, M., 2011. Nonpollen palynomorphs: Indicators of salinity And environmental change in the Caspian-Black Sea-Mediterranean corridor. The Geological Society of America Special Paper 473:1 – 27.

Murray, J.W., Stewart, K., Kassakian, S., Krynytzky, M., DiJulio, D., 2007. Oxic, suboxic, and anoxic conditions in the Black Sea. In: Yanko-Homback, V., Gilbert, A.S., Panin, N., Dolukhanov, P.M., (eds) The Black Sea flood question: changes in coastline, climate and human settlement. Springer, Dordrecht, pp. 1 – 22.

Obbink, E., Carlson, A., Klinkhammer, G., 2010. Eastern North American freshwater discharge during the Bølling-Allerød warm periods. Geology 38 (2): 171 – 174.

Özdoğan, M., 2011. Westward Expansion of the Neolithic way of life: sorting the

Neolithic package into distinct packages. Current Anthropology 52(S4): S415 – S430.

Peltier, W.R., Fairbanks, R.G., 2006. Global glacial ice volume and Last Glacial Maximum duration from an extended Barbados sea level record. Quaternary Science Reviews (25) 23 – 24:3322 – 3337.

Pienkowski, A.J., 2011. Late Holocene environmental conditions in Coronation Gulf, Southwestern Canadian Arctic Archipelago; evidence from dinoflagellate cysts, Other non-pollen palynomorphs, and pollen. Journal of Quaternary Science 26 (8): 839 – 853.

Rochon, A., De Vernal, A., Turon, J.-L., Matthiessen, J. and Head, M.J., 1999. Distribution of dinoflagellate cysts in surface sediments from the North Atlantic ocean and adjacent basins, and quantitative reconstruction of sea-surface parameters. American Association of Stratigraphic Palynologists 35:250.

Ryan, W.B.F., Pitman, W.C.III., Major, C.O., Shimkus, K., Moskalenko, V., Jones, J.A., Dimitrov, P., Görür, N., Sakınç, M., Yüce, H., 1997. An abrubt drowning of Black

Sea shelf. Marine Geology 138:119 – 126.

Ryan, W.B.F., and Pitman, W. C. III., 1999. Noah's Flood: the New Scientific Discoveries about the Event That Changed History. New York: Simon & Schuster.

Ryan, W.B.F., Major, C.O., Lericolais, G., and Goldstein, S.L., 2003. Catastrophic flooding of the Black Sea. Annual Review of Earth and Planetary Sciences 31:525 – 554.

Sarıkaya, M.A., Zreda, M., Çiner, A., 2009. Glaciations and paleoclimate of Mount Erciyes, central Turkey, since the Last Glacial Maximum, inferred from ^{36}Cl cosmogenic dating and glacier modeling. Quaternary Science Reviews 28: 2326 – 2341.

Siani, G., Paterne, M., Arnold, M., Bard, E., Métivier, B., Tisnerat, N., Bassinot, F., 2000. Radiocarbon reservoir ages in the Mediterranean Sea and Black Sea. Radiocarbon 42(2):271 – 280.

Sluijs, A., Pross, J., and Brinkhuis, H., 2005. From greenhouse to icehouse: organic-walled dinoflagellate cysts as paleoenvironmental indicators in the Paleogene.

Earth-Science Reviews 68:281 – 315.

Sperling, M., Schmiedl, G., Hemleben, Ch., Emeis, K.C., Erlenjeuser, H., Grootes, P.M., 2003. Black Sea impact on the formation of eastern Mediterranean sapropel S1? Evidence from the Marmara Sea. Palaeogeogr Palaeoclimatol Palaeoecol 190:9 – 21.

Stuiver, M. and Braziunas, T.F., 1993. Modeling atmospheric ^{14}C Influences and ^{14}C ages of marine samples to 10,000 BC. Radiocarbon 35 (1):137 – 189.

Thode, H.G., 1991. Sulphur isotopes in nature and the environment: an overview. In: Krouse, H.R., Grinenko, V.A. (Eds.) Chapter 1: Stable Isotopes in the Assessment of Natural and Anthropogenic Sulphur in the Environment. John Wiles and Sons, 1 – 26.

Traverse, A., 1988. Paleopalynology. Boston: Unwin Hyman.

Turney, C.S.M., and Brown, H., 2007. Catastrophic early Holocene sea level rise, human migration and the Neolithic transition in Europe. Quaternary Science Reviews 26:2036 – 041.

Tzedakis, P.C., Roucoux, K.H., de Abreu, L., Shackleton, N.J., 2004. The duration of forest stages in southern Europe and interglacial climate variability. Science 306 (5705):2231 – 2235.

Ünal, Y., Kindap, T., Karaca, M., 2003. Redefining the climate zones of Turkey using Cluster analysis. International Journal of Climatology 23:1045 – 1055.

Urğulu, E., Roleček, J., Bergmeier, E., 2012. Oak woodland vegetation of Turkey – a first overview based on multivariate statistics. Applied Vegetation Science, online at Doi: 10.1111/j,1654-109X.2012.01192.x

Vidal, L., Ménot, G., Joly, C., Bruneton, H., Rostek, F., Çağatay, M.N., Major, C., Bard, E., 2010. Hydrology in the Sea of Marmara during the last 23 ka: implications for timing of Black Sea connection and sapropel deposition. Paleoceanography 25:1 – 16.

Watanabe, T., Naraoka, H., Nishimura, M., Kinoshita, M., and Kawai, T., 2003. Glacial-Interglacial changes in organic carbon, nitrogen and sulfur accumulation in Lake Baikal sediment over the past 250 kyr. Geochemical Journal 37:493 – 502.

Zattin, M., Cavazza, W., Okay, A.I., Federici, I., Fellin, M.G., Pignalosa, A., Reiners, P., 2010. A precursor of the North Anatolian Fault in the Marmara Sea region. Journal of Asian Earth Sciences 39:97 – 108.

Zonneveld, K.A.F., Versteegh, G., Kodrans-Nsiah, M., 2008. Preservation and organic Chemistry of late Cenozoic organic-walled dinoflagellate cysts: A review. Marine Micropaleontology 68:179 – 197.

Plates

Plate I. Pollen and spore taxa characteristic of pollen assemblage zones in MAR02-89P. Scale bar is 10 microns. Sample depth of specimens is shown in cm; archive slides are at Memorial University of Newfoundland Dept., Earth Sciences. All images are from MAR02-89P except where noted.

A. *Pinus*, 750cm; B. *Quercus* small, 800cm; C. *Quercus* large, 600cm; D. *Corylus*, 60cm; E. *Artemesia*, 600cm; F. *Centaurea*, 800cm; G. *Taraxacum*-type pollen, 410cm; H. Chenopodiaceae *Suaeda*-type pollen, 600cm; I. Chenopodiaceae *Salicornia*-type pollen, 600cm; J. Chenopodiaceae *Noaea*-type pollen, 550cm; K. Poaceae small, 600cm; L. Poaceae large, from MAR02-88P, 0cm; M. *Ephedra*, 440cm; N. *Castanea*, 600cm; O. *Alnus*, 40cm; P. *Picea*, 660cm; Q. *Abies*, 580cm; R. *Acer*, 600cm; S. *Betula*, 20cm; T. *Ulmus*, 600cm; U. *Carpinus*, 60cm; V. *Tilia*, 600cm; W. *Pistacia*, 120cm; X. *Juniperus*, 600cm; Y. Aster-type, 460cm; Z. *Cirsium*-type pollen, 600cm; AA. *Juglans*, from MAR05-45G, 90cm; BB. *Olea*, from MAR05-13P, 0cm; CC. *Quercus* small, infilled with pyrite, 260cm; DD. *Polypodium vulgare*, from MAR02-77P, 0cm; EE. Polypodiaceae without perine, 600cm; FF. *Dryopteris*, from Black Sea core 342, 110cm; GG. Unknown trilete, from MAR02-77P, 0cm; HH. *Anthoceros*, from Black Sea core 342, 110cm; II. *Thelypteris*, from Black Sea core 342, 110cm; JJ. *Lycopodium annotinum*, from MAR05-04G, 10cm.

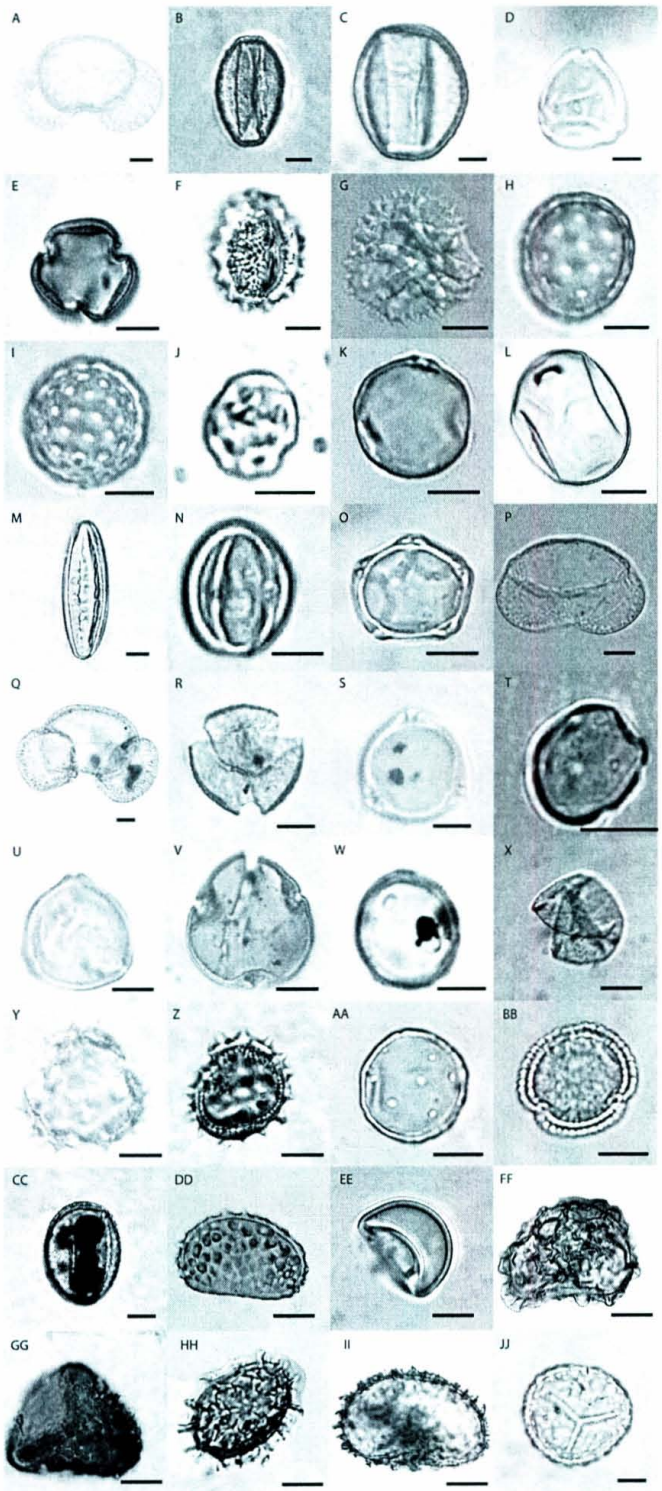
A
B
C
D
E
F
G
H
I
J
K
L
M
N
O
P
Q
R
S
T
U
V
W
X
Y
Z
AA
BB
CC
DD
EE
FF
GG
HH
II
JJ

Plate II. Dinocyst taxa characteristic of dinocyst assemblage zones in MAR02-89P. Scale bar is 10 microns. Sample depth of specimens is shown in cm; archive slides are at Memorial University of Newfoundland Dept., Earth Sciences. All images are from MAR02-89P except where noted.

A1. *Spiniferites cruciformis* form 1, ventral view, hi focus, 780cm; A2. *S. cruciformis* form 1, dorsal view, low focus, 780cm; B1. *S. cruciformis* form 2, ventral view, high focus, 780cm; B2. *S. cruciformis* form 2, dorsal view, low focus, 780cm; C. *Pyxidinopsis psilata*, dorsal view, low focus, 440cm; D. *Lingulodinium machaerophorum* with clavate processes, ventral view, high focus, 60cm; E. *L. machaerophorum* short spine form, dorsal view, low focus, 120cm ; F. *Brigantedinium* sp., dorsal view, low focus, 60cm; G1. *Operculodinium centrocarpum*, dorsal view, low focus, 440cm; G2. *O. centrocarpum*, ventral view, high focus, 440cm; H. *Caspidinium rugosum*, dorsal view, high focus, 540cm; I. *Impagidinium caspiensis*, dorsal view, low focus, 780cm; J. *Tectatodinium pellitum*, dorsal view, low focus, 0cm; K1. *Spiniferites ramosus*, from MAR02-88P, ventral view, high focus, 90cm; K2. *S. ramosus*, from MAR02-88P, dorsal view, low focus, 90cm; L. *Spiniferites mirabilis*, from MAR02-88P, ventral view, mid focus, 0cm; M. *Protoperidinium stellatum*, dorsal view, high focus, 120cm; N1. *Pyxidinopsis* "*londeixii*", ventral view, high focus, 120cm; N2. *P.* "*londeixii*", dorsal view, low focus, 120cm; O. reworked *Tuberculodinium vancampoae*, high focus, 600cm; P. reworked c.f. *Wetzeliella*, high focus, 600cm; Q. reworked *Homotryblium*, high focus, 540cm; R. *Nematosphaeropsis labyrinthus*, ventral view, high focus, 0cm; S. *Romanodinium areolatum*, ventral view, high focus, 540cm.

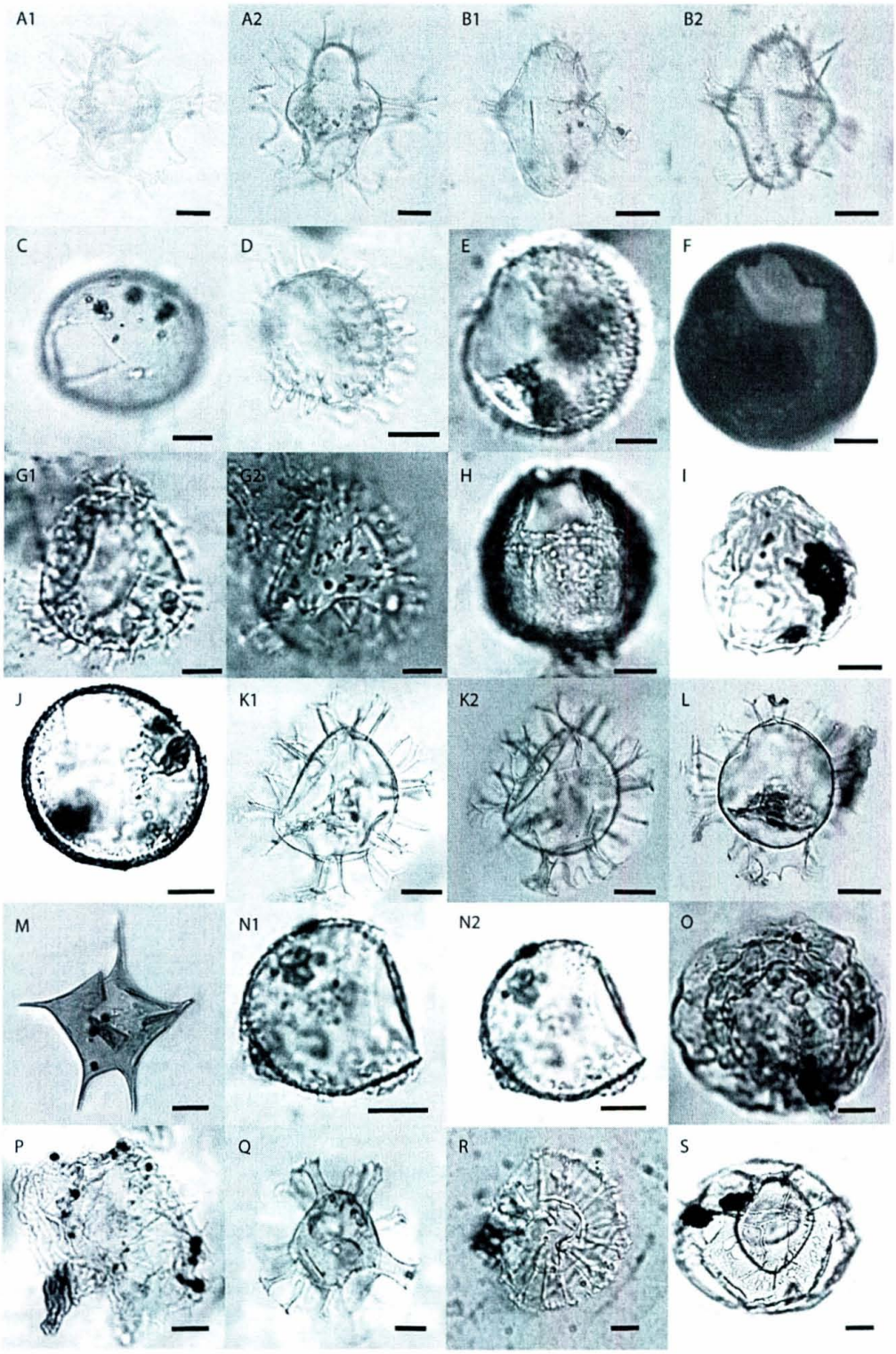
A1
A2
B1
B2
C
D
E
F
G1
G2
H
I
J
K1
K2
L
M
N1
N2
O
P
Q
R
S

Plate III. Non-Pollen Palynomorphs (NPP) taxa characteristic of MAR02-89P. Scale bar is 10 microns. Sample depth of specimens is shown in cm; archive slides are at Memorial University of Newfoundland Dept., Earth Sciences. All images are from MAR02-89P except where noted.

A. *Pediastrum boryanum*, 440cm; B. *Pediastrum simplex*, 440cm; C. *Botryococcus*, 260cm; D. *Staurastrum tetracerum* with 3 spines, 60cm; E. *Staurastrum tetracerum* with 4 spines, 60cm; F. *Multiplicasphaeridium*-type sp. with 3 processes, 780cm; G. *Multiplicasphaeridium*-type sp. with 5 processes, 260cm; H. *Glomus* sp., from MAR02-45P, 450cm; I. *Glomus* sp., from MAR05-4G, 0cm; J. Microforaminiferal lining, 260cm; K. Microforaminiferal lining, 550cm; L. Neorhabdocoel egg capsule, 550cm.

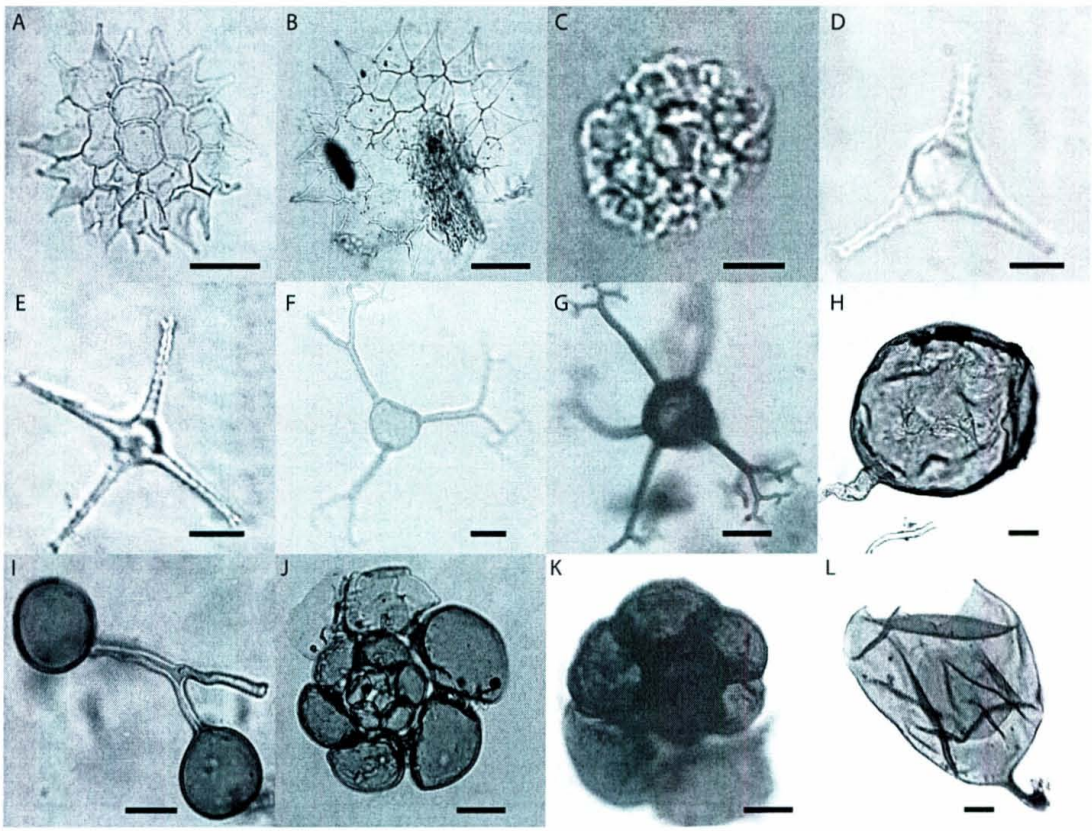

Appendix I

depth	cal. yr BP	%sand	Carbon wt.%	d13C VPDB	Sulfur wt. %	d34S VCDT	TS/TOC
0	8391	2.22804718	1.62	-25.15	0.9	-39.54	0.55555556
10	8564	2.27272727	1.93	-25.35	1.44	-38.73	0.74611399
20	8737	1.52380952	2.37	-25.44	1.54	-36.45	0.64978903
30	8910	0.44378698	2.36	-25.6	1.7	-36.17	0.72033898
40	9084	0.60483871	2.67	-25.54	1.67	-35	0.62546816
50	9257	3.19961796	2.58	-24.88	1.61	-34.23	0.62403101
60	9430	0.26773762	2.39	-24.95	1.55	-33.75	0.64853556
70	9603	0.76419214	1.96	-25.57	1.65	-35.4	0.84183673
80	9776	0.76775432	2.41	-26.15	1.49	-33.73	0.61825726
90	9949	0.40595399	2.46	-25.93	1.54	-33.86	0.62601626
100	10123	0.35335689	1.71	-26.14	1.77	-36.45	1.03508772
110	10296	0.93023256	1.73	-26.51	1.58	-35.22	0.9132948
120	10469	0.28409091	1.44	-26.48	1.77	-36.02	1.22916667
130	10642	0.12217471	1.48	-26.44	1.83	-35.75	1.23648649
140	10815	0.67076579	1.61	-26.37	1.85	-33.62	1.14906832
150	10988	0.1216545	1.24	-26.71	1.6	-35.66	1.29032258
160	11162	0.19788918	1.3	-26.57	1.45	-35.22	1.11538462
170	11335	0.74982958	1.566	-26.97	1.146	-34.32	0.73180077
180	11508	0.66401062	1.226	-26.411	1.24	-33.169	1.01141925
190	11681	1.39037433	1.23	-26.611	1.237	-34.064	1.00569106
200	11854	1.16207951	2.257	-27.455	1.365	-33.611	0.60478511
210	12027	1.11358575	1.563	-27.071	1.345	-32.377	0.86052463
220	12201	1.558753	1.663	-26.935	1.609	-33.928	0.96752856
230	12374	1.56641604	1.79	-27.243	1.656	-32.958	0.92513966
240	12547	0.89285714	1.39	-27.134	1.568	-33.98	1.12805755
250	15567	4.62656973	0.864	-26.835	1.683	-35.863	1.94791667
260	16913	7.58699373	0.535	-26.603	2.165	-33.918	4.04672897
270	18258	4.57013575	0.398	-25.758	2.055	-21.003	5.16331658
280	18733	2.09397344	0.387	-25.884	1.592	-13.847	4.11369509
290	19207	4.02298851	0.403	-25.807	0.596	-21.459	1.47890819
300	19262	1.27632419	0.39	-25.379	0.812	-19.892	2.08205128
310	19316	1.20415982	0.424	-25.809	0.211	-18.444	0.49764151
320	19371	1.13830393	0.417	-25.857	0.063	-14.747	0.15107914
330	19425	3.22946176	0.431	-25.831	0.102	-20.422	0.23665893
340	19480	2.10593491	0.877	-27.014	0.085	-18.141	0.09692132
350	19534	1.04166667	0.441	-25.661	0.051	-11.98	0.11564626
360	19589	0.83194676	0.451	-25.699	0.047	-8.788	0.10421286
370	19643	1.21668598	0.499	-26.021	0.061	-2.249	0.12224449
380	19698	0.50476725	0.445	-25.885	0.052	-1.913	0.11685393
390	19752	1.23131047	0.439	-25.645	0.062	2.486	0.14123007
400	19807	0.84196891	0.478	-26.416	0.563	22.163	1.17782427
410	19861	2.32964473	0.481	-26.057	1.224	23.844	2.54469854
420	19916	1.77830468	0.473	-25.871	0.791	16.14	1.67230444
430	19970	0.83682008	0.478	-26.585	0.567	6.801	1.18619247
440	20025	1.15406809	0.463	-25.843	0.161	0.066	0.34773218
450	20079	0.84269663	0.47	-26.27	0.11	-8.58	0.23404255
460	20288	8.14717477	0.45	-25.88	0.08	-5.68	0.17777778
470	20497	0.40816327	0.45	-25.76	0.07	-4.16	0.15555556
480	20705	0.65406977	0.42	-25.54	0.07	1.8	0.16666667
490	20914	0.73710074	0.44	-25.8	0.04	-0.52	0.09090909
500	21347	0.72954664	0.55	-26.16	0.79	14.89	1.43636364
510	21780	0.6155303	0.48	-25.65	1.06	18.45	2.20833333
520	22081	1.35135135	0.55	-26.13	1.16	6.88	2.10909091
530	22383	0.75825156	0.48	-25.67	0.94	8.49	1.95833333
540	22684	0.68270481	0.49	-26.37	0.59	15.96	1.20408163
550	22986	0.3652968	0.5	-25.64	0.74	19.89	1.48
560	23287	0.47281324	0.5	-25.64	0.94	22.52	1.88
570	23589	2.05859066	0.44	-25.98	1.27	26.17	2.88636364
580	23890	0.26809651	0.5	-25.57	0.97	1.33	1.94
590	24192	1.33795837	0.49	-25.8	0.7	8.15	1.42857143
600	24493	0.46583851	0.5	-25.82	0.84	17.13	1.68
610	24795	0.90996169	0.53	-26.18	1.04	9.94	1.96226415
620	25096	0.76154212	0.52	-26.06	0.77	8.66	1.48076923
630	25397	0.7068803	0.51	-26.03	0.97	7.8	1.90196078
650	25699	2.08030963	0.41	-26.28	0.03	5.5	0.07317073
660	26000	1.20948234	0.44	-25.91	0.1	22.41	0.22727273
670	26302	1.93584071	0.43	-25.77	0.12	9.19	0.27906977
680	26603	1.99063232	0.41	-25.83	0.05	13.47	0.12195122
690	26905	2.01229737	0.41	-25.74	0.04	7.72	0.09756098
700	27206	1.63599182	0.38	-25.66	0.04	2.51	0.10526316
710	27508	2.52317199	0.38	-25.65	0.04	5.94	0.10526316
720	27809	1.66666667	0.43	-25.9	0.03	1.48	0.06976744
730	28111	1.27919911	0.43	-25.54	0.35	52.75	0.81395349
740	28412	2.66930302	0.43	-25.75	0.09	9.47	0.20930233
750	28692	1.76366843	0.44	-25.72	0.04	2.98	0.09090909
760	28972	1.68949772	0.44	-25.67	0.05	3.81	0.11363636
770	29252	1.1740684	0.45	-25.84	0.04	3.2	0.08888889
780	29531	1.89663348	0.48	-25.4	0.08	3.09	0.16666667
790	29811	2.03291384	0.42	-25.65	0.04	2.29	0.0952381
800	30091	2.67898383	0.85	-27.23	0.05	2.97	0.05882353
810	30371		1.2	-27.77	0.04	-0.53	0.03333333

Appendix II

Systemic list of generic and specific names used in text, with complete authorships. Further information on the taxonomy and nomenclature of these taxa can be found in Fensome and Williams (2004) and Fensome et al. (1990).

Phytoplankton and Acritarchs in MAR02-89P

Acritarcha

Multiplicasphaeridium Staplin, 1961

cf. *Multiplicasphaeridium* sp.of Strother, 1996

Chlorococcales

Botryococcus Kützing

Botryococcus braunii Kützing, 1849

Pediastrum F.J.F. Meyen, 1829.

Pediastrum boryanum (Turpin 1828) Meneghini 1840

Pediastrum simplex Meyen, 1829

Prasinophyta

Cymatiosphaera O. Wetzel, 1993 (syn. Pterosperma Pouchet, 1893 [Parke et al., 1978] phycoma)

Cymatiosphaera globulosa Takahashi, 1964 (= *Pterosperma* sp. phycoma)

Desmidiaceae (sometimes classified in a separate order, Desmidiales)

Staurasturum tetracerum Ralfs ex Ralfs 1848

Fern and Fern Allies

Equisetaceae

Class Spenopsida

Equisetum

Polypodiales

Polypodiaceae

Asplenium

Dryopteridaceae

Dryopteris-type

Dennstaedtiaceae

Pteridium

Lycopodiopsida

Lycopodium annotinum

Anthocerotaceae

Anthoceros

Dinoflagellates

Ataxiodinium choane Reid 1974

Brigantedinium spp. Reid 1977 ex Lentin et Williams, 1993 = *Protoperidinium* spp.

Brigantedinium simplex Wall 1965) Reid 1977 = cyst of *Protoperidinium conicoides* (Paulsen) Balech

Caspidinium rugosum Marret in Marret et al., 2004

Impagidinium caspienense Marret in Marret et al., 2004

Impagidinium sp. Stover and Evitt, 1978

Lingulodinium machaerophorum (Deflandre et Cookson 1955) Wall 1967

Lingulodinium machaerophorum forms with short club-shaped processes (vars. A-D of Marret et al., 2004)

Lingulodinium machaerophorum form with short truncate processes of Mudie et al., 2001

Operculodinium centrocarpum sensu Wall and Dale 1966 = cyst of *Protoceratium reticulatum* (Claparède et Lachmann) Bütschli 1885

Protoperidinium stellatum (Wall) Balech 1994

Pyxidinopsis psilata Wall and Dale 1973; Head, 1994a

Pyxidinopsis sp. of Londeix et al, 2009

Spiniferites cruciformis Wall and Dale, 1973

Spiniferites cruciformis morphotype C of Marret in Marret et al., 2004

Spiniferites elongatus Reid, 1974

Spiniferites mirabilis (Rossignol 1964) Sarjeant 1970

Spiniferites ramosus (Ehrenberg, 1838) Mantell, 1854

Tectatodinium pellitum Wall, 1967; Head, 1994a

Homotryblium plectilum Drugg and Loeblick, 1967

Apteodinium Eisenack, 1958b

Wetzeliella sp. Eisenack, 1938

Tuberculodinium vancampoae (Rossignol, 1962) Wall, 1967

Polysphaeridium zoharyi (Rossignol, 1962) Bujak et al., 1980

Fungi

Glomus L. R. and C. Tulasne, 1845 chlamydospore-type

Prasinophyta

Cymatiosphaera globulosa K. Takahashi

Foraminiferida: planktonic and benthic microforaminiferal linings

Copepoda

Copepod egg-type of *Cobricosphaeridum* Harland and Sarjeant, 1970 emend Head et al.,

2003

Pollen Taxa

Aceraceae

Acer

Alismataceae

Sagittaria

Chenopodiaceae *Suaeda*

Atriplex

Haloxylon

Noaea

Salsola

Salicornia

Sarcobatus

Anacardiaceae

Pistacia

Asteraceae

Anthemis

Artemisia

Aster

Bidens

Calendula

Carduus

Centaurea

Cirsium

Serratula

Taraxacum

Xanthium

Betulaceae

Alnus

Betula

Corylus

Cupressaceae

Juniperus

Ephedraceae

Ephedra

Fagaceae

Castanea

Fagus

Quercus

Oleaceae

Fraxinus

Olea

Pinaceae

Abies

Cedrus

c.f. Larix

Picea

Pinus

Poaceae

Salicaceae

Salix

Tiliaceae

Tilia

Ulmaceae

Ulmus

Appendix III

DEPTH (cm)	0	10	20	30	40	50	60	70	80	90	100	110	120	130	140	150	160	170	180	190	200	210	220	230	240	250	260	270	280	290	300	310	320	330	340	360	370	380	390	400
cal. ka BP	8391	8564	8737	8910	9084	9257	9430	9603	9776	9949	10123	10296	10469	10642	10815	10988	11162	11335	11508	11681	11854	12027	12201	12374	12547	15567	16913	18258	18733	19207	19262	19316	19371	19425	19480	19589	19643	19698	19752	19807
Pinus - Cedrus	24		2	7	4		7	2	1	3	5	6	4	4	1	4	3	3	2			1	1	6	15	13	17	21	8		4	1	6	7	7	14	11	11	8	12
Picea			2				1	2	1								1	2		3			1	1	2	3	0	3	1		7	3	2	3	9	5	5	5	7	7
Abies	5			2		3	5	2	4	1	1	2	4	7		1		1		3		2		2	7	3	0	0	0			1			1	2	1	1	2	3
cf Larix										1	1			1												1	0	0	0				1		1					2
Juniperus	1	5	8	8	2	2	3	1	1	3	3	5	3	6		2	1	1	1	3	1	1		1	0	4	4	8	1		7	9	9	9	9	13	11	11	7	7
CTC												4		1																										
Quercus	87	19	30	58	30	23	47	41	28	29	33	67	36	70	16	30	30	37	15	13	17	24	25	49		22	19	2			5	5	7	8	12	13	9	4	5	8
Acer	3						1			1	1	2		2										1	4	3	3				3		1	1	1	3		2	3	2
Castanea	3		1	1	1			2	1					2	3		1	1		4		4	4	6	2	1	1				2	4		3	4	3	1		2	
Fagus					1					3	3	1	2	1	3				3						4															
Fraxinus	3	1	5	3		4	7	6	8		1								2		1	1	1									1	2			3				
Tilia	1					2	1																																	
Ulmus										2	2	1													1															
Corylus	4	12	10	13	7	12	10	8	9	2	1	4		1		6	1	5	3	1			4	5			1				2	3	4	3	1	7	5	5	6	4
Pistacia											1	1	2												2														
Betula	6	1	5	2		3	4	6	7			1	1	1						1		1	2	7		1						2	1		2			1		1
Carpinus	1									1	3	6	4	2	2	2	3	2		2					1															
Salix				1	1		1		1		1													1	3						2	2	1		2	1		1		
Alnus	3	1	2	5	3	3	1	2	6	1	1	4		10	1		3				1			5	4	2	1				1	1		1	1		2		1
Olea							5	2	1															1							1	4		1		1	1	1	3	1
Cornus	1										1																													
Juglans																																								
Ilex																										3						1							
Buxus										1															0	1														
Cistus										1															0	2														
Cornus					2	2				1	1														1															
Ericales												1		1										1		2	1		1										1	
c.f. Polygala sp.																																								
Potentum										2	1		5	4	2										1	1		1												
Prunus Malus																																								
Rhamnus													4																											
Ribes						2		1				1				1			1		1			2						1										
Sambucus																									1															
Vitis																																								
Apiaceae												2		14											3															
Anthemis-type				1			3			1								2	1	2		1																		
Artemisia	17	4	7	11	7	9	8	13	11	5	10	20	16	32	13	6	11	48	63	50	34	70	62	18	33	26	8	3	1		10	5	4	7	9	7	9	4	11	8
Total Chenos	10	2	1	4	1	2	5	7	16	7	8	14	7	18	7	5	5	10	14	16	12	20	14	16	22	26	14	6		1	5	9	8	10	4	5	1	11	3	7
Ephedra spp.	1		1							1		2	2	5					1		2				6	8	7	1						1	2			1	1
Aster-type	1							1		2		2			2						1		1	1	3	2	1	1			1	2	1	3		2	2	2	2	3
Centaurea												1		2								1			2			2	1	1	4	3	3	7	3	5	2	3	2	1
Calendula																																								
Bidens-type									1																3															
Carduus															2											1														
Cirsium-type																										5	2		2											
Serratula-type	1							1	1					1							1				1		1				1									
Taraxacum-type				2		1	1		1		1		1	4				1								2	2				4	1	3	1	1	1	2	5	2	2
Poaceae - small	9	10	24	28	6	8	6	14	25	1	9	9	4	17	2	9	4	5	9	6	5	8	7	17	2	13	7	2	1	1	15	10	11	14	17	26	11	19	9	15
Poaceae - large	1	1	4	3	1		1		1	1				13		3	1		1			2	4	3	1	4	6	1			5	4	1	3	6	7	2	4	6	1
Butomus																										1														
Brassicaceae													2													2														
Liguliflorae - Asterac																																							
Caryophyllaceae														1											1	4														
Cyperaceae											2	1		2	1										2	7		1												
Cyperaceae - Rhynchospora																																								
Boraginaceae												1																												
Euphorbia peplis																																								
Lamiaceae										2		16		7												1		7												
Fabaceae										1	4		3	1																										
Glaucium																																								
Herniaria																																								
Hippophae																																								
Hypericum																																								
Illecebrum																																								
Lemna																										1														
Liliaceae																																								
Lythrum										3	1	1	1																											
Melampyrum																																								
c.f. Myriophyllum sp.																																								
Nymphaea												2																												
Pinguicula																																								
Polygonum	1		1									1																		1	1	2				1	4	1	
Potamogeton												2													1															
Plantago														1															1											
Ranunculaceae											1				1																									
c.f. Proserpinaca																																								
Rosaceae	3										1	1		1											1	1	4													
Rubiaceae																										1														
Rumex					1					1	5		1	4											3	1		2												
Sagittaria												1		1												1														
Sambucus										3																														
Scutellaria																										3														
Shepherdia canadensis																																								
Silene																																								
Solanaceae												5		2	1											1		1												
Saxifraga	5					1											1										1												
Stachys																										4														
Thalictrum		1	2		1	1															1	1					1					1		1		2			
Typha																																								
Urtica				2	1		1	1	1					2					1											1		2		1			3	
Unknown triolpate	15	1	1	6	6	1	3	9	2	2	1	3	2	5		1	1			2	2	1	1	1	1	4	2				2	2	1	3	1	4	3	4	1	3
Unknown triolporate	1			2	1	1	2		3			2		3		3		4	2		1	4	4	1		1	5	2			1	3	1	1	1	1				
Unknown various	13	4	3	6	9	7	11	6	3	2		5		1	1	8	5	6	3	5	4	6	7	7		6					7	7	7	4	4	6	3	4	6	5
Indeterminate	83	30	22	49	28	22	32	34	26	7	7	3	2	8	1	11	28	21	11	15	20	8	13	21	11	12			2	6	4	13	6	11	14	13	7	10	6
Total Q. Pollen	274	92	131	214	113	109	166	161	159	91	111	199	106	258	59	92	99	149	133	126	104	157	151	172	86	112	128	65	16	5	98	88	90	98	110	147	95	111	101	100
Pollen a	56293	68993	64555	139064	63154	61905	91845	56923	103552	42801	72224	56602	54818	56008	52983	33718	32683	51074	44958	56914	78648	73613	73194	103944	27453	4095	8922	3071	3317	2260	3564	3279	5903	3391	3943	4982	3076	3917	3838	3570
Lycopodium	67	21	27	23	25	24	22	36	20	27	21	49	33	28	73	16	41	39	38	45	33	19	29	31	25	37	308	172	256	55	24	306	301	167	319	308	331	333	316	305	322

DEPTH (cm)	410	420	430	440	450	460	470	480	490	530	540	550	560	570	580	590	600	610	620	630	650	660	670	680	690	700	710	740	750	760	770	780	790	800
cal. ka BP	19861	19916	19970	20025	20079	20288	20497	20705	20914	22383	22684	22986	23287	23589	23890	24192	24493	24795	25096	25397	25699	26000	26302	26603	26905	27206	27508	28412	28692	28972	29252	29531	29811	30091
Pinus = Cedrus	15	14	12	35	20	41	24	32	41	40	61	58	36	66	46	28	71	49	53	54	12	38	37	18	30	37	6	19	14	29	11	42	13	78
Picea	8	6	8	3	9	17	14	9	15	19	10	3	2	22	14	18	2	24	23	32	5	18	12		4			9		1			2	4
Abies	2	1	1			2	2	1	4	9	8			3	3			4	4	6	1	4	9	1	2	3		2	3	1	5	7		
cf Larix						1													1			2			3	1		1						
Juniperus	9	5	5	18	1	18	3	1	6	28	20	28	10	18	5	14	4	13	19	14	6	18	10	8	8	6	1	9	8	4	12	5	3	23
CTC																																		
Quercus	9	10	5	6	9	6	2	4	9	28	13	15	10	10	15	16	20	10	12	13	7	17	7	9	10	15	7	12	8	10	3		6	8
Acer				1	1	3	2	2	1	8	4				3	3	3	1	3	1	3	2	3	2		1		3	1	1	2			
Castanea	1			5		1		1	1	5	3	9	1	6	7	3	2	1	6	3	2	2	4	2	2	4	1	2	2	5	6		2	2
Fagus																												2						
Fraxinus							1							3																2				
Tilia																	1																	
Ulmus														2								1												
Corylus	2	6	4	2	3	7		4	3		4	7	2	2	5	7		4	3	3	1	2	9	1	2	8	4	3	2	1	1			
Pistacia																																		
Betula	3	1		1	1	2				2				1		1	1	2	1	1								1						
Carpinus				1	1									1												1								
Salix				2		1					1			2	1			1			2	4			1			2						1
Alnus		1	1	3					1	1	2			3			2			3			1			1		2	2	4	2	1		3
Olea	2		1		1			2	2	3	2	3				1		6	6															
Cornus				2									1	5																3				
Juglans																														1				7
Ilex																														1				
Buxus																																		
Cistus																																		
Cornus																																		
Ericales		1	1						1	1	1						1					2	1					4	1		2	1		
c.f. Polygala sp.																													1	1				
Poterium																									1									
Prunus Malus																																		
Rhamnus																																		
Alnus	1				1					1												2												
Sambucus																																		
Vitis																																		
Apiaceae																						1			5									
Anthemis-type																						1			1									
Artemisia	7	10	1	19	8	5		6	6	26	12	16	13	13	22	13	15	16	7	9	3	16	7	7	15	12	4	3	8	21	4	1	6	19
Total Cheno	6	3	2	11	10	3	1	1	6	13	13	9	8	10	8	11	6	3	6	5	8	10	5	1	4	8	1		5	8	2	2	5	9
Ephedra spp.			1	4		1			2	2	2	3	1	3	4	5	1	3	2	1		1					1		2	5	1	1	2	2
Aster-type	1	2	2	5	2	9		3		5	2		3		2	1	6	1	1	2		10	6	4	5	1	1	1		3	3		7	5
Centaurea	5	6	4	10	7	6	1	7	11	7	5			2	2	5		2	1	4	5	7	4	4	8	7	4	3		6	3		4	2
Calendula																																		
Bidens-type				1													2																	
Carduus										2														1		1								
Cirsium-type											3	1			3	3		1				1						1	1					
Serratula-type							1										2		1						1									1
Taraxacum-type	5	2	1	2	3	2	3	6	3	2	1				3	1	1	1	1	1	3	8	3	4	3	2	4	3	5	6	1	6	6	5
Poaceae - small	19	22	12	4	9	14	3	14	9	20	39	23	5	7	27	29	5	5	13	11	6	23	1	3	4	3		1	5	3	6	1	3	
Poaceae - large	6	4	7	4	1	2	2	3	2	9	8	5		5	1	1		1	1		1			1	3		1		1	1	2	1	1	
Butomus																																		
Brassicaceae																																		
Liguliflorae - Asterac.																																		
Caryophyllaceae																						5		1										
Cyperaceae																						5		2										
Cyperaceae - Rhynchospora																						1												
Boraginaceae																								1										
Euphorbia peplis																																		
Lamiaceae													1																					
Fabaceae																									3									
Glaucium																						2				1								
Hernaria																																		
Hippophae																						1				1								
Hypericum																								1		1								
Illecebrum																								1										
Lemna																										1								
Liliaceae																																		
Lythrum																						3												
Melampyrum																									1						1			5
c.f. Myriophyllum sp.																										1								
Nymphaea																						1												
Pinguicula																						5	2			2	2	1		1	1		3	
Polygonum		1	1		2	5	1	6	1	3	5		2	2		1				5		2												
Potamogeton																									1									1
Plantago																						2												
Ranunculaceae																									1									
c.f. Proserpinaca																						2												
Rosaceae											3			1																				
Rubiaceae					1					1				3																				
Rumex														1										3								1		
Sagittaria																						1												
Sambucus																																		
Scutellaria																																		
Shepherdia canadensis														1								1												
Silene																									1									
Solanaceae																						2												
Saxifraga													2									1								1				
Stachys																									1									
Thalictrum					4								3	1																	2		1	5
Typha																																		
Urtica	1	3	1	3		1	1				2	2		1	2	2	1	2				1		3	1		1	1	1					
Unknown tricolpate	5	2	1	12	2	1		1	4	6	2	3	5	4	5	7	5	2	3	2	1	9			3	2		1		4	3	1	5	5
Unknown tricolporate				2				1	3	3		1			1	1	5	1	2			2		1				2		2		1		
Unknown various	5	2	1	22	7	10	1	8	9	21	7	5	1	20	3	6	4	8	7	1	1	9	1	1	2	4	1	3	2	19	1	1	3	
Indeterminate		6	4	1	6	15	2	7	8	15	12	12		7	6	8		5	4	5		4	4	6	6	5		9	9	8	4	2	5	
Total Q. Pollen	112	108	76	185	105	173	64	121	148	281	242	206	108	226	188	185	160	165	185	171	69	246	126	87	143	126	39	100	84	155	80	73	79	185
Pollen g	3933	3851	2756	5435	3669	5657	2154	2926	4986	9633	9085	8089	4455	7541	7232	7130	4206	6459	7946	6145	2436	8648	4337	1903	3263	4383	1410	3289	2660	4412	4173	2380	2476	5698
Lycopodium	326	306	316	397	331	341	348	499	335	359	300	297	290	354	309	302	415	297	275	328	329	761	341	541	522	341	328	300	355	384	225	327	369	362

Appendix IV

DEPTH (cm)	0	10	20	30	40	50	60	70	80	90	100	110	120	130	140	150	160	170	180	190	200	210	220	230	240	250	260	270	280	290	300	310	320	330	340	360	370	380	390	400
cal. ka BP	8391	8564	8737	8910	9084	9257	9430	9603	9776	9949	10123	10296	10469	10642	10815	10988	11162	11335	11508	11681	11854	12027	12201	12374	12547	15567	16913	18258	18733	19207	19262	19316	19371	19425	19480	19589	19643	19698	19752	19807
?Achomosphaera																																								
Batiacasphaera species																																								
Dubridinium												2		1															3												
Echinidinium sp.												2																												
c.f. Islandium minutum												1																								1				
Pentapharsodinium faroe											2				2																										
Pyxidinopsis psilata			1						2	3	7	2	2	3	6					1		2	4	4	3	7	1	3	0		1								1	2
Pyxidinopsis "Londerii"													4	3	11																									
Spiniferites cruciformis			1			3	5			2	2		1	12			1		1				6	12	6	33	10	4	3			1			2	1				2
Caspidinium rugosum																										1														
Impagidinium caspiensis											1		1		2																									
Impagidinium sp.																		2																						
Tectatodinium pellitum	1										4	4			5												2													
Operculodinium centrocarpum	47	10	21	23	47	16	26	60	43	28	20	131	33	13	23	2		5		3	1		1	1				1			1		1		5	4			1
Lingulodinium machaerophorum	15	7	10	19	8	5	7	3	4	12	18	14	35	14	13			1	2					1							1			1		1			2	9
Spiniferites belerius										2		2		3																										
Spiniferites bentori										1			1	1																										
Spiniferites delicatus	2									1																														
Spiniferites elongatus	1		1	2		1	3		1		1					1																								
Spiniferites ramosus/hyperacanthus	4									8	4	5	3	5	3											1				2										
Spiniferites lazus																																								
Spiniferites mirabilis	7	7	5	8	5	4	3	5	2		1					1						1	2																	
Spiniferites species unknown	15								1	1	5	2		3													8													
Romanodinium areolatum																																1								
Hemicystodinium																																								
Ataxiodinium sp.										1	2	4																												
Protoperidinium stellatum			1	2						1			2																										
Brigantedinium sp.			1	1			2			1		3			1																									
Scrippsiella trifida											1																													
Quinquecuspis concreta	1													1	1											1														
Xandarodinium variable												1																												
Dinocyst: Unknown					1	1						6		5				2									31	1	3											
Dinocysts: Reworked	3				1	1			2			4						1	1		1	1	1					5	7		1		1		3	5	1			1
Pre-quaternary Acritarch						1																									2			2	1	1	1	1		
Total Q. Dinocysts	94	25	41	55	61	30	46	70	54	62	68	179	82	65	67	4	1	10	3	4	1	3	14	20	9	45	55	9	9	2	4	2	2	1	10	10	2	1	4	18
Dino/g	19312	18748	20204	35741	34092	17038	25451	24749	35169	29161	44245	50914	42406	12599	60167	1466	330	3428	1014	1807	756	1407	6786	12087	2873	1645	3834	425	1866	904	145	75	131	35	358	339	65	35	152	643
Lycopodium	67	21	27	23	25	24	22	36	20	27	21	49/33	28	73	16	41	39	38	45	33	19	29	31	25	37	308	172	236	55	24	306	301	167	319	308	331	333	316	305	322

DEPTH (cm)	410	420	430	440	450	460	470	480	490	530	540	550	560	570	580	590	600	610	620	630	650	660	670	680	690	700	710	740	750	760	770	780	790	800
cal. ka BP	19861	19916	19970	20025	20079	20288	20497	20705	20914	22383	22684	22986	23287	23589	23890	24192	24493	24795	25096	25397	25699	26000	26302	26603	26905	27206	27508	28412	28692	28972	29252	29531	29811	30091
?Achomosphaera																																		
Batiacasphaera species				2										1																				
Dubridinium																																		
Echinidinium sp.																																		
c.f. Islandium minutum																																		
Pentapharsodinium faroe																																		
Pyxidinopsis psilata	1	1	3	2	1		1		9	10	6	5		2	5	3		3	4	1		1	5	1	4	6	3	6		1		1	1	2
Pyxidinopsis "Londeixii"																																		
Spiniferites cruciformis		1	1			1	2		1	10	4			1	7	4	6	1	2	5	3	3	1	3	3		2	2	2	2		7	2	19
Caspidinium rugosum			1	1																				1										
Impagidinium caspiensis																								1										
Impagidinium sp.																																		
Tectatodinium pellitum				1																														
Operculodinium centrocarpum	3			8	2	2		1					5	1	2		1						1					1	2	1				1
Lingulodinium machaerophorum			1		1		2		2	4	3	2	2	2	6	2	2	2	3	5	1	5	5	1	5	5	4	1	1	2	2			1
Spiniferites belerius																									1									
Spiniferites bentori																																		
Spiniferites delicatus																																		
Spiniferites elongatus																																		
Spiniferites ramosus/hyperacanthus																		1								1								
Spiniferites lazus																	1																	
Spiniferites mirabilis																																		
Spiniferites species unknown				1						1		1	2	1			2	1		1					1				1			1		4
Romanodinium areolatum																																		
Hemicystodinium																																		
Ataxiodinium sp.																																		
Protoperidinium stellatum																																		
Brigantedinium sp.										1				3		1				2	1		2	2		1	3							
Scrippsiella trifida																																		
Quinquecuspis concreta																																		
Xandarodinium variable																																		
Dinocyst: Unknown				14										2			3																	3
Dinocysts: Reworked							1		1	6	2	1	3	10			1	1		1				1	3			1	3	4	7	5	3	
Pre-quaternary Acritarch	1	1				2			1	4	1	4																						
Total Q. Dinocysts	5	4	8	29	4	6	6	1	13	40	19	16	11	19	20	13	16	11	12	16	5	10	16	11	15	16	13	15	12	8	8	11	3	30
Dino/g	176	143	288	852	140	196	202	24	438	1371	713	628	454	634	769	501	421	429	515	575	177	148	551	241	342	557	470	493	380	228	417	359	94	924
Lycopodium	326	306	316	397	331	341	348	499	335	359	300	297	290	354	309	302	415	297	275	328	329	761	341	541	522	341	328	300	355	384	225	327	369	362